Molecular Fingerprinting of VNUT-containing Compartments in Neuro-2a Cells

by

Gabrielle Jensen

B.Sc. (Biological Sciences), Simon Fraser University, 2018

A.Sc. (Biology), Kwantlen Polytechnic University, 2015

Thesis Submitted in Partial Fulfillment of the
Requirements for the Degree of
Master of Science

in the
Department of Biomedical Physiology and Kinesiology
Faculty of Science

SIMON FRASER UNIVERSITY

Fall 2021

Declaration of Committee

Name:	**Gabrielle Jensen**
Degree:	**Master of Science**
Title:	**Molecular Fingerprinting of VNUT-containing Compartments in Neuro-2a Cells**
Committee:	**Chair:** **Dawn Mackey** Associate Professor, Biomedical Physiology and Kinesiology
	Damon Poburko Supervisor Associate Professor, Biomedical Physiology and Kinesiology
	Charles Krieger Committee Member Professor, Biomedical Physiology and Kinesiology
	Michael Silverman Committee Member Professor, Biological Sciences
	Tom Claydon Examiner Professor, Biomedical Physiology and Kinesiology

Abstract

Vesicular ATP release is involved in regulating biological processes like nociception, blood glucose, and vascular tone. ATP-containing vesicles are filled by the vesicular nucleotide transporter (VNUT) and are molecularly distinct from catecholaminergic vesicles of sympathetic neurons. This work sought to identify the molecular fingerprint of VNUT-containing vesicles. Fluorescence microscopy in Neuro-2a, HeLa, and HEK293 cells showed VNUT being widely dispersed throughout the cells with a perinuclear enrichment. VNUT failed to colocalize with known markers of synaptic vesicles, lysosomes, dense cored vesicles, and catecholaminergic vesicles. Bioinformatic analyses of mammalian VNUT C-terminus identified a unique KDEL-like HEDL motif, as well as a lack of classic synaptic vesicle-targeting dileucine-like and tyrosine-based motifs. This work suggests that VNUT likely resides primarily in the Golgi-ER complex, a previously unconsidered location for what is thought to be a vesicle-associated translocase.

Keywords: *SLC17A9*; purinergic signalling; sympathetic co-transmission; VNUT-EGFP; immunocytochemistry; nearest-neighbour colocalization analysis

This thesis is dedicated to my encouraging husband for believing in me, to my family for their unwavering support, and to my friends who hiked this mountain with me.

Acknowledgements

First and foremost, I would like to thank my husband for his unconditional support. Josh, you have been my rock through the ups and downs of grad school. When I wanted to quit, you supported me. You also supported me when I immediately changed my mind like the stubborn person I am. Thank you for making sure I ate, drank water, and took breaks. I cannot express my gratitude for your patience, love, and understanding.

I owe a further debt of gratitude to my family. Thank you for waiting for me to eat supper, even when I came home from the lab at 11 o'clock at night. Thank you for helping look after Buffy, for listening to my trials and tribulations, and for all the hugs.

I would not have been able to collect as much data as I have without the help of my lab mates. Thank you, Anita, Emaan, Irvin, Jiru, and Lara. You are all superstars! I appreciate all your hard work and wish you all the best in your future endeavours.

I would not have known what to do with my data if not for my supervisor and mentor, Damon Poburko. Thank you for the guidance you have given me over the last 3 years. Thank you for your understanding when life threw some curve balls my way and for your patience when I struggled with data analysis and writing.

Finally, thank you to Drs Michael Silverman and Vera-Ellen Lucci. Your words of encouragement were spoken when I most needed to hear them.

Table of Contents

List of Tables

List of Figures

List of Acronyms

ADP	Adenosine 5'-diphosphate
AMP	Adenosine 5'-monophosphate
AMPA	α-amino-3-hydroxy-5-methyl-4-isoxazolepropionic acid
ANOVA	Analysis of variance
AP-2	Assembly polypeptide adaptor complex 2
ATP	Adenosine 5'-triphosphate
BAPTA-AM	Acetyloxymethyl 2-[N-[2-(acetyloxymethoxy)-2-oxoethyl]-2-[2-[2-[bis[2-(acetyloxymethoxy)-2-oxoethyl]amino]phenoxy]ethoxy]anilino]acetate
BDNF	Brain-derived neurotrophic factor
BIP	Binding immunoglobulin protein
$Ca2^{+}$	Calcium ion
CaV2.2	Voltage-gated calcium channel 2, isoform 2
CaV2.3	Voltage-gated calcium channel 2, isoform 3
CCTOP	Constrained Consensus TOPology Prediction
CD44	Cluster of differentiation 44
CGA	Chromogranin A
COX4	Cytochrome c oxidase, subunit 4
CRELD2	Cysteine-rich with EGF-like domains 2
C-terminus, termini (plural)	Carboxyl terminus, termini
dFromP	Distance from perimeter
DIDS	Diisothiocyanatostilbene disulfonic acid
DM	Differentiation media
DMEM	Dulbecco's Modified Eagle Medium
DsiRNA	Dicer-substrate short interfering RNA
EEA1	Early endosome antigen 1
EGFP	Enhanced green fluorescent protein
ELKS1	Protein rich in the amino acids E (glutamic acid), L (leucine), K (lysine), and S (serine) 1
ER	Endoplasmic reticulum
ERGIC	Endoplasmic-reticulum-Golgi intermediate compartment
FBS	Fetal bovine serum
FFL	Firefly luciferase

FWHM	Full width at half maximal fluorescent intensity
GABA	Gamma aminobutyric acid
GFP	Green fluorescent protein
GM	Growth media
GOLPH3	Golgi phosphoprotein 3
GPCR	G protein-coupled receptor
GRAB	GPCR activation-based
GTP	Guanosine 5'-triphosphate
HEK	Human epithelial kidney
HeLa	Henrietta Lacks
HEPES	4-(2-hydroxyethyl)-1-piperazineethanesulfonic acid
HWHM	Half width at half maximal fluorescent intensity
ICC	Immunocytochemistry
IgG1	Immunoglobulin G1
IgG2a	Immunoglobulin G2a
ITP	Inosine 5'-triphosphate
JACoP	Just Another Colocalization Plugin
KCN	Potassium cyanide
LAMP-1	Lysosome-associated membrane protein-1
MANT-ATP	(2'-(or-3')-O-(N-Methylanthraniloyl) Adenosine 5'-Triphosphate
MES	2-(N-morpholino)ethanesulfonic acid
MINER	Multi-image nearest neighbour analysis tool
mRNA	Messenger ribonucleic acid
MTS	Mitochondrial targeting sequence
Munc protein	Mammalian uncoordinated protein
N2a	Neuro-2a, Neuroblastoma-2a
NA	Numerical aperture
Na.But, Na.Butyrate	Sodium butyrate
NANC	Non-adrenergic, non-cholinergic
NCBI	National Center for Biotechnology Information
NEM	N-ethylmaleimide
NGS	Normal goat serum
NH_4Cl	Ammonium chloride
NLS	Nuclear localization sequence

NN	Nearest neighbouring
NPT	Sodium-dependent phosphate transporter
NSF	N-ethylmaleimide sensitive factor
N-terminus, termini (plural)	Amine terminus, termini
$P2X_n$	ATP-gated ion channel, subunit n
$P2Y_n$	G-protein coupled ATP receptor, subunit n
Panx1	Pannexin-1
PBS	Phosphate buffered saline
PC12	Pheochromocytoma 12
PDI	Protein disulphide-isomerase
PFA	Paraformaldehyde
PI_4P	Phosphatidylinositol 4 phosphate
PLL	Poly-L lysine
PTS	Peroxisomal targeting sequence
QD	Quad band dichroic mirror
Rab3	Ras-related protein Rab3
RFP	Red fluorescent protein
RIPA	Recursive ImageJ particle analyzer tool
ROI	Region of interest
RRP	Readily releasable pool
SD	Standard deviation
SERCA	Sarcoendoplasmic reticulum calcium ATPase
shRNA	Short/small hairpin RNA
siRNA	Short interfering RNA
SLC	Solute carrier
SLC17A	Solute carrier family 17
SLC17An	Solute carrier family 17, member *n*
SLC18A	Solute carrier family 18
SLC18An	Solute carrier family 18, member *n*
SNAP-25	Synaptosomal-associated protein, 25 kDa
SNARE	Soluble NSF attachment protein receptor
SV2a	Synaptic vesicle glycoprotein 2A
SV40	Simian vacuolating virus 40
Syt	Synaptotagmin

TGN	Trans-Golgi network
TIRF	Total internal reflection fluorescence
TMD	Transmembrane domain
TOM	Translocases of the outer mitochondrial membrane
TRIS	Tris(hydroxymethyl)aminomethane
Tukey HSD	Tukey honestly significant differences
UTP	Uridine 5'-triphosphate
UV	Ultraviolet
VAChT	Vesicular acetylcholine transporter
VAMP2	Vesicle-associated membrane protein 2
V-ATPase	Vesicular/vacuolar ATP-driven proton pump
VEAT	Vesicular excitatory amino acid transporter
VEGF	Vascular endothelial growth factor
VGLUT	Vesicular glutamate transporter
VMAT	Vesicular monoamine transporter
VNUT	Vesicular nucleotide transporter

Chapter 1.

Introduction

1.1. Purinergic Signaling

Vesicular ATP release has been demonstrated in a variety of cell types and tissues (Bodin & Burnstock, 2001; Burnstock, 2007; Meldrum & Burnstock, 1983), yet the molecular composition of primarily ATP-containing vesicles has not been characterized. With implications for several biological processes like vision, cognition, nociception, blood glucose regulation, bladder tone, and vascular tone (Bodin & Burnstock, 2001), this research aims to lay the groundwork for understanding the regulatory mechanisms of vesicular ATP release by characterizing the molecular constituents of purinergic vesicles. Identifying the molecular fingerprint of vesicular nucleotide transporter (VNUT)-containing vesicles, particularly in comparison to vesicles containing other neurotransmitters, could provide additional insight into the molecular mechanisms underlying co-transmission and co-release.

For the purposes of this research, co-transmission refers to the carefully regulated release of two or more neurotransmitters from different vesicle populations, while co-release describes the release of different neurotransmitters from the same vesicle population. An example of co-transmission can be seen in the peripheral nervous system. Sympathetic nerves regulate vascular tone by releasing ATP and norepinephrine onto the adjacent smooth muscle lining of blood vessels, resulting in vasoconstriction. Each neurotransmitter is released in different proportions, allowing for fine tuned control of vascular tone. A greater proportion of ATP is released in response to lower frequency stimuli, while more norepinephrine is released after higher frequency stimuli (Todorov, Mihaylova-Todorova, Bjur, & Westfall, 1999). The release of norepinephrine can be sustained over a longer period of time than that of ATP (Todorov, Mihaylova-Todorova, Craviso, Bjur, & Westfall, 1996; Westfall, Todorov, Mihaylova-Todorova, & Bjur, 1996). Both ATP release and the post-junctional response to ATP are short-lived (Todorov et al., 1999; Westfall et al., 1996), while norepinephrine-induced contractions are tonic in nature, unlike the phasic response to ATP (Sneddon & Westfall,

1984). The differences in release kinetics suggest that ATP and norepinephrine are regulated by co-transmission, although co-release has not been definitively ruled out.

The vesicular nucleotide transporter (VNUT) is thought to be responsible for loading vesicles with ATP (Sawada et al., 2008). VNUT function is dependent on a positive internal membrane potential that is generated by the vesicular ATPase (V-ATPase) therefore, the V-ATPase must be a component of purinergic vesicles (Sawada et al., 2008). Previous work in the Poburko lab attempted to identify whether ATP and norepinephrine were co-released from peripheral nerves of the rat tail artery by assessing colocalization of VNUT and the vesicular monoamine transporter (VMAT2), which loads vesicles with catecholamines such as norepinephrine (Wimalasena, 2011). Colocalization, indicated by both proteins being present on the same synaptic vesicle membrane, would suggest that ATP and norepinephrine are co-released. However, VNUT and VMAT2 were anti-colocalized in the peripheral nerves of rat tail artery (Kalkhoran et al., 2019). Vesicles containing the VMAT2 did associate with classic synaptic vesicle proteins like SV2a, synaptophysin, and synaptotagmin 1 (Kalkhoran et al., 2019). Additionally, my colleagues identified preferential association between VMAT2-containing puncta and the voltage-gated calcium channel CaV2.2, while VNUT associated with CaV2.3 (Kalkhoran et al., 2019). These results suggested that VNUT and VMAT2 resided within different vesicle populations, but the molecular components of VNUT-containing vesicles remained unclear.

My thesis research sought to characterize the molecular fingerprint of a VNUT-containing vesicle. The literature provided evidence for localization of VNUT to lysosomes, which might explain the lack of colocalization with synaptic vesicle markers seen in my colleagues' research. Immunocytochemical analyses of several vesicle and lysosome markers did not colocalize with VNUT. Additional possible subcellular localizations were investigated by assessing the VNUT peptide sequence for known targeting motifs. Due to time constraints, I focused my study on the C-terminal region of VNUT, since the C-terminal tails of VMAT2, VAChT, and VGLUT2 are required for targeting these transporters to their respective vesicle populations (Colgan, Liu, Huang, & Liu, 2007; Haiyan Li, Santos, Park, Dobry, & Voglmaier, 2017; Varoqui & Erickson, 1998).

1.1.1. ATP as a Neurotransmitter

In 1929, ATP was discovered was identified and presumed to be involved in extracellular signaling, particularly with respect to muscle contraction (Bodin & Burnstock, 2001; Verkhratsky & Krishtal, 2009). A 1959 study identified ATP as being released from sensory neurons (Holton, 1959), officially implicating ATP as a neurotransmitter. The subsequent discovery of receptors that recognized ATP and its derivatives, ADP, AMP, and adenosine, as well as other nucleotides, birthed the field of purinergic signaling (Bodin & Burnstock, 2001).

Purinergic receptors fall into two main classes, P1 and P2. P1 receptors recognize adenosine, while P2 receptors recognize ATP and ADP (Y. Moriyama, Hiasa, Sakamoto, Omote, & Nomura, 2017). The P2 receptor family further consists of metabotropic P2Y receptors and ionotropic P2X receptors. Both P2 receptor types are calcium sensitive and subsequently activate ATP release channels, like pannexin (Locovei, Scemes, Qiu, Spray, & Dahl, 2007; Pelegrin & Surprenant, 2006). Figure 1.1 summarizes the purinoceptors and their ligands, as well as their relationship with the Pannexin1 (Panx1). How the purinoceptors activate Panx1 secretion of ATP is not well understood.

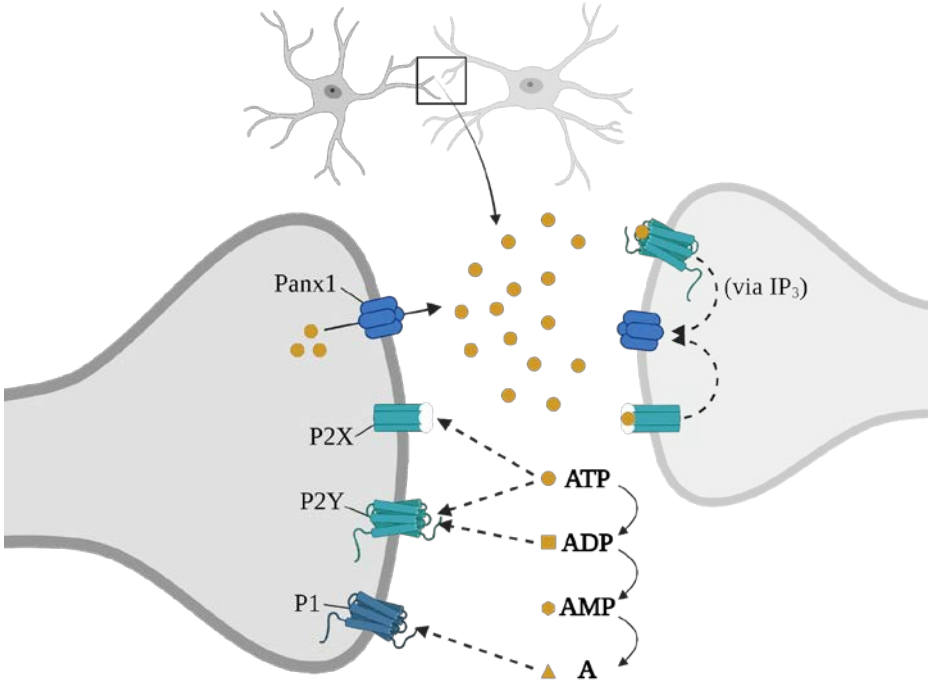

Figure 1.1 The cycle of ATP signaling via purine receptors and PanX1
The P2X subgroup of purine receptors recognize ATP, while the G-protein coupled P2Y receptors recognize ATP and ADP. Adenosine (A) is the main ligand for P1 receptors. Upon activation by

their respective ligands, the P2 receptor activation initiates calcium influx via permeable channels. These receptors also activate Panx1 pannexin channels, although the details of Panx1 activation are unknown. Dotted lines indicate activation. Solid lines indicate direction of transport. In the synaptic cleft, ATP is hydrolyzed by ectonucleotidases. Created with BioRender.com.

The idea of ATP being a neurotransmitter resulted in conflict. ATP is commonly described as cellular energy currency. Having such a critical role within the cell, a role as an extracellular messenger that was deliberately released seemed counter intuitive (Bodin & Burnstock, 2001; Verkhratsky & Krishtal, 2009). Indeed, one school of thought believed ATP could not be a neurotransmitter due to its critical intracellular presence (Burnstock, 2007; Verkhratsky & Krishtal, 2009). Evidence to support the contrary included the discovery of purinergic receptors, visualization of vesicles and measuring ATP release therefrom, and identification of non-adrenergic, non-cholinergic (NANC) transmission (Bodin & Burnstock, 2001; Burnstock, 2007; Burnstock, Cocks, Kasakov, & Wong, 1978; Verkhratsky & Krishtal, 2009). NANC transmission does not rely on acetylcholine or norepinephrine, but NANC transmitters are often released concurrently with acetylcholine or norepinephrine (Offermanns & Rosenthal, 2004)

1.1.2. ATP in Sympathetic Neurons and Vesicle Release Kinetics

Co-transmission allows cells to fine-tune post-junctional responses due to the different effects of transmitters. For example, post-junctional smooth muscle cells of the urinary bladder are more sensitive to acetylcholine after exposure to ATP, resulting in a stronger response to the acetylcholine (Burnstock, 2007). The release of acetylcholine from the pre-junctional motor nerves in the same neuromuscular junction is mediated by adenosine, a breakdown product of ATP (Verkhratsky & Krishtal, 2009). The effects of ATP can be regulated by itself as well as other transmitters. For example, the release of ATP from vascular sympathetic nerves is regulated by norepinephrine (Verkhratsky & Krishtal, 2009). The importance of regulating the relative amounts of co-released neurotransmitters is illustrated by the electrical stimulation of sympathetic nerves in the guinea pig vas deferens, resulting in altered ratios of ATP and norepinephrine released depending on the frequency of the electrical stimulus applied. At lower frequencies (8 Hz), α_2-adrenoceptors inhibit the amount of norepinephrine released with ATP, resulting in rapid yet short-lived post-junctional responses to ATP. As the stimulation frequency increases, α_2-adrenoceptor inhibition of norepinephrine release is reduced. More norepinephrine is released, resulting in pre-junctional regulation to reduce ATP release.

Post-junctional responses to norepinephrine are tonic, slow to start, yet lasts longer than that of ATP (Todorov et al., 1999). By altering which neurotransmitter is released, when it is released, and how much is released, neurons can adjust post-junctional responses as needed.

Despite the functional importance of co-transmission, the mechanism that coordinates the differential storage and release of neurotransmitters is not well understood. What is understood is that neurotransmitters are transported and stored in highly regulated intracellular vesicles. These vesicles are stored in specialized areas near the cell plasma membrane called active zones (Denker & Rizzoli, 2010). Active zones are the sites of vesicle fusion, neurotransmitter release, and re-uptake of the vesicle membrane components (Suedhof, 2012). Vesicles may fuse with the plasma membrane in three ways: full-collapse fusion, kiss-and-run, and compound exocytosis (L. G. Wu, Hamid, Shin, & Chiang, 2014). During complete fusion, the vesicle membrane fuses with the plasma membrane. Some transmembrane components mix with the plasma membrane components while others are retained in clusters for re-internalization. Some vesicles undergo a maturation process consisting of repeated fusion and retrieval from the plasma membrane, called vesicle recycling. Mature vesicles are re-loaded with transmitters by the action of vesicular transporters. Newly loaded vesicles are docked to the plasma membrane by cytoskeletal components and SNARE complexes in preparation for immediate release, forming the ready releasable pool (RRP) (Denker & Rizzoli, 2010). The vesicles of the RRP are fusion competent due to the presence of fusion chaperones such as syntaxin, SNAP-25/SNARE complexes, and Munc proteins (Suedhof, 2012). Proximity to the plasma membrane is facilitated by tethers between proteins of the vesicle and plasma membranes as well as scaffolding proteins like ELKS (Held & Kaeser, 2018). While proximity does help with physical fusion mechanics, scaffolds and tethers also help cluster vesicles around calcium channels allowing influxes of calcium to quickly bind to the calcium-depend fusion facilitator synaptotagmin-1 (Held & Kaeser, 2018; Suedhof, 2012). In comparison, the recycling vesicle pool resides further away from the site of fusion and consists of 10-20% of synaptic vesicles; these vesicles fuse and release their contents in response to moderate stimuli (Denker & Rizzoli, 2010). High-frequency stimulation induces the release of the reserve vesicle pool, a collection of vesicles that must travel the furthest to fuse with the plasma

membrane. It is unclear what specific marker, if any, designates vesicles as fated to the RRP, the recycling pool, or the reserve pool (Denker & Rizzoli, 2010).

Due to the speed of release in response to lower frequency stimuli, ATP is likely released from synaptic vesicles within the RRP. It is not clear if co-transmitters such as norepinephrine are released from a shared or separate RRP. In the guinea pig vas deferens, ATP-containing vesicles are released during low frequency stimuli (up to 8 Hz) and are depleted after 30 seconds. On the contrary, noradrenaline is released during higher frequency stimuli of greater than 8 Hz for up to 60 seconds before depletion (Westfall et al., 1996). Norepinephrine release is significantly impacted by reserpine, an inhibitor of norepinephrine vesicle loading, with 99% of initial release lost (Kirkpatrick & Burnstock, 1987). ATP release is unaffected by reserpine (Kirkpatrick & Burnstock, 1987). Similarly, blockage of norepinephrine re-uptake and inhibition of α_2-adrenoceptors with cocaine and phenoxybenzamine, respectively, did not reduce ATP release (Stjärne, 2001). These results provide further evidence for the differential loading of ATP and norepinephrine, but it is not clear if vesicles containing the latter were incapable of fusion since vesicle loading was impeded, not fusion. However, these data in combination with the loss of co-release at higher stimulation frequency (Stjärne, 2001), the preferential association of norepinephrine- and ATP-containing vesicles with different isoforms of voltage-gated calcium channels (Kalkhoran et al., 2019; Smythe, Yamboliev, & Mutafova-Yambolieva, 2008), provide promising evidence of ATP and norepinephrine being sorted into and released from separate vesicle pools.

1.1.3. Characterizing Different Vesicle Populations

Neurotransmitters are associated with different vesicle proteins and vesicle populations, accordingly. Norepinephrine and related catecholamine transmitters are commonly found in dense core vesicles (Burnstock, 2009; Haiyan Li et al., 2005). The size and density of these vesicles can be seen on an electron micrograph. Dense core vesicles can be as large as 80-200 nm or similar in size to synaptic vesicles, about 45-60 nm (Merighi, 2018; Nagwaney et al., 2009). The high electron density of dense core vesicles is caused by chromogranins, which are soluble precursors of neuropeptides and may have a role in sorting catecholamines. Chromogranin A and B are associated with catecholaminergic vesicles as established by colocalization with the vesicular monoamine transporter 2 (VMAT2) (Kloukina-Pantazidou, Chrysanthou-Piterou, Havaki,

& Issidorides, 2013; Haiyan Li et al., 2005). VMAT2 is a transporter that loads catecholamines such as dopamine, serotonin, and norepinephrine into vesicles. VMAT2, and by association norepinephrine, is also associated with common synaptic vesicle proteins like synaptotagmin 1 (Syt1), synaptophysin, and synaptic vesicle glycoprotein-2a (SV2a) (Freyberg et al., 2016; Kalkhoran et al., 2019; Haiyan Li et al., 2005). In contrast, the vesicular nucleotide transporter (VNUT), which loads ATP into cellular compartments, did not colocalize with Syt1, synaptophysin, or SV2a in sympathetic neurons of the rat tail artery (Kalkhoran et al., 2019). The lack of canonical vesicle protein association and the differences in release kinetics suggest that ATP resides in a different vesicle population from norepinephrine. Precedent for different synaptic vesicle pathways for co-released transmitters, including synthesis and recycling, is documented in midbrain and hippocampal neurons with the vesicular glutamate transporter (VGLUT) and VMAT2. VMAT2 was more dispersed across the plasma membrane than VGLUT, suggesting slower or perhaps less efficient recycling mechanics. Compared to VMAT2, VGLUT is sorted to a different vesicle population that is more readily released and undergoes faster endocytosis after an exocytotic event (Onoa, Li, Gagnon-Bartsch, Elias, & Edwards, 2010).

The vesicle population to which ATP belongs is not well-understood. ATP can be present in catecholaminergic and cholinergic vesicles (Aberer, Stitzel, Winkler, & Huber, 1979; Gualix, Pintor, & Miras-Portugal, 1999) but does not typically share vesicles with glutamate or γ-aminobutyric acid (GABA) (Pankratov, Lalo, Verkhratsky, & North, 2006). To add to the complexity, some reports claim that ATP is secreted from lysosomes in epithelial cells, glial cells, and neurons (Jung, Shin, Konishi, Lee, & Kiyama, 2013; J. Liu, Liu, & Yang, 2016; Oya et al., 2013). ATP secretion via lysosomes might explain the lack of association between VNUT and synaptic vesicle proteins. However lysosomal localization of VNUT might occur in a cell- or tissue-dependent manner. The canonical lysosome marker lysosome-associated membrane protein-1 (LAMP-1) did not colocalize with VNUT in microglia and cerebellar granule neurons (Imura et al., 2013; Menéndez-Méndez et al., 2017). VNUT knockout studies in COS1 monkey fibroblast cells and C2C12 mouse myoblast cells support a critical role of VNUT in loading ATP into lysosomes (Zhong, Cao, Sun, & Dong, 2016). Conversely, other researchers provide evidence for ATP release from non-lysosomal compartments in epithelial cells, endocrine cells, and neurons (Aberer et al., 1979; Bjelobaba, Janjic, & Stojilkovic, 2015;

Y. Moriyama et al., 2017; Obermüller et al., 2005). The identification of VNUT-containing vesicles is complex due to the variety of compartments that may release ATP and as well as the mixed, perhaps cell-dependent localization of VNUT to lysosomes.

For clarity, I will define several vesicle populations that I have investigated throughout my thesis work as well as any markers used to identify each vesicle population. Secretory vesicles of peripheral nerves are large vesicles that primarily contain peptides like vascular endothelial growth factor (VEGF). Another group of secretory compartments are lysosomes. With no clear distinction between traditional lysosomes and secretory lysosomes, the collective population of lysosomes are identified as containing LAMP-1. Synaptic vesicles are defined as small vesicles that contain synaptic vesicle associated proteins like SV2a, synaptophysin, or synaptotagmin. Within the context of peripheral nerves, two subcategories of synaptic vesicles are investigated: ATP-containing purinergic vesicles and norepinephrine-containing catecholaminergic vesicles. Localization of VNUT to synaptic vesicles, secretory vesicles, or lysosomes is not well characterized in N2a cells, with indirect evidence suggesting localization to vesicles (Gutiérrez-Martín et al., 2011; Menéndez-Méndez, Díaz-Hernández, & Miras-Portugal, 2015). Various studies have characterized vesicular ATP release in N2a cells, but lack colocalization analyses to confirm VNUT localization to purinergic vesicles (Menéndez-Méndez et al., 2015; P. Y. Wu et al., 2009). If VNUT associates with secretory vesicles, typical markers of these vesicles should colocalize with VNUT. Two markers of secretory vesicles expressed in murine Neuro-2a neuroblastoma (N2a) cells are VEGF and CGA (Meister et al., 1999; Weng et al., 2017). An important note: CGA is not specific to a single vesicle population (i.e., catecholaminergic vesicles) as peptidergic vesicles also contain CGA (D'amico, Ghinassi, Izzicupo, Manzoli, & Di Baldassarre, 2014). If VNUT localizes to lysosomes, LAMP-1 should colocalize with VNUT. To account for the transient fusion and separation of lysosomes and endosomes, the endosome-associated protein EEA1 is a common early endosome marker that distinguishes colocalization of VNUT with lysosomes from that of endosomes. VNUT and synaptophysin have been studied in mouse retina photoreceptor cells, Neuro-2a neuroblastoma cells, and cerebellar granule neurons with colocalization being defined by partial overlap of each channel colour. (Menéndez-Méndez et al., 2015, 2017; S. Moriyama & Hiasa, 2016). For example, in mouse retinal tissues VNUT is stained with a red probe while synaptophysin is stained green with the resulting overlap producing a

yellow signal. While some partial overlap was observed in retinal tissue, the scale of these images did not show vesicular or organellar colocalization of VNUT and synaptophysin. Rather, these data demonstrated the co-expression of these proteins in retinal tissue (Menéndez-Méndez et al., 2015). In N2a cells and granule neurons, immunolabeling demonstrated punctate VNUT and synaptophysin signals, albeit slightly blurry. If VNUT and synaptophysin reside within synaptic vesicles, then all VNUT-containing vesicles would colocalize with synaptophysin and vice versa. The data suggest otherwise, with few instances of overlapping puncta. The “most prominent” clusters of synaptophysin- and VNUT-containing are noted, but even these puncta do not demonstrate consistent overlap (Menéndez-Méndez et al., 2015). These data would benefit from further investigation of VNUT and synaptophysin colocalization using a blob-based analysis method (Fletcher, Scriven, Schulson, & Moore, 2010), as described later in this introduction and used in my research. VNUT colocalization with synaptic vesicle markers SV2a and synaptotagmin-1 has not been demonstrated in neurons, although the latter might be colocalized with VNUT in PC12 cells (Sawada et al., 2008). One goal of this thesis work is to provide additional and perhaps more conclusive data to determine the degree of colocalization between VNUT and markers of various vesicle populations, summarized in Table 1.1, in a neuron-like cell model.

Table 1.1 Summary of Vesicle Subpopulation Markers

	Small, synaptic vesicles (45-60 nm)		Large, secretory vesicles (80-200 nm)		
Vesicle Subtype	Purinergic	Catecholaminergic	Peptidergic	Lysosomes	Endosomes
Chromogranin(s) Present?	No	Yes	Yes	No	No
Solute Carrier(s)	VNUT	VMAT1, VMAT2	VMAT1, VMAT2	VNUT(?)	No
Vesicle Markers	Synaptotagmin(?), Synaptophysin (?)	SV2a, Synaptophysin, Synaptotagmin, Synaptobrevin (VAMP2)	BDNF, VEGF	LAMP-1, LAMP-2	EEA-1

1.2. Studying ATP Storage and Release

ATP is released in three ways; exocytosis is the release of ATP from vesicles. Channel-dependent release, such as through pannexin hemichannels, allow cells to release

cytosolic ATP. Finally, uncontrolled ATP release can occur via ruptures in the plasma membrane due to stress or damage (Bodin & Burnstock, 2001; Boudreault & Grygorczyk, 2002; Y. Moriyama et al., 2017; Murana et al., 2017; Sabirov, Dutta, & Okada, 2001). Figure 1.2 illustrates the three primary modes of ATP release. ATP release is primarily studied through measuring extracellular concentration of sequential media collections using the luciferin-luciferase bioluminescence assay. The amount of ATP released is related to the intensity of light emitted by the luciferin-luciferase reaction within a liquid sample (Marques & Esteves Da Silva, 2009). However, the assay lacks spatial and temporal resolution of release events and is unable to differentiate between vesicular and non-vesicular ATP release.

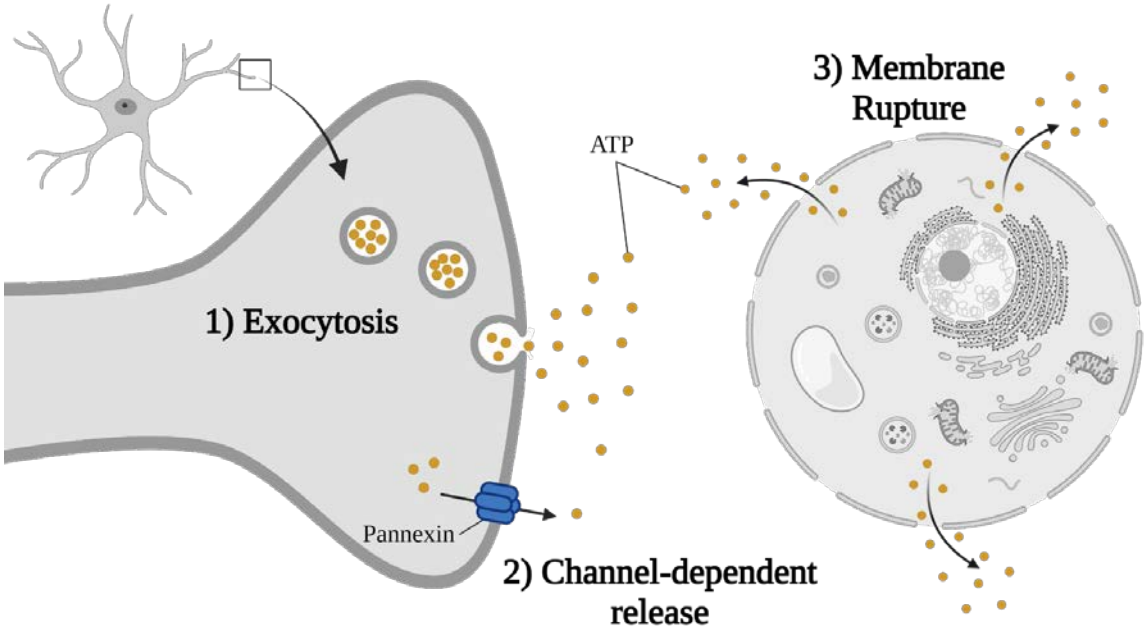

Figure 1.2 Modes of ATP release
In a healthy cell, left, ATP (orange) can be released from vesicles, or through hemichannels like pannexin (blue). Ruptures in the plasma membrane occur in cells that have sustained trauma, often resulting in cell death. The trauma can be physical or biological and result in the release of ATP in an uncontrolled manner. Created with BioRender.com.

Several fluorescent probes are used to study intracellular ATP compartmentalization. Quinacrine is a fluorescent dye that is recruited to acidic organelles including vesicles, endosomes, and lysosomes (Pierzynska-Mach, A Janowski & Dobrucki, 2014). Quinacrine staining is challenging to interpret for three reasons. First, acidic compartments swell over time when cells are exposed to quinacrine, likely due to stress from phototoxic species generation. Second, nucleic acid staining occurs with prolonged exposure during live cell imaging and readily in fixed cells (Pierzynska-Mach, A Janowski & Dobrucki, 2014). Although reported as a marker of ATP-containing vesicles (Akopova et al., 2012; Geisler et al., 2013; J. Liu et al., 2016), pH driven localization means there is little specificity for ATP-containing vesicles over vesicles containing other transmitters, like norepinephrine, or acidic compartments like lysosomes (Roy, Gagné, Fernandes, & Marceau, 2013). MANT-ATP is a fluorescent analogue of ATP. Like quinacrine, MANT-ATP has been used to confirm VNUT localization to ATP-containing compartments (Imura et al., 2013), as well as demonstrating vesicular release of ATP from dopaminergic neurons in real time (Ho et al., 2015). Both fluorescent molecules exhibit strong colocalization with VNUT in dorsal root ganglia, microglia, C2C12 myoblast cells, retinal and cortex tissues (Cao et al., 2014; Ho et al., 2015; Imura et al., 2013; Jung et al., 2013). However, MANT-ATP indiscriminately accumulates in ATP-containing compartments including vesicles and lysosomes. Quinacrine and MANT-ATP are useful tools for studying intracellular ATP, but interpretating synaptic vesicle localization of VNUT is limited due to the non-specific accumulation of these probes.

A new tool for studying real time ATP release, called the $GRAB_{ATP1.0}$ sensor, was recently developed by and generously gifted from Yulong Li (Peking University). The $GRAB_{ATP1.0}$ sensor is a GFP-conjugated, P2Y1 G-protein-coupled receptor that has been decoupled from its G-protein (Z. Wu et al., 2021). Instead of triggering a secondary messenger cascade, the $GRAB_{ATP1.0}$ sensor fluoresces upon binding to ATP. The sensor has a half maximal effective concentration of 45 nM in neurons and is a promising tool for real-time imaging of ATP release (Z. Wu et al., 2021).

Due to the localization of the sensor to the plasma membrane, the sensor does not detect intracellular ATP. An advantage of the $GRAB_{ATP1.0}$ sensor is the ability to visualize instances of ATP release in real time. See Figure 1.3 for an illustration of the workings of the $GRAB_{ATP1.0}$ sensor, including activation upon ATP binding. In the same way that the $GRAB_{ATP1.0}$ sensor is a powerful new tool for recording extracellular ATP, studying subcellular vesicle-like pools of ATP was made possible by the discovery of VNUT.

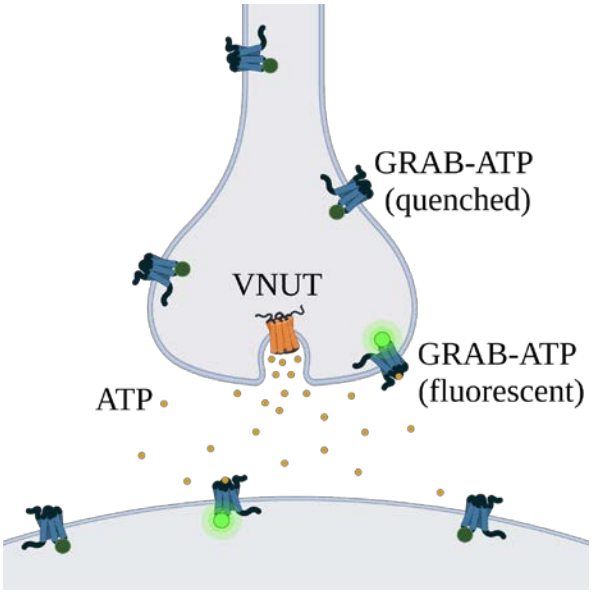

Figure 1.3 Activation of the $GRAB_{ATP1.0}$ sensor in response to ATP
The $GRAB_{ATP1.0}$ sensor is a genetically encoded probe that detects exogenous ATP. The diffusion of ATP upon release can be observed by the sequential activation of neighbouring sensors. Created with BioRender.com.

1.2.1. The Vesicular Nucleotide Transporter

The field of purinergic signaling gained powerful molecular tools to study ATP localization, such as immunostaining and expression vectors, when the Moriyama lab identified the vesicular nucleotide transporter (VNUT) as the protein that loads ATP into vesicles (Sawada et al., 2008). VNUT is encoded by the *SLC17A9* gene of the solute carrier 17 family. The SLC17 family is a group of anion transporters that includes the vesicular glutamate transporters (VGLUT1-3) and sialin (Rudnick, 2008; Sawada et al., 2008). Table 1.2 lists the gene and protein names of each SLC17A family member.

In order of efficacy, VNUT preferentially transports ATP, UTP, GTP, ITP, ADP, and AMP (Y. Moriyama et al., 2017). Like the other SLC17A transporters, VNUT function depends on the positive luminal membrane potential that is established by the H^+ electrochemical gradient generated by the vesicular ATPase (V-ATPase) (Y. Moriyama et al., 2017; Omote & Moriyama, 2013; Rudnick, 2008; Sawada et al., 2008). The V-ATPase inhibitor bafilomycin severely impairs mechanically-induced ATP release from primary cultures of rat hippocampal astrocytes and mouse cortical astrocytes (Coco et al., 2003; Xiong, Sun, Teng, Jin, & Zhou, 2018) as well as ionomycin-induced ATP release from primary cultures of rat cortical microglia (Imura et al., 2013). As a consequence of driving protons

into the vesicle lumen, the V-ATPase also establishes an inside acidic pH gradient, which is a component of neurotransmitter/proton antiport in the SLC18A family of transporters (Y. Moriyama et al., 2017; Omote & Moriyama, 2013; Rudnick, 2008; Sawada et al., 2008). Unlike the SLC18A family members, VNUT function is not dependent on pH (Sawada et al., 2008).

Table 1.2 Summary of SLC17A family protein names

Gene Name	Gene-based Protein Name	Protein Common Name	Abbreviation used in Thesis
SLC17A1	Solute Carrier Family 17, Member 1	Sodium/phosphate cotransporter 1	NPT1
SLC17A2	Solute Carrier Family 17, Member 1	Sodium/phosphate cotransporter 3	NPT3
SLC17A3	Solute Carrier Family 17, Member 1	Sodium/phosphate cotransporter 4	NPT4
SLC17A4	Solute Carrier Family 17, Member 1	Sodium/phosphate cotransporter homolog	NPT2
SLC17A5	Solute Carrier Family 17, Member 1	Silain	Sialin
SLC17A6	Solute Carrier Family 17, Member 1	Vesicular Glutamate Transporter 2	VGLUT2
SLC17A7	Solute Carrier Family 17, Member 1	Vesicular Glutamate Transporter 1	VGLUT1
SLC17A8	Solute Carrier Family 17, Member 1	Vesicular Glutamate Transporter 3	VGLUT3
SLC17A9	Solute Carrier Family 17, Member 1	Vesicular Nucleotide Transporter	VNUT

Inhibitors of VNUT include Evans blue, diisothiocyanatostilbene disulfonic acid (DIDS), and atractyloside (Geisler et al., 2013; Gualix et al., 1999; Y. Moriyama et al., 2017; Oya et al., 2013; Yin et al., 2019). While these compounds do inhibit VNUT, they are not specific to VNUT. For example, Evans blue prevents glutamate uptake by allosterically inhibiting AMPA and kainate receptors as well as the excitatory amino acid transporter and vesicular glutamate transporters. Clodronate is an anti-osteoporotic drug that is used to treat osteoporosis and neuropathic pain. In 2017, clodronate was found to inhibit pain by inhibiting VNUT through competition with the chloride binding site (Y. Moriyama & Nomura, 2017). With a half maximal inhibitory concentration of 15.6 nM and no apparent off-target inhibition of other SLC transporters, clodronate is currently the most selective inhibitor of VNUT (Kato et al., 2017; Y. Moriyama & Nomura, 2017).

VNUT has a critical role in ATP release, illustrated by several studies using VNUT deficient mice (Imura et al., 2013; Y. Moriyama et al., 2017; Y. Moriyama & Nomura, 2017). Mice that do not express *SLC17A9* experience severely impaired ATP release from neurons, neuroendocrine, and microglial cells (Kato et al., 2017). Dorsal horn neurons are involved in peripheral nerve injury pain perception, which is lost in *SLC17A9*$^{-/-}$ mice. General pain sensation, such as tail- or paw-flicks, remains intact (Masuda et al., 2016), but inflammatory responses such as edema are significantly reduced compared to wild-type mice (Kato et al., 2017). VNUT deficient mice do not release ATP from adrenal chromaffin cells in response to high K^+. This lack of ATP release causes a subsequent decrease in noradrenaline secretion because purinergic $P2Y_{12}$ and $P2X_{4\text{-}7}$ receptors regulate vesicular catecholamine release (Sakamoto et al., 2014). In the islets of Langerhans (pancreatic β cells) of *SLC17A9*$^{-/-}$ mice, glucose-stimulated ATP release is lost while glucose-stimulated insulin secretion is 1.5-fold greater than in wild-type mice (Sakamoto et al., 2014). VNUT deficient mice have enhanced glucose tolerance. Blood glucose readings are approximately 100 mg/dL less than those of wild-type mice between 30 and 120 minutes after oral administration of glucose, indicating a role in ATP release in blood glucose homeostasis (Sakamoto et al., 2014). Hippocampal neurons isolated from *SLC17A9*$^{-/-}$ mice do not release ATP in response to high K^+ (Miras-Portugal et al., 2019). Similarly, hippocampal astrocytes are less responsive to the anti-depressant fluoxetine, which stimulates ATP release causing reduced depression-like behaviour in mice. Conversely, over-expression of VNUT improved the therapeutic effects of fluoxetine (Kinoshita et al., 2018; Miras-Portugal et al., 2019). These results point to a regulatory role of VNUT-mediated ATP release in depression. Although not explicitly related to VNUT deficient mice, a study on glaucomatous mice identified a positive correlation between *SLC17A9* expression and glaucoma progression. As *VNUT* expression and ATP release increased, the glaucoma became more severe (Miras-Portugal et al., 2019; Pérez de Lara et al., 2015). At the organism level, *SLC17A9*$^{-/-}$ mice appear to be healthy. This puzzling observation suggests that VNUT-dependent ATP release is not life-sustaining or else the lack of *SLC17A9* expression may stimulate compensational upregulation of ATP release channels, such as pannexins, to rescue ATP release (Mihara, Uchida, Koizumi, & Moriyama, 2018; Y. Moriyama et al., 2017).

VNUT-mediated ATP release has also been demonstrated using cultured cell lines. RNA interference studies support a critical role for VNUT in ATP release with ~50% reduction in N2a cells (Menéndez-Méndez et al., 2015) and PC12 cells (Sawada et al., 2008) and nearly abolished release in hippocampal primary culture (Larsson et al., 2012). The role of VNUT in ATP release in microglia and PC12 cells appears to be dependent on plasmalemmal depolarization and subsequent activation of voltage-gated calcium channels, inferring that VNUT-mediated ATP release is vesicular (Imura et al., 2013; Sawada et al., 2008). ATP release in response to elevated intracellular Ca^{2+} may suggest a vesicular mechanism of release. Knocking down VNUT in microglia reduced ATP release in response to ionomycin, a Ca^{2+} ionophore, by approximately 68% (Imura et al., 2013). In microglia, Ca^{2+}-dependent VNUT-mediated ATP release is regulated by the SNARE complex. Botulinum A is a neurotoxin that inhibits SNAP-25, a key component of the core SNARE complex (Smythe et al., 2008). In the presence of botulinum A, ionomycin-triggered ATP release was reduced by approximately 32% (Imura et al., 2013). The Ca^{2+} chelator BAPTA-AM also impaired vesicular ATP release, as did the vesicle transport inhibitor brefeldin A (Imura et al., 2013). These results all implicate VNUT in vesicular ATP release and presumably its localization to vesicles.

In addition to strong evidence for vesicular ATP release, there is also evidence for VNUT localization to lysosomes. Lysosomes isolated from COS1 monkey kidney fibroblast cells took up less ATP when exposed to VNUT inhibitors DIDS and Evans Blue. As previously discussed, these inhibitors are not specific to VNUT, thus interpreting these results is limited. However, inhibitors of connexin and pannexin hemichannels carbenoxolone and niflumic acid did not reduce ATP uptake into the lysosome-containing fractions of kidney fibroblast-like cells (Zhong et al., 2016). VNUT shRNA expression in C2C12 murine myoblast cells significantly impacted ATP uptake into lysosome lysates, inducing a 10-fold decrease in ATP uptake compared to the scrambled shRNA control (Zhong et al., 2016). Further evidence in support of VNUT localization to lysosomes include studies using optic nerve head astrocytes and retinal epithelial cells (Beckel et al., 2018), cochlear marginal cells (J. Liu et al., 2016), cerebellar granule neurons (Menéndez-Méndez et al., 2017), Schwann cells (Shin, Lee, & Jung, 2012), and human epithelial kidney cells (Cao et al., 2014). These studies highlight the complexity of VNUT localization studies as well as assessing lysosomal and vesicular ATP release.

1.2.2. VNUT: A Comparison in Structure and Targeting

The secondary structure of VNUT is based on homology to other SLC17A family members (Sawada et al., 2008). In addition to providing a basis for predicting the structure of VNUT, the vesicular glutamate transporters and sialin might provide a clue to the subcellular localization of VNUT as these transporters localize to synaptic vesicles in neurons. The peptide sequences of VGLUT1-3 contain a synaptic vesicle targeting dileucine motif that is preceded by an acidic residue: [D/E]XXXLL (Haiyan Li et al., 2017), where X can be any amino acid. The dileucine motif is also present in synaptic vesicle proteins synaptobrevin and synaptotagmin-1 (Colgan et al., 2007; Prado & Prado, 2002). SLC18A family members VMAT1-2 and the vesicular acetylcholine transporter (VAChT) also have dileucine motifs of *EEKMAIL* and *SERDVLL*, respectively, which are thought to participate in internalization and vesicle targeting (Colgan et al., 2007; Prado & Prado, 2002; Varoqui & Erickson, 1998). The dileucine motif is often found on the cytosolic C-terminus of synaptic vesicle associated proteins. This motif recruits adaptor proteins, which subsequently recruit clathrin to the vesicle.

In addition to the three-wild card dileucine-like motif, a two-wild card [D/E]XXLL motif and a tyrosine-based YXXθ motif facilitate internalization of clathrin-dependent cargo at the plasma membrane through recognition by adaptor protein-2 (AP-2) (Pandey, 2009; Prado & Prado, 2002). Additionally, the NPXY internalization motif is typically found on the C-terminal domain of cell surface proteins like the low density lipoprotein receptor (Bonifacino & Traub, 2003) and is recognized by adaptor proteins and clathrin (Bonifacino & Traub, 2003; Pandey, 2009). Adaptor protein-clathrin interaction is integral to vesicle protein sorting and vesicle trafficking (Schmid, 1997). In contrast to the VGLUTs, VMATs, and VAChT, the presence of dileucine-like motifs and other known targeting motifs, which will be discussed in the next section, have not been identified in VNUT.

1.2.3. Vesicle Sorting and Membrane Targeting

Identification of targeting sequences is achieved via mutational studies where segments of a protein are removed or replaced with inert residues and the resultant functional changes are observed. A general motif can be deduced in some instances, such as the nuclear localization sequence (NLS) that allows targeted proteins to enter the nucleus.

However, sequence variation between species and/or proteins result in generalized motifs. General rules are established, such as the peroxisomal targeting sequence (PTS) containing clusters of basic residues (Gould, Keller, & Subramani, 1987), or the numerous functional variants of the ER-targeting KDEL-based motif (Raykhel et al., 2007). General rules can also be shared by different motifs. For example, basic residues also occur in NTSs (Kalderon, Roberts, Richardson, & Smith, 1984; Lange et al., 2007). For this reason, trafficking studies are required to confirm the dependence of protein localization on a particular motif.

Protein sorting to lysosomes appears to be driven by the tyrosine motif YXXθ, where θ can be any hydrophobic amino acid (Bonifacino & Traub, 2003). LAMP-1 is a canonical marker of lysosomes and has an 11-amino acid C-terminal tail containing the YXXθ motif. A CD44 and LAMP-1 C-terminus fusion protein resulted in targeting of the cell surface protein to lysosomes. This experiment identified the C-terminus of LAMP-1 as being necessary for lysosomal targeting (Guarnieri, Arterburn, Penno, Cha, & August, 1993). However, lysosomal localization appears to be driven by a modified variant of this motif. Isolated and purified LAMP-1 from mice livers lacked two C-terminal residues predicted from the cDNA sequence. Instead of the predicted octameric sequence SHAGYQTI, the isolated peptide contained six residues: SHAGYQ (Guarnieri et al., 1993). Proteolytic modification of the YXXθ motif might explain the differential targeting of LAMP-1 and VAChT. In VAChT, the intact YXXθ motif is necessary and sufficient for targeting to synaptic vesicles and is also required for internalization (Colgan et al., 2007; Varoqui & Erickson, 1998). It is unclear which targeting motifs are present within VNUT or if those motifs are modified, but motif modifications or splice variants might explain the differential trafficking of VNUT to different membranes.

For completeness, since cells do not only contain vesicular or lysosomal membranes to which proteins can be sorted, I will describe some additional targeting sequences. Di-lysine endoplasmic reticulum (ER) and Golgi retention motifs, such as KKXX or [K/H]DEL, are typically found on the C-terminal tail of soluble resident proteins (Banfield, 2011; Teasdale, Jackson, & Johnson, 1996). The lysine residues of the former motif cannot be substituted for other amino acids. Replacement of either lysine residues with similarly basic arginine or histidine residues does not rescue the motif (Teasdale et al., 1996). The critical role of lysine residues in targeted sorting of Golgi proteins is well characterized in yeast, where Golgi proteins are missorted to lysosome-like structures

(Banfield, 2011). While the ER and Golgi work closely to synthesize proteins for secretion, they are functionally different with different molecular components. The [K/H]DEL motif allows escaped ER residents to be retrieved from the Golgi network via the action of the KDEL receptor. Relative to the ER, the acidic pH of the Golgi (pH ~6.5) creates ideal binding conditions for the KDEL receptor. Retrograde transport of the cargo to the ER exposes the receptor to a less acidic pH~7, allowing the receptor to release its cargo. Other explanations for differences in targeting between the Golgi and ER include transmembrane domain structure for Golgi targeting and differences in peripheral binding proteins (Banfield, 2011; Teasdale et al., 1996). Further, [F/L][L/I/V]XX[R/K] is a Golgi-specific targeting sequence that is recognized by peripheral Golgi protein GOLPH3 (Banfield, 2011). In yeast, changes to this sequence prevents recognition by peripheral Golgi proteins, resulting in proteins being sorted to lysosome-like structures and degraded (Banfield, 2011). It is worth noting that mammalian glycosyltransferases lack the [F/L][L/I/V]XX[R/K] motif and instead require phosphatidylinositol 4 phosphate (PI_4P)-binding of GOLPH3 for retention to the Golgi (Banfield, 2011).

A nuclear localization sequence (NLS) is a motif that allows nuclear import of proteins containing these sequences by NLS receptors. NLSs can be monopartite or bipartite, indicating the number of sequence segments within the entirety, and are typically clusters of basic amino acids. An example of a monopartite sequence is PKKKRKV of the SV40 large T antigen. An example of a bipartite sequence is KRPAATKKAGQAKKKK of nucleoplasmin, wherein two sequence segments are underlined (Lange et al., 2007).

A mitochondrial targeting sequence (MTS) allows protein transport to mitochondria as well as navigation through the mitochondrial import pathway. For example, *COX4* encodes a subunit of cytochrome c oxidase, which is involved in the electron transport chain. This mitochondrial protein undergoes nuclear transcription. To enter the mitochondria, mitochondrial preprotein receptors called Translocases of the Outer Mitochondrial membrane (TOM) recognize N-terminal amphipathic helices (M. Li et al., 2010). The COX4 subunit requires the N-terminal sequence MLSLRQSIRFFKPATRTLCSSRYLLA for mitochondrial targeting and TOM-mediated import (“Intracellular transport: 4.2 Peptide signal sequences,” 2020).

Like NTSs and MTSs, peroxisome targeting sequences (PTSs) do not have characterized motifs. Instead, specific sequences are known. For example, the LIKAKKGGKSKL sequence at the carboxyl terminus of firefly luciferase is perhaps the best-known PTS (Gould et al., 1987). Generally, peroxisomal membrane proteins have a PTS with a transmembrane segment that is preceded by a cluster of basic amino acid residues (Van Ael & Fransen, 2006). Nuclear, mitochondrial, and peroxisomal sequences are not identifiable by distinct unique motifs, making the study of these sequences difficult.

A comparative study of lysosomal, peroxisomal, mitochondrial, nuclear, and vesicular signaling motifs within VNUT and related transporters remains to be reported. While the secondary structure of VNUT was predicted using homology comparisons within the SLC17A family (Sawada et al., 2008), these comparisons did not include targeting motifs. The evolutionary conservation of the VNUT peptide sequence was briefly explored across ten species (Sawada et al., 2008). However, this initial comparison would benefit from a comprehensive expansion that includes multiple representatives of each Class of Kingdom Animalia. Combined with a targeting motif analysis of the C-termini, this data could provide insight into the evolution-driven changes in VNUT and perhaps changes in function because of novel mutations. These aspects of the VNUT peptide sequence are explored in Chapter 4.

1.3. Analyzing Colocalization

The use of fluorescence microscopy to label and observe the subcellular localization of two or more proteins of interest in relation to each other is a common method of ascribing the degree of colocalization between said proteins. Although a useful tool for observing organellar localization patterns of chosen probes, fluorescence microscopy cannot determine functional relationships or interactions between proteins (Dunn, Kamocka, & McDonald, 2011). Perhaps even less well defined is the threshold of colocalization at which one can claim that two probes are sufficiently overlapping to be considered residents of the same cellular compartment and thus colocalized.

Colocalization can describe two main relationships between probes: co-occurrence and correlation (Dunn et al., 2011). Co-occurrence is the spatial overlap of the probes while correlation refers to the relative amount of signal. In the case of VNUT, there might be

one to two molecules per vesicle, which contains considerably more ATP. In this example, VNUT and ATP co-occur. The absolute amount of VNUT and ATP do not affect colocalization analysis because these molecules present a high degree of covariance. Most ATP blobs should contain a VNUT blob, and the relative fluorescent intensities of these probes should be positively correlated. A common visual evaluation of colocalization consists of two-channel images presented side-by-side with a final merged image. Side-by-side and merged images can create intuitive, easy-to-follow figures to illustrate colocalization (or lack thereof) but they do not sufficiently quantify colocalization. Visual evaluation is prone to error as differences in signal intensity can affect the interpretation of the merged image. Quantification of colocalization should accompany merged channel images to allow more accurate and less biased interpretation of data (Dunn et al., 2011). An example of a quantifiable analysis is a scatterplot, which illustrates the co-variance of the signal intensity of each probe using the Pearson's Correlation Coefficient. The theory of the Pearson Correlation Coefficient is straightforward and intuitive, but the execution requires careful consideration of the many limitations. The coefficient describes the co-variance of two probes by defining the x and y axes of a scatterplot as the signal intensities of each probe. In the case of colocalization, the resulting dots exhibit a positive correlation along a linear regression (Bolte & Cordelières, 2006). If the ratio between the probe intensities co-vary equally, the coefficient approaches one. Otherwise, the coefficient approaches negative one in instances of negative correlations of co-variance or minimal colocalization, and zero if no correlations can be made (Bolte & Cordelières, 2006). The Pearson Correlation Coefficient is limited by its susceptibility to over-represent the covariance between probes in whole fields of view or when regions of interest (ROIs) are not accurate (Dunn et al., 2011). Further, intra- and extracellular background pixels (noise), bleed through of one probe into the emission spectra of the other probe, or different probe ratios within the sample will falsely contribute to the representation of pixels for which the intensities are low, skewing the data towards larger values of variance (Bolte & Cordelières, 2006; Dunn et al., 2011).

Other methods of quantifying colocalization include the Manders Overlap Coefficient and fractional overlap. The Manders Overlap Coefficient is related to the Pearson's Correlation Coefficient except it measures pixel intensity while largely ignoring differences in probe intensity (Dunn et al., 2011). The ImageJ colocalization tool JaCoP

uses the Manders Overlap Coefficient (Dunn et al., 2011). A better measure of spatial overlap is the fractional overlap, which measures the amount of overlap between probes after the minimum fluorescent values (i.e., background grey levels) have been subtracted from each signal (Dunn et al., 2011).

Tools for assessing colocalization are available via the ImageJ plugins Coloc 2 and JaCoP (“Colocalization Analysis,” 2020). Coloc 2 performs pixel intensity correlation analyses based on several statistical principles of colocalization (including those discussed above) while JaCoP is a compiled set of tools like common colocalization indicators and visualizations. Additional colocalization resources, which are used in my research, are ImageJ macros that identify puncta using user-defined parameters and then calculate relative distances between puncta, named the Recursive ImageJ Particle Analyzer (RIPA) and Multi-Image Nearest Neighbour Colocalization (MINER), respectively (Kalkhoran et al., 2019; Poburko, n.d.). The RIPA macro allows user input of parameters that best describe the probe signal such as circularity, solidity, upper and lower threshold limits, and minimum and maximum area, to draw ROIs. RIPA helps reduce the influence of intensity differences between signal and background, resulting in unbiased ROI selection.

MINER is a nearest neighbour analysis tool that recognizes the ROIs generated by RIPA and records multiple characteristics of each punctum based on user input. Users can tell MINER which channel contains the reference puncta and how many other channels are being analyzed relative to the reference, denoted as nearest neighbour (NN) channels. The intensity of each ROI is fitted to a Gaussian curve along the major and minor axis and the resultant full-width half-max value is recorded. The distance of each NN puncta is measured relative to the perimeter and/or center of the reference channel puncta, as per user preference (Kalkhoran et al., 2019). All output files can then be imported to statistical analysis software such as JMP. Together, MINER and RIPA allow a semi-automatic, high-throughput workflow.

1.4. Mouse Neuroblastoma-2a Cells

The neuroblastoma Neuro-2a (N2a) cell line is derived from the neural crest and can be differentiated into neuron-like cells (Tremblay et al., 2010) that are easy to maintain compared to primary neuronal cultures. This cell line is capable of transfection and

grows rapidly in culture (Shastry, Basu, & Rajadhyaksha, 2001). N2a cells have been used extensively to study neuronal differentiation, cytoskeletal stability, axonal growth, neurodegenerative disorders, and signaling pathways (Gutiérrez-Martín et al., 2011; S. Kim et al., 2013; Menéndez-Méndez et al., 2015; Namsi et al., 2018; Swayne, Sorbara, & Bennett, 2010; Tremblay et al., 2010; Wicki-Stordeur, Dzugalo, Swansburg, Suits, & Swayne, 2012; P. Y. Wu et al., 2009; Xu et al., 2018).

In the context of studying purinergic signaling, N2a cells are able to release ATP via pannexin channels and vesicular-like mechanisms alike (Gutiérrez-Martín et al., 2011; Menéndez-Méndez et al., 2015; Swayne et al., 2010; Xu et al., 2018). Although not selective for ATP, Pannexin1 (Panx1) pores are the main mediator for channel-dependent ATP release (Dahl, 2015) and are expressed in N2a cells (Wicki-Stordeur et al., 2012). The channel undergoes conformational changes to allow ATP release in response to mechanistic changes to the plasma membrane, hypoxic conditions, high extracellular K^+, and purinergic receptor activation (Dahl, 2015). Activated metabotropic P2Y and ionotropic P2X receptors mediate cytosolic calcium levels (Dahl, 2015; Menéndez-Méndez et al., 2015). The resultant increase in intracellular calcium activates pannexin channels, although the mechanism of calcium activated Panx1 activation is not well understood. N2a cells express $P2X_1$, $P2X_3$, $P2X_4$, and $P2X_7$, but only the $P2X_7$ receptor is functional (Gómez-Villafuertes et al., 2009). Co-immunoprecipitation of $P2X_7$ and Panx1 in HEK cells highlights the close physical receptor-channel relationship (Pelegrin & Surprenant, 2006), while electrophysiological recordings and fluorescence microscopy in 1321N1 human astrocytoma cells provide evidence of a close functional relationship (Locovei et al., 2007). In addition to Panx1 mediated release, N2a cells are thought to release ATP from vesicles (Gutiérrez-Martín et al., 2011; Menéndez-Méndez et al., 2015).

Vesicular fusion and neurotransmitter release requires SNARE complexes, which consist of several vesicle membrane and plasma membrane associated proteins. The alpha helical domains of these proteins twist into each other, pulling the vesicle membrane into close proximity to the plasma membrane (Yoon & Munson, 2018). Additional regulatory factors like the calcium sensor synaptotagmin and cytoskeleton associated tethers like ELKS mediate the proximity of the two membranes such that fusion occurs in response to an influx of calcium (Held & Kaeser, 2018; Yoon & Munson, 2018). The SNARE complex inhibitor N-ethylmaleimide (NEM) drastically reduced

ionomycin-induced ATP release (Gutiérrez-Martín et al., 2011), providing evidence that N2a cells release ATP using vesicular mechanisms. Since VNUT is thought to load vesicles with ATP, knocking down VNUT should inhibit vesicular ATP release by preventing vesicle filling. Compared to cells overexpressing VNUT and a scrambled shRNA construct, N2a cells that were co-transfected with VNUT shRNA and the VNUT expression construct exhibited approximately 50% decrease in luminescence using the luciferin-luciferase assay (Menéndez-Méndez et al., 2015). These data support a VNUT-mediated vesicular release of ATP from N2a cells. However, Panx1-mediated ATP release accounts for approximately 40% of KCl-induced ATP release (Wicki-Stordeur et al., 2012). Like synaptic release, Panx1 channels are calcium-activated. Inhibition of pannexin channels should result in only vesicular release while inhibition of VNUT and/or SNARE complexes should result in channel-dependent release. If VNUT is localized to synaptic vesicles, the application of the inhibitor clodronate should result in a similar reduction of ATP release as NEM inhibition of SNARE complexes. Finally, inhibition of basal release from Panx1 with probenecid and vesicular release using NEM and/or clodronate should abolish most ATP release in response to calcium ionophores such as ionomycin and A23187.

While endogenous VNUT expression is low in N2a cells (Miras-Portugal et al., 2019), overexpression can be induced by transfecting the cells with exogenous expression constructs. VNUT overexpression changes the morphology of the cells, resulting in stunted neurite growth. Contrarily, neuritogenesis is increased when VNUT expression is knocked down (Menéndez-Méndez et al., 2015). The effect of overexpressed VNUT is presumably due to the increased ATP release (Menéndez-Méndez et al., 2015), subsequently increasing the activation of P2X7 receptors, which in turn inhibit neurite formation (Gómez-Villafuertes et al., 2009). These results demonstrate the functionality of both endogenous and overexpressed VNUT in N2a cells.

Finally, previous work to develop fluorescently labeled, pH-sensitive VNUT and VMAT2 reporters for studying ATP and catecholamine corelease was facilitated by the relatively quick culture time and robust post-transfection survival of the N2a cells (B. Kim, 2019). These characteristics, in addition to the expression of purinergic signaling components, combined with previous working knowledge of these cells point to the N2a cell line being an advantageous model for this research.

1.5. Thesis Hypotheses

The overarching hypothesis of this research was that VNUT localization to a molecularly unique population of purinergic vesicles is driven by synaptic vesicle targeting motifs. This hypothesis was elaborated through two sub-hypotheses that are tested in their respective Aims. Aim 1 hypothesized that VNUT is localized to a population of purinergic synaptic vesicles that is distinct from catecholaminergic synaptic vesicles. This hypothesis was tested using fluorescent microscopy-based colocalization analyses to identify the molecular fingerprint of VNUT-containing vesicles, discussed in Chapter 3. Aim 2 hypothesized that a signaling motif that is responsible for targeting VNUT to synaptic vesicles resides in the C-terminal domain. Bioinformatic analyses of VNUT and other solute carriers were performed to answer this question and are described in Chapter 4. Initially, a third aim was developed to test the hypothesis that VNUT-mediated, Ca^{2+}-dependent ATP release from N2a cells is vesicular. Some experimental troubleshooting was completed and is described in Appendix A, but this hypothesis could not be tested due to COVID-19-related complications.

Chapter 2.

General Methods

2.1. Cell Culture

2.1.1. N2a Cell Maintenance and Differentiation

Neuro-2A (N2a) neuroblastoma cells (American Type Culture Collection CCL-131) are cancer cells that can be differentiated into postganglionic-like phenotypes resembling dopaminergic neurons. The N2a cells were maintained in growth media (GM) consisting of Dulbecco's Modified Eagle Medium (DMEM) with high glucose and sodium pyruvate (4.5 g/L D-glucose, L-glutamine, 110 mg/L sodium pyruvate, ThermoFisher Scientific, cat # 10569), supplemented with 10% fetal bovine serum (FBS, Seradigm LIFE SCIENCE, cat# 97068-085) and 1X antibiotic-antimycotic (ThermoFisher Scientific, cat# 15240-062), in cell culture treated 75 cm^2 flasks (ThermoFisher Scientific, cat# FB012937). Cells grown in GM were typically round with few neurite-like extensions. The spherical cell bodies of in Figure 2.1, image A and inset, illustrate the proliferative phenotype observed when the cells are grown in growth media. Differentiation was induced via serum starvation using a retinoic acid differentiation media (DM). DM was prepared using the same DMEM supplemented with 0.1% FBS and 5 µM retinoic acid (Millipore-Sigma, cat# R2625). The differentiated cells had smaller cell bodies and elongated neurites with occasional varicosity-like swellings (Fig 2.1B). Unless otherwise stated, all culture wear is tissue culture treated. Cells were trypsinized using TrypLE (ThermoFisher Scientific, cat# 12604013) incubated at 37°C for 3 minutes. When not in use during experiments or imaging, live cells were stored in a humidified cell culture incubator at 37°C with 5% CO_2 and 95% air.

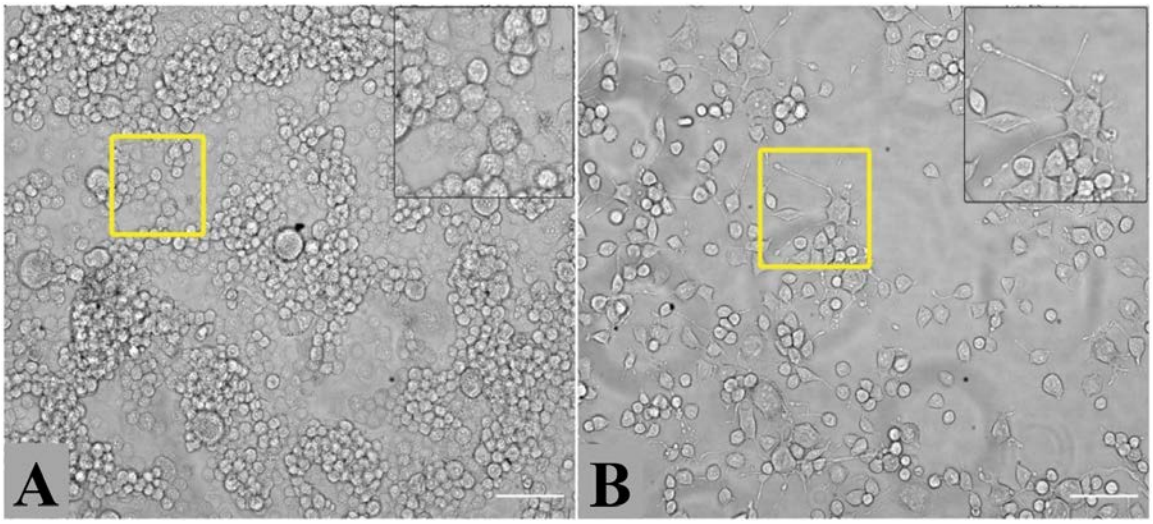

Figure 2.1 Proliferative and differentiated phenotypes N2a cells
Phase contrast images were taken at 20X magnification after a three-day incubation in GM (A) or DM (B). Yellow-bounded regions are enlarged in the insets. Scale bar = 100 µm.

N2a cells were seeded onto autoclaved #1 12 mm glass coverslips (ThermoFisher Scientific, cat# 12-545-80). Prior to cell culture, coverslips were aseptically transferred into a 24-well plate (VWR, cat# 10861-558). Approximately 100 µL of 10 µg/mL laminin in PBS (Corning via VWR, cat # 354232) was applied to the coverslips and allowed to cure at room temperature within the biosafety cabinet during cell harvesting and maintenance, about 20 minutes. The excess laminin was aspirated, GM was added to the wells and the cells were seeded down at 10-20 K cells per well. Note: Autoclaved coverslips were stored at room temperature in a sterile container.

2.1.2. Transfection

One day after seeding, cells were transfected with fluorescently labeled expression constructs at a 1:2 ratio of DNA to jetPRIME reagent using the jetPRIME DNA transfection kit and protocol from Polyplus (cat# 114-07). For example, 0.5 µg of DNA and 1 µL jetPRIME reagent was used to transfect one well of a 24-well plate. After application of the transfection mixture, cells were incubated at 37°C for four hours, followed by careful aspiration of the transfection media and replacement with fresh warmed GM. Cells recovered from transfection for one day prior to subsequent steps such as differentiation. See Table 2.1 for a list of expression constructs used. The LAMP-1-GFP and CGA-GFP constructs were gifted from SFU researcher Michael

Silverman. The $GRAB_{ATP1.0}$ and VAMP2-mCherry constructs were gifted from Yulong Li of Peking University, China.

Table 2.1 Expression constructs used

Construct Name	Probe	Source	Cat #
$GRAB_{ATP1.0}$	GFP (green)	Li Lab, Peking University	Patent Pending
LAMP-1-GFP	GFP (green)	Silverman Lab, SFU	Plasmid #16290
LAMP-1-RFP	RFP (red)	AddGene.org	Plasmid #1817
CGA-GFP	GFP (green)	Silverman Lab, SFU	n/a
VAMP2-mCherry	mCherry (red)	Li Lab, Peking University	n/a

2.2. Immunocytochemistry

2.2.1. Immunostaining Workflow

After three days of retinoic acid-induced differentiation, the cells were fixed using 4% paraformaldehyde (PFA) in PBS (Electron Microscopy Sciences, cat# 15710) for 15 minutes, then washed three times with PBS for 2 minutes each. All incubation times occurred in the dark (i.e., a drawer) at room temperature unless otherwise stated. Cell were permeabilized with 0.1% Triton-X 100 (Millipore-Sigma, T8787) in PBS for 15 minutes, followed by three PBS washes and a one-hour incubation in blocking solution (4% normal goat serum (NGS) (Millipore-Sigma, cat# NS02L) in PBS). Primary antibodies were diluted in the blocking solution, applied the diluted antibodies to the cells, and incubated overnight at 4°C. The next day, a 20-minute wash with 1 µg/mL Hoechst-33342 (Invitrogen Molecular Probes, cat# H3570) was followed by two PBS washes of 5 minutes each. Secondary antibodies were diluted in blocking solution, applied to the cells, and allowed to incubate for one hour. After three five-minute PBS washes, cells were post-fixed with 4% PFA for 15 minutes then washed three times with PBS for two minutes per wash. Coverslips were mounted onto glass slides using ProLong Glass Antifade Mountant (ThermoFisher Scientific, cat# P36984), cured overnight, and stored until imaging. Unmounted coverslips were stored in PBS at 4°C until use. Table 2.2 summarizes all antibodies used. Figure 2.2 illustrates all three experimental workflows, ICC-only (Fig 2.2A), transfection-only (Fig 2.2B), and hybrid ICC and transfection (Fig 2.2C).

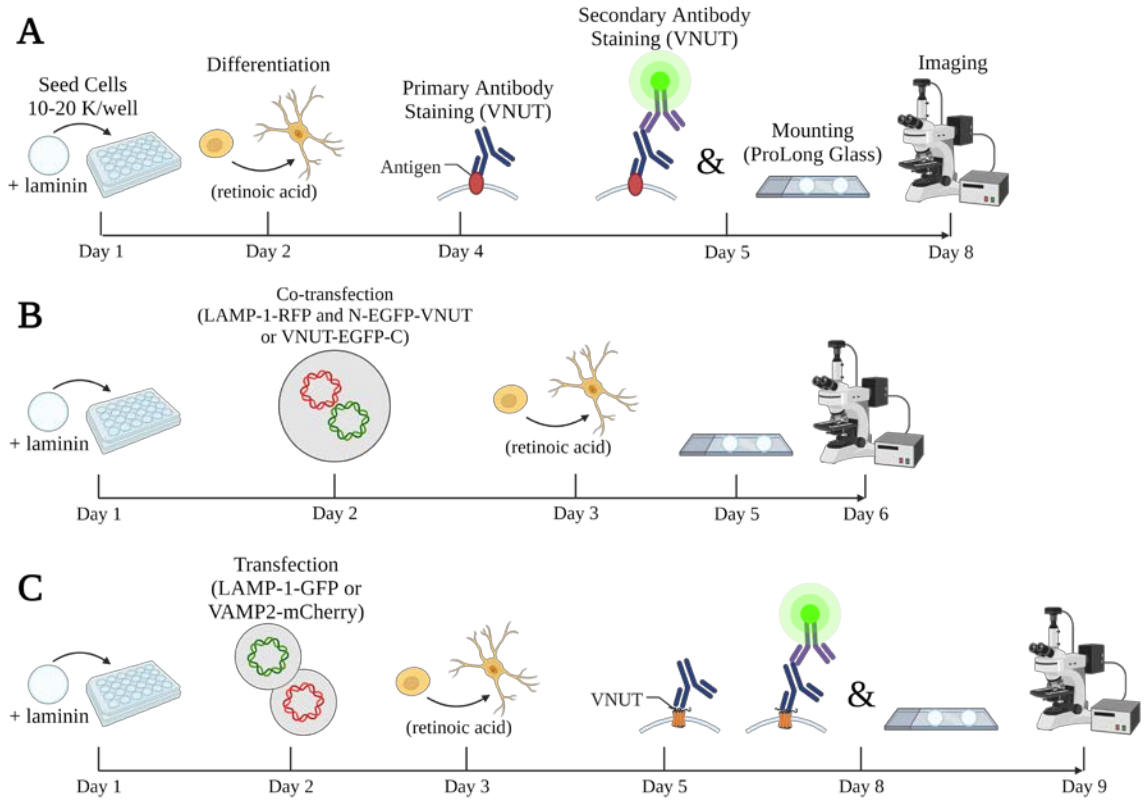

Figure 2.2 Workflow for immunocytochemistry-based, transfection-based, and hybrid experiments

A: Immunocytochemical preparation of cells for colocalization analysis. Although only one antigen is show in the figure, VNUT and one or two other antigens were stained at the same time. B: Co-transfection experiments were used to corroborate immunocytochemical findings. In these experiments, LAMP-1-RFP was co-transfected with an N-terminal EGFP tagged VNUT or a C-terminal EGFP tagged VNUT. C: Hybrid experiments were used to assess VNUT colocalization with VAMP2-mCherry or LAMP-1-GFP. This figure shows a secondary antibody with a green fluorophore, which was been used with VAMP2-mCherry. Not shown is a red fluorophore-conjugated secondary antibody that was used in conjunction with LAMP-1-GFP. Created with BioRender.com.

Table 2.2 Antibodies used

Poburko Lab ID	Target	Species	Isotype(s)	Source, Cat #	Dilution
CGA	Chromogranin A	Mouse	IgG1	Silverman Lab, Invitrogen (MA5-13096)	100X
LAMP-1	LAMP-1	Mouse	IgG2a	Silverman Lab, Millipore Sigma (AMAB91170)	100X
Synapsin	Synapsin	Mouse	IgG1	Silverman Lab	200X
Syp	Synaptophysin	Mouse	IgG1	Abcam (AB8049)	200X
Syt 1	Synaptotagmin 1	Mouse	IgG2a	Abcam (AB13259)	200X
Syt 2	Synaptotagmin 2	Mouse	IgG1	Santa Cruz (SC-136089)	200X
Syt 5	Synaptotagmin 5/9	Mouse	IgG2a	Santa Cruz (SC-398837)	200X
Syt 7 Atto	Synaptotagmin 7	Mouse	IgG2b	StressMarq Biosciences (SMC-424)	200X
SV2a	SV2a	Mouse	IgG1	Abcam (AB49572)	200X
ELKS	ELKS	Mouse	IgG2a	Millipore Sigma (E4531)	200X
VMAT2 (D-4)	VMAT2	Mouse	IgG1	Santa Cruz Biotech (SC-3902285)	100X
SLC17A9 (T-12), lot G1812	VNUT	Rabbit	Polyclonal	Santa Cruz Biotech (SC-86313)	200X
SLC17A9 (T-12), lot J1215	VNUT	Rabbit	Polyclonal	Santa Cruz Biotech (SC-86313)	200X
SCL17A9, ANT-085	VNUT	Rabbit	Polyclonal	Alomone Labs (ANT-085)	2000X
gArb555	Rabbit IgG	Goat	Polyclonal	Invitrogen (A21429)	1000X
647 IgG2a	Mouse IgG2a	Goat	IgG2a	Invitrogen (A21241)	1000X
647 IgG1	Mouse IgG1	Goat	IgG1	Invitrogen (A21240)	500X
AF647 GaR	Rabbit IgG	Goat	Polyclonal	Invitrogen (A21244)	1000X
gArb 488	Rabbit IgG	Goat	Polyclonal	Invitrogen (A11034)	1000X
555 IgG2a	Mouse IgG2a	Goat	IgG2a	Invitrogen (A21137)	500X
gAm546	Mouse IgG	Goat	IgG	Invitrogen (A11030)	1000X

2.3. Fixed Cell Imaging

Fluorescent microscopy was done using a CFI Plan Apo Lambda 100X 1.45 NA objective on a Nikon Ti-E scope and attached Zyla 5.5 CMOS camera as previously described (Kalkhoran et al., 2019). Images were acquired at z-steps of 200 nm, about 11 steps per image, to capture the depth of the cell body, neurites, and varicosities. All channels of a multi-coloured image were acquired at each z-step to ensure axial alignment.

2.4. Image Analysis

2.4.1. ImageJ/FIJI

All image data was processed using ImageJ/FIJI (Schindelin et al., 2012). Fixed cell image stacks were compressed into a single z-plane through the Extended Depth of Field plugin (Aguet et al., 2008). Cell parts (e.g., neurites, somas, varicosities) were hand-traced and labeled. The RIPA macro generates ROIs through a series of thresholds, bounding each punctum based on user inputs such as fluorescent intensity relative to background, puncta size in pixels, puncta circularity, and puncta solidity, Figure 2.3 (Kalkhoran et al., 2019). Prior to analysis, images were preprocessed with a 10-pixel rolling ball background subtraction and a 1-pixel radius two-dimensional Gaussian blur. If necessary, conjoined ROIs were separated using a unsharp mask radius of 0.8 pixels. Images were watershed on the final loop of RIPA, then the final ROIs were drawn. All input parameters were saved in the output RIPA folder, allowing repeat iterations.

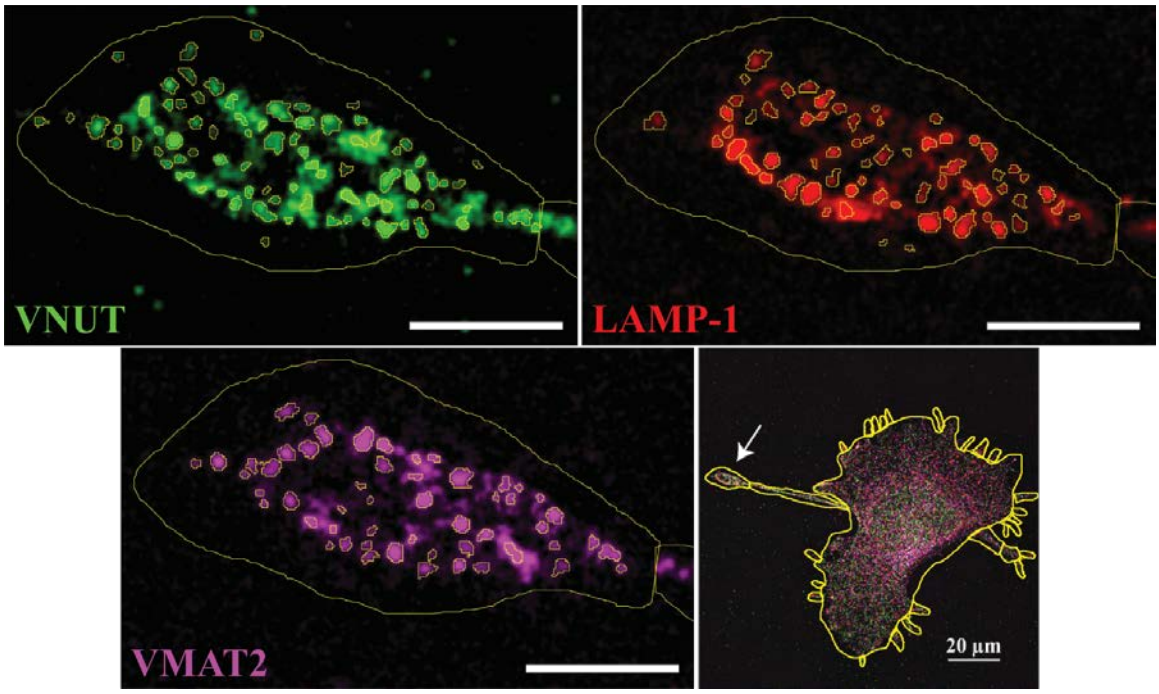

Figure 2.3 RIPA bounding of ROIs based on user input
RIPA-drawn ROIs are shown around puncta in each channel of a three-channel image containing immunolabeled VNUT (green), LAMP-1 (red), and VMAT2 (purple). Lower right image shows the hand-traced cell parts (yellow). The arrow indicates the terminal varicosity in which RIPA bounded puncta ROIs are shown. While RIPA will bound all ROIs in an image through multiple steps of thresholding, only the ROIs that are within a cell part are analyzed. This excludes most instances of background fluorescence from analysis. RIPA-drawn ROIs were bounded using conservative input parameters ($0.7 \leq$ circularity ≤ 1; $0.7 \leq$ solidity ≤ 1; $9 \leq$ area ≤ 100 pixels; exclude 5 pixels from edge of image). Scale bar = 5 µm unless otherwise stated.

MINER analysis followed, which fitted the RIPA-drawn ROIs with a Gaussian fit to identify the full-width half-max of the major and minor axes (Kalkhoran et al., 2019). The nearest neighbor analysis then identified puncta that are closest to puncta from the reference channel, as selected by the user, within each cell part. Figure 2.4 exemplifies the FWHM calculations, as well as the identification of nearest neighboring (NN) LAMP-1 and VMAT2 puncta to the VNUT reference puncta.

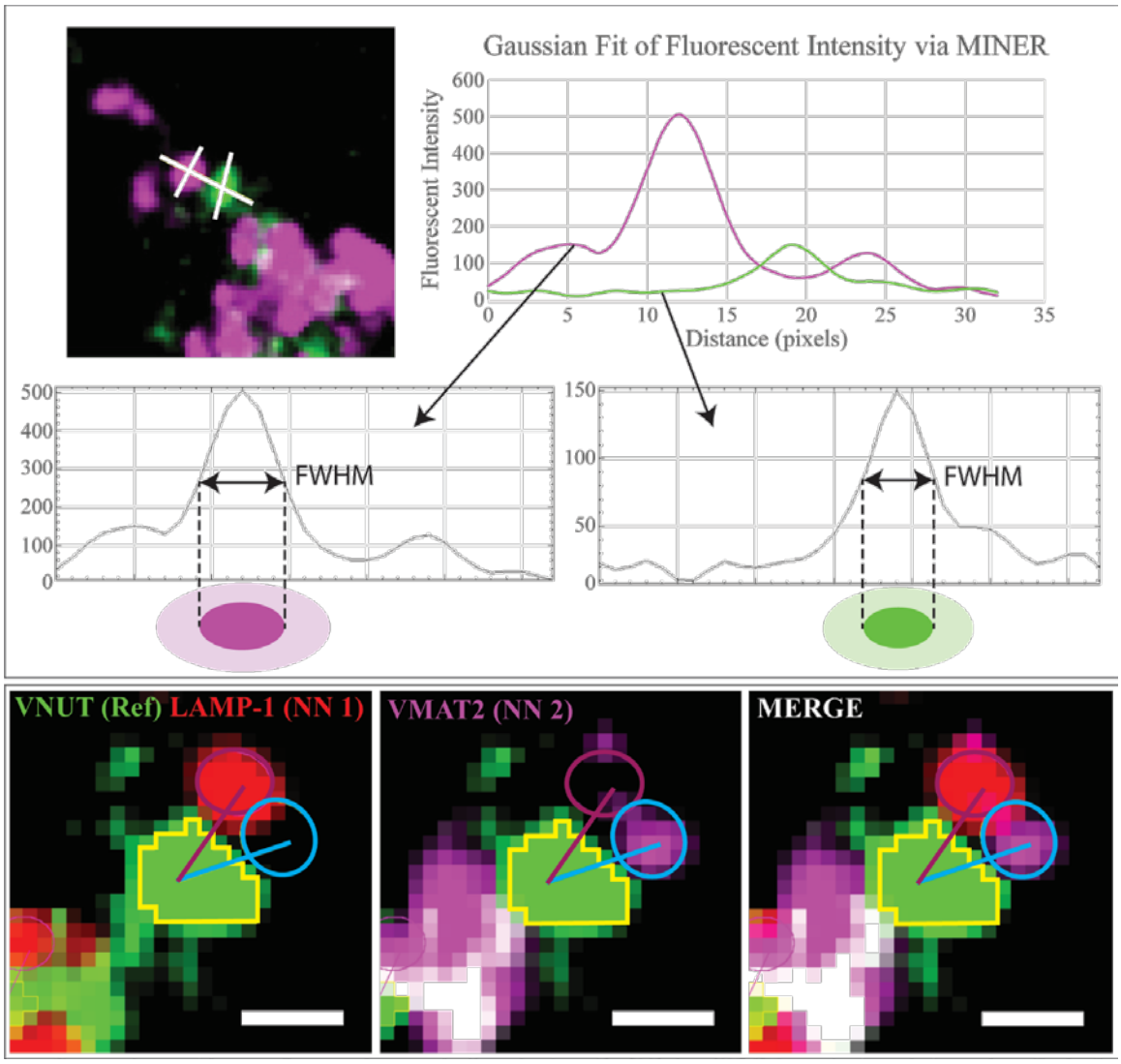

Figure 2.4 MINER workflow and outputs
Top: Graphs show the change in fluorescent intensity of puncta along the path of the white line in the two-channel image. The FWHM of each punctum is calculated using the average of the FWHM values along the major and minor axes (white) of each punctum. Bottom: The VNUT reference punctum was assessed for NN puncta. For images containing multiple NN channels, such as LAMP-1 and VMAT2, each reference punctum is assigned an NN puncta for each NN channel. Image contrasts were scaled by puncta. Original images were not saturated. Scale bar = 500 nm.

The MINER macro was validated as a tool for colocalization analysis. In this validation, the LAMP-1 and VMAT2 channels of a previous colocalization analysis image were separated out of the image, isolating the VNUT channel and corresponding ROIs. This VNUT image was copied, and the puncta were randomized using the Poburko lab macro RandomizeByROIsV1.5.4. This macro uses the ImageJ/FIJI random number generator to assign the ROIs new (x,y) co-ordinates within a boundary ROI. Instead of using cell

part ROIs, the MINER validation test and the randomization trial (described in the next paragraph) used whole cell ROIs that were generated by thresholding the images to create tight cell outline. I wanted to minimize expanding the cell ROI area in which the VNUT puncta would be randomized. Hand tracing is prone to increasing the cell ROI size, which would then underestimate the frequency of colocalization. An example of cell ROI generation and subsequent randomization of VNUT ROIs within the cell boundary is shown in Figure 2.5. The image containing the randomized puncta was then merged with the original image as an additional channel. The resultant two-channel image contained the randomized VNUT puncta that were pseudocoloured magenta and the original, green VNUT puncta. The MINER macro was used to analyze this image using the original arrangement of VNUT puncta as the reference channel. The reference puncta were assessed for having nearest neighbouring (NN) randomized VNUT puncta or original VNUT puncta channel within their perimeter or touching their periphery as described in the previous colocalization analysis.

The likelihood of random colocalization compared to experimentally observed colocalization was quantified using a randomization trial. VNUT puncta from 8 cells were scrambled throughout the cell boundary ROIs using the RandomizeByROIsV1.5.4 macro. The VMAT2 and LAMP-1 puncta were unchanged. The MINER macro was used to analyze the frequencies of colocalization between the randomized or original VNUT reference puncta and their assigned NN LAMP-1 and VMAT2 puncta. These frequencies were compared to those of the original analyses.

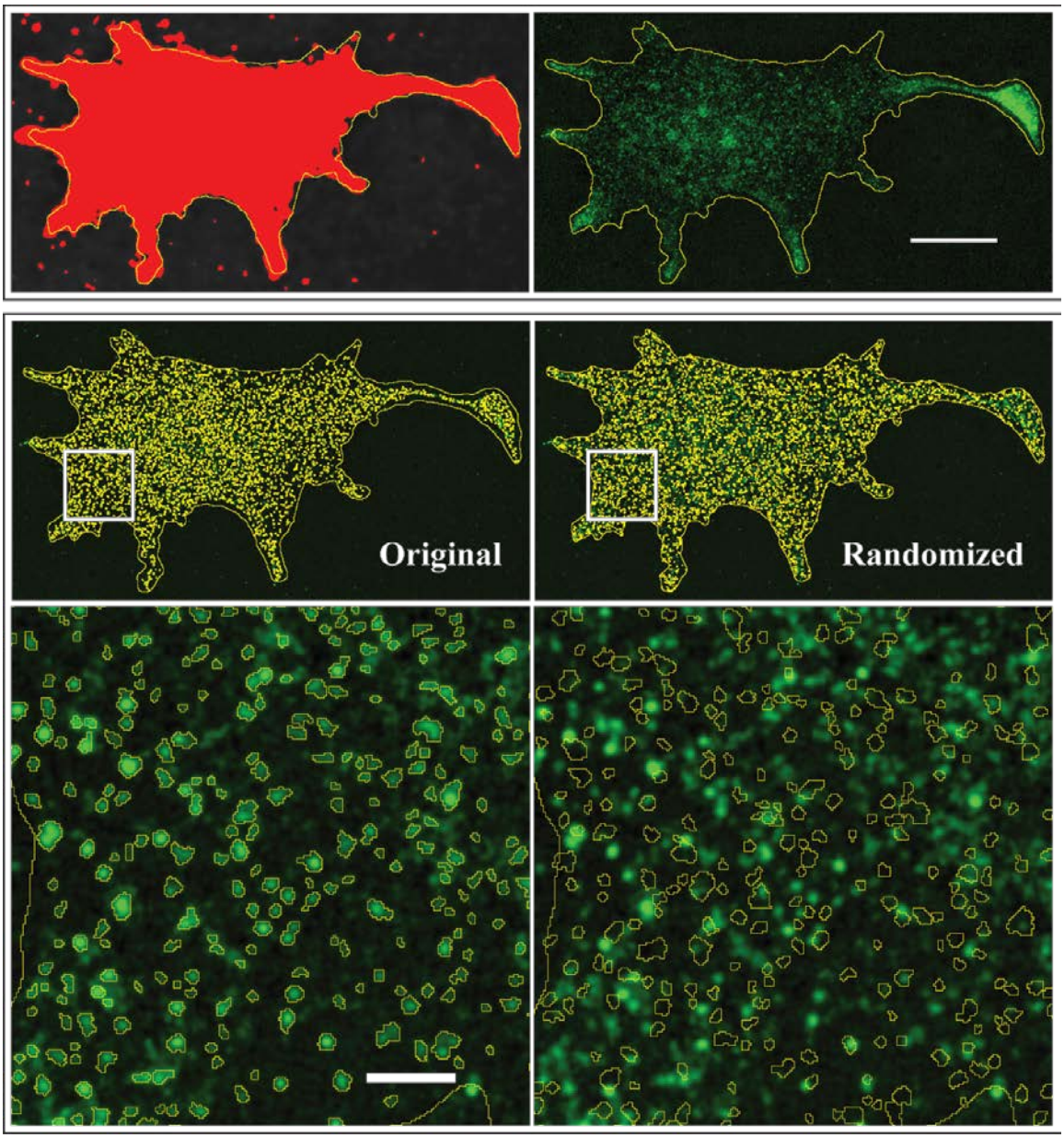

Figure 2.5 Randomization of VNUT puncta
Top: The ImageJ thresholding tool was used to generate cell outlines that were tighter than the hand-drawn cell part ROIs. Scale bar = 20 µm. Bottom: The ROIs and the pixels contained within them (square zoom, left) were randomized within the cell boundary. The outlines of the randomized ROIs are overlayed on the original imaging (square zoom, right). Scale bar = 2.5 µm. The randomized coordinates were saved for each ROI and these ROIs were treated as an additional channel in subsequent randomization analyses.

2.4.2. JMP and Statistical Analysis

I analyzed my data using JMP software (JMP®, Version 15. SAS Institute Inc., Cary, NC, 1989–2021). Colocalization was calculated between the assessed markers and VNUT by measuring puncta size and the distance from the perimeter of the reference puncta to the center of the nearest neighbour (NN) puncta. Colocalized puncta were defined as reference puncta that contained their NN puncta **within** their periphery (i.e., overlapped such that the center of the NN puncta was within the bounds of the reference). **Touching** puncta were defined when the NN center and the perimeter of a reference ROI was less than the half-width at half-maximal intensity (HWHM) of the NN puncta. Puncta were defined as **not touching** if the distance between the reference punctum perimeter was greater than the HWHM of the NN punctum. Figure 3.3 in Section 3.2 illustrates the physical relationships defined above. The reported mean values for fraction of within, touching, and not touching puncta were calculated from the percent of reference puncta from each category out of the total population of reference puncta. Statistical significance testing of different degrees of colocalization for each marker between cell parts was assessed using an ANOVA. Where significant differences were detected, a Tukey honestly significant differences (HSD) *post hoc* test was used to identify which cell part means were significantly different. The Student's T Test was used to identify significant differences between means of randomized VNUT puncta and the original puncta arrangement in the randomization trial.

Reversed MINER analyses were used to assess the relative proportion of colocalization between markers and VNUT. The analysis workflow was the same as described above except the marker was the reference channel and VNUT was the NN channel.

2.4.3. Adobe Illustrator and Figure Building

Figures were built by importing JMP graphs into Adobe Illustrator, where I consolidated data for each marker as appropriate. I finalized formatting, spacing, sizing, fonts, and colours for consistency and readability.

2.4.4. Microbiology

Expression constructs were transformed into DH10β (ThermoFisher Scientific, Cat# EC0113) or NEB5α *Escherichia coli* (New England BioLabs, cat# C2987H) for amplification. The plasmids were extracted using the PureYield Plasmid Midiprep System (Promega, cat# A2392) and stored at -20°C until transfection. Bacterial glycerol stocks were prepared using a 1:1 solution of LB Broth and 40% glycerol in water and stored at -80°C. I followed the AddGene protocol for glycerol stocks, including the preceding instructions “Inoculating an Overnight Liquid Culture,” which can be found at https://www.addgene.org/protocols/create-glycerol-stock/.

2.4.5. Bioinformatic Analysis of VNUT

GenBank sequences for VNUT, VMAT2, VAChT, VGLUT1-3, and sialin were retrieved *en masse* from NCBI, encompassing approximately 800 sequences from kingdom Animalia with representatives from Classes Mammalia, Aves, Reptilia, Amphibia, Chondrichthyes, Actinopterygii, Hyperoartia, Bivalvia, Trematoda, and Insecta. An in-house, regex-based motif searching R script was used to analyze the peptide sequences for signaling sequences or motifs. The R script can be found on GitHub: https://github.com/dpoburko/bioInformaticsTools/blob/master/motifSearch.R. Positive motif matches were listed in an output Excel file, which were then compiled into JMP for analysis and graphing. VNUT sequences were compared to SLC17A and SLC18A family members using the R script. Comparisons between VNUT and other solute carriers across all Classes were visualized in JMP.

Alignment analyses of amino acid and nucleic acid sequences were completed using CLC Genomics Workbench. Structural comparisons between human transporters were built with the Constrained Consensus Topology prediction server (CCTOP), CLC, and the secondary structure visualization tool Protter. CCTOP was used to predict transmembrane domains, while Protter and CLC were used to illustrate secondary structure and amino acid sequences, respectively.

Chapter 3.

Inconclusive VNUT Localization to Vesicle-Like Compartments

3.1. Rationale

The subcellular localization of VNUT varies depending on cell type. Evidence for localization to lysosomes includes the reduction of ATP uptake into lysosomes isolated from COS1 cells when exposed to non-specific inhibitors of VNUT DIDS and Evans Blue (Cao et al., 2014; Zhong et al., 2016). Since DIDS and Evans blue inhibit other transporters, it is unclear how much of the reduction in ATP uptake can be attributed to VNUT. Inhibitors of connexin and pannexin hemichannels, carbenoxolone and niflumic acid, did not reduce ATP uptake into lysosome fractions (Cao et al., 2014; Zhong et al., 2016). VNUT shRNA expression in C2C12 cells significantly decreased ATP uptake into lysosome lysates while overexpression of GFP-tagged VNUT resulted in faster uptake of ATP (Cao et al., 2014). Studies of primary cortical astrocytes also suggest VNUT is localized to lysosomes via immunocytochemistry and live-cell imaging using LysoTracker (Oya et al., 2013), although data derived from pH-sensitive dyes requires careful interpretation due to non-specific accumulation. For example, LysoTracker accumulates in acidified compartments and as such is sold as a lysosome marker. However, vesicles and endosomes are also acidic organelles that can be stained with LysoTracker (S. Li et al., 2014; Moreno, Ramalho-Santos, Chan, Wessel, & Schatten, 2000). A study using astrocytes provides what is arguably the most direct evidence of ATP release from lysosomes (Zhang et al., 2007). Instead of relying on the bioluminescence assay or pH-sensitive probes, extended incubation of astrocytes with the AM1-43 dye resulted in selective staining of lysosomes, confirmed by colocalization with lysosomal membrane markers LAMP-1 and CD-63. Exocytosis-induced lysosomal de-staining was observed in response to ATP as well as chemically induced hypoxia with potassium cyanide (KCN). The calcium chelator BAPTA-AM inhibited de-staining while ionomycin increased AM1-43 de-staining (Zhang et al., 2007). To demonstrate lysosomal exocytosis of ATP, the cells were stained with GFP-conjugated lysosomal marker CD63 and MANT-ATP to confirm MANT-ATP localization to lysosomes. The

subsequent MANT-ATP de-staining in response to KCN provides strong evidence of lysosomal exocytosis of ATP (Zhang et al., 2007).

Microglia cells provide strong evidence of vesicular ATP release (Imura et al., 2013). Ionomycin-induced ATP release is significantly reduced in the presence of the calcium chelator BAPTA-AM, the vesicle trafficking inhibitor brefeldin A, the V-ATPase inhibitor bafilomycin, and the SNARE complex inhibitor botulinum A (Imura et al., 2013). These results support vesicular ATP release. VNUT knockdown via siRNA reduced ATP release in response to ionomycin and ATP by approximately 32% and 50%, respectively (Imura et al., 2013). Colocalization of quinacrine and MANT-ATP to VNUT-RFP puncta was observed in murine MG5 cells using total internal reflection fluorescence (TRIF) microscopy. Quinacrine and MANT-ATP de-staining was observed in response to ionomycin and ATP. Immunostaining for LAMP-1 and VNUT did not corroborate the lysosomal localization of VNUT as these puncta were distinctly anti-colocalized (Imura et al., 2013). These data strongly point to VNUT localization to purinergic vesicles and the vesicular release of ATP. N2a cells are able to release ATP via pannexin channels and SNARE complexes (Gutiérrez-Martín et al., 2011; Menéndez-Méndez et al., 2015; Xu et al., 2018). Lysosomal release of ATP has not been demonstrated in N2a cells.

3.2. Assessing the Subcellular Localization of VNUT

In Aim 2 of my thesis, I sought to quantify colocalization between VNUT and markers of exocytotic compartment(s) such as synaptic vesicles, secretory vesicles, and secretory lysosomes, with the goal of generating a molecular fingerprint of VNUT-containing vesicles. Briefly, immunocytochemistry and transfection techniques visualized fluorescent probes for VNUT and the vesicle population markers. After image acquisition, processing, and analysis, I quantified colocalization by categorizing nearest neighbouring (NN) marker puncta into three groups, as described two paragraphs below this one and illustrated in Figure 3.3. Possible vesicle population markers were discussed in Chapter 1, Section 1.2.3, but I will take a moment to review the markers that I studied as shown in Figure 3.1. Due to the possibility of VNUT associating with lysosomes, LAMP-1 colocalization with VNUT was assessed. Chromogranin A (CGA) was used as a marker of secretory vesicles, while VMAT2 was used to identify catecholaminergic synaptic vesicles. ELKS was used as an active zone marker.

Synaptic vesicle proteins synapsin, SV2a, synaptophysin, and synaptobrevin (VAMP2) were used as markers of synaptic vesicles.

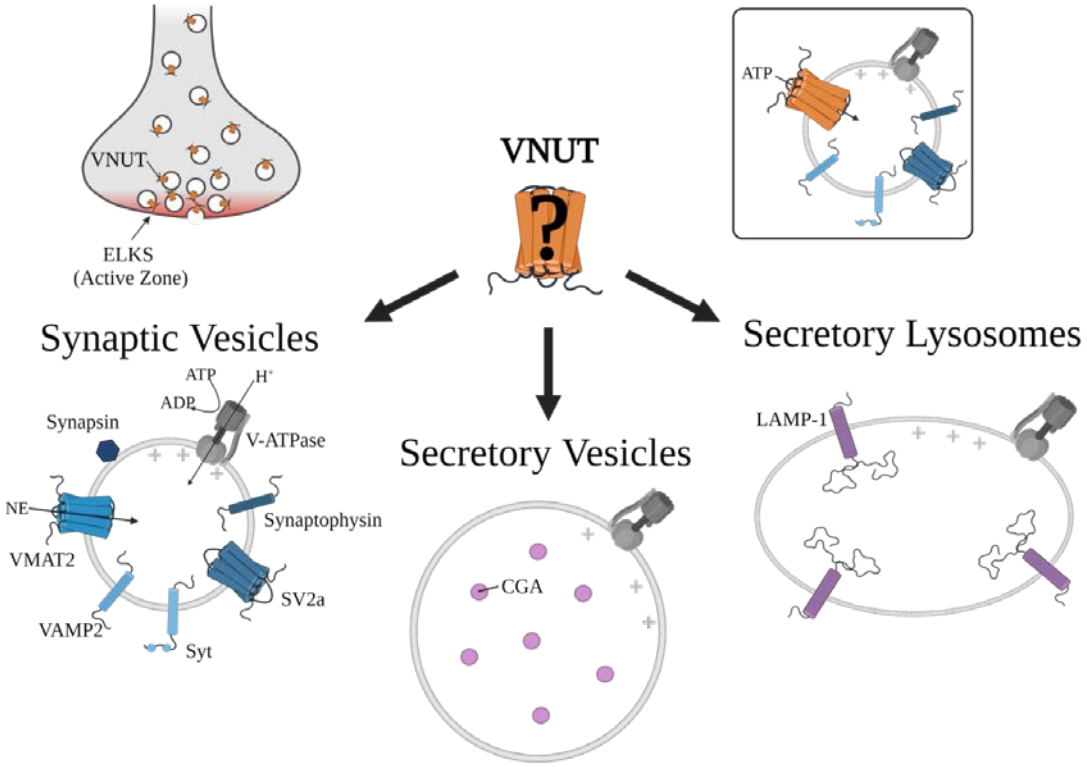

Figure 3.1 Identifying the molecular fingerprint of VNUT-containing vesicles
Each of the assessed markers are shown within their associated membranes. ELKS, a soluble scaffolding protein that is concentrated in active zones, is shown as a red gradient in the cartoon at upper left. The upper right cartoon depicts the predicted molecular architecture of a VNUT-containing vesicle. Created with Biorender.com.

In addition to the previously mentioned synaptic vesicle proteins, I analyzed the frequency of overlap of four calcium-sensitive synaptotagmin isoforms with VNUT: Syt1, Syt2, Syt5 (also known as Syt 9), and Syt 7. Isoforms 1, 2, and 5/9 reside in synaptic vesicle membranes and mediate vesicle fusion in a calcium-dependent manner (Maximov, 2009). Syt7 has a role in mediating asynchronous release of neurotransmitters as well as the replenishment of synaptic vesicles during tonic transmission (H. Liu et al., 2014). The anti-Syt7 antibody was non-specific, as shown in Figure 3.2, thus no Syt7 data was acquired. A fifth isoform, Syt4, is associated with secretory vesicles (Dean et al., 2009; Mori & Fukuda, 2011), the Golgi apparatus (Arthur, Dean, Pagratis, Chapman, & Stowell, 2010; Ibata, Fukuda, Hamada, Kabayama, & Mikoshiba, 2000), and retrograde signaling (Yoshihara, Adolfsen, Galle, & Littleton,

2005). Syt4 is expressed in N2a cells (data not shown) but was not tested for colocalization with VNUT due to incompatible antibody species.

I will outline some general notes for analyzing the characteristics of each vesicle marker. First, puncta size was calculated from the average of the major and minor FWHM values of fluorescent puncta. When calculating puncta size, I included all data regardless of whether the VNUT reference puncta had unique nearest neighbour (i.e., vesicle marker) puncta. In some cases, one NN puncta might be the closest puncta in the NN channel to multiple reference puncta. In our analyses, a NN puncta was only allowed to be assigned to its closest puncta in the reference channel. The more distant reference puncta were designated as not having a NN puncta.

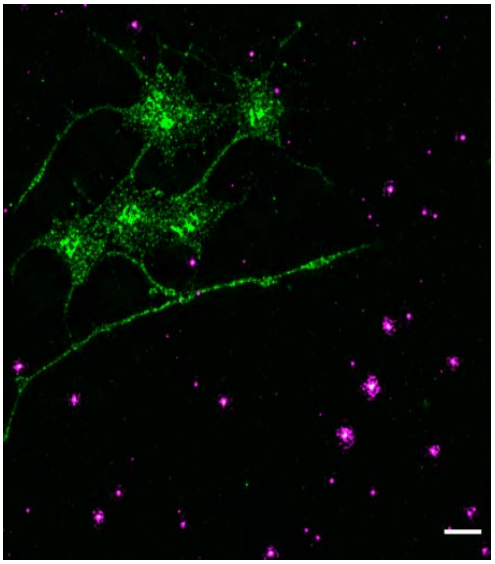

Figure 3.2 Anti-Syt7 antibody shows non-specific binding
This is a representative image showing the extracellular staining of the anti-Syt7 antibody, shown in magenta. Anti-VNUT staining is largely restricted to the cells and is shown in green. Scale bar = 20 µm.

Second, when performing the colocalization analysis, I characterized reference puncta into three groups: reference puncta that do not touch a NN punctum, reference puncta that touch a NN punctum, and reference puncta that contain their NN puncta within their periphery as drawn by RIPA. Figure 3.3 illustrates example arrangements of puncta from each group described above.

Lastly, colocalization data were assessed using an ANOVA comparison, followed by a Tukey HSD *post hoc* test. Statistically significant data are denoted in the figures of this chapter by an asterisk. Only significant comparisons, defined as $p<0.05$, are annotated.

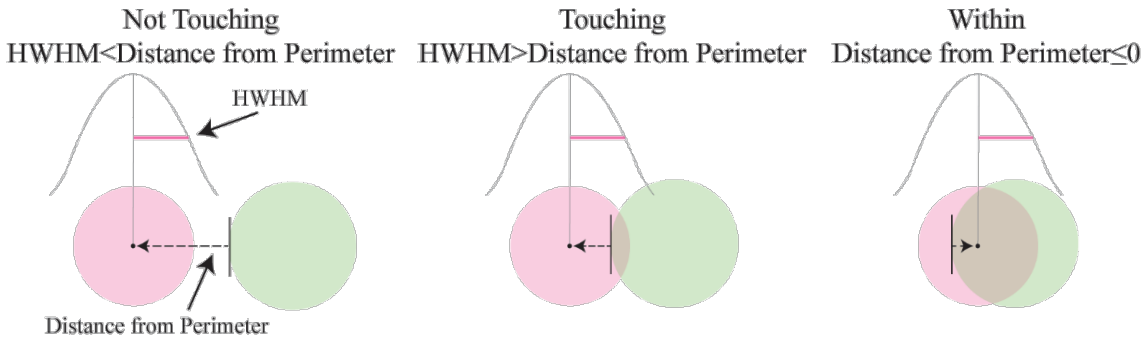

Figure 3.3 Categorization of nearest neighbouring puncta based on degree of colocalization with reference puncta
The nearest neighbour (NN) punctum is r2epresented by the left sphere (pink) while the reference punctum is on the right (green) of each pairing. The Gaussian fit of the fluorescent signal from the NN punctum is illustrated above the corresponding sphere, under which the half-width, half-max (HWHM) value of the NN puncta is illustrated by a pink line. The distance to the center of the NN punctum is measured from the perimeter of the reference punctum.

3.2.1. Validation of Semi-Automatic, High-Throughput Colocalization Analysis using MINER in N2a Cells

VNUT Self-Colocalization Trial

To test the accuracy of the MINER colocalization analysis, I analyzed the frequency of colocalization between two arrangements of VNUT puncta within an N2a cell. Using the original puncta as the reference channel, I analyzed the frequency of reference puncta that had an NN randomized or original puncta within their perimeter or were touching their NN puncta using the MINER macro. Panel B in Figure 3.4 shows the MINER output, which highlights the reference and NN puncta in relation to each other. The resultant analysis illustrated the accuracy with which MINER detected 98% of original NN puncta as residing within their reference puncta (Fig 3.4D), indicated in Table 3.1. The average distance from the reference perimeter to the center of the assigned original NN puncta was -76 nm (Figure 3.4C). Throughout this thesis, this is the only negative mean Distance From Perimeter (dFromP) value reported. Since the original NN puncta were not moved, the 2% of “other” puncta (i.e., reference puncta that did not touch their NN puncta) indicates the error rate of the MINER analysis method (Table 3.1). Moreover, the fraction of reference puncta containing their nearest neighbouring randomized VNUT puncta within their periphery was 10% with an average distance from perimeter (dFromP) of 291+/-233 nm (Table 3.1). These data suggest that the NN puncta were sufficiently randomized throughout the cell by the ROI-randomizing macro in ImageJ/Fiji.

Table 3.1 Results of VNUT self-colocalization analysis

NN Puncta	Within	Touching	Other	dFromP (nm)
Original	97.7	0	2.3	-75.6 (86.9)
Randomized	10	13.5	76.5	290.5 (233)

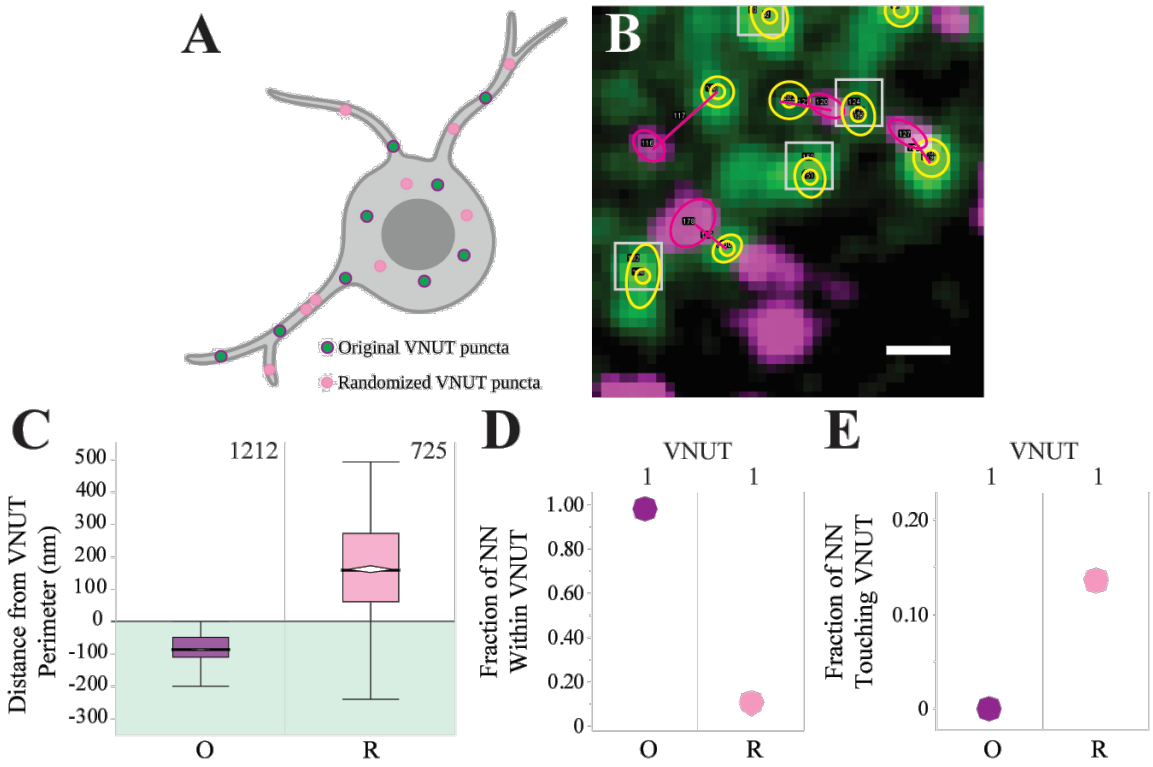

Figure 3.4 Validation of MINER via VNUT self-colocalization analysis
A: This cartoon illustrates the original arrangement of the VNUT puncta within the N2a cell (green dots). The purple borders indicate that these puncta were analyzed as NN puncta in a self-analysis and correspond to the purple boxplot in C and the purple dots in D and E. The VNUT puncta in the randomized arrangement (pink dots) are the NN puncta that were analyzed using the original puncta as the reference channel. The analysis of these puncta is colour coded in panels C, D, and E as a pink boxplot and pink dots, respectively. B: The MINER output shows all analyzed ROIs. The reference ROIs are highlighted with yellow outlines, the randomized VNUT ROIs are outlined in magenta, and the magenta lines connect NN puncta to their nearest reference puncta. Grey boxes highlight reference puncta not assigned to an NN puncta. Scale bar = 0.5 µm. C: Numbers above each boxplot refer to n, number of puncta; diamonds illustrate 95% confidence interval of mean; bar indicates median value. D,E: Numbers above each dot indicate the N, number of cells; NN, nearest neighbour. C,D,E: O, original; R, randomized.

Assessing Colocalization of Randomized VNUT Puncta with LAMP-1 and VMAT2 in N2a Cells

I sought to develop thresholds at which I could deem a protein to be colocalized with VNUT. Due to difficulties developing and acquiring an shRNA-based negative control condition, my next best option was to use the acquired data to create a randomized control condition. The randomization of ROIs is described in Section 2.4.1. The randomized VNUT puncta of 8 cells were assessed in parallel to the original images, using the RIPA and MINER macros as previously described. The distances from the perimeter of the VNUT reference puncta to the centers of the nearest neighbouring LAMP-1 and VMAT2 puncta were compared. The frequencies of reference puncta containing their NN puncta within their perimeter and touching their NN puncta were also compared. The Student's T test was used to test for significant differences between the mean frequency of reference puncta containing NN within periphery for the randomized and original VNUT puncta, Figure 3.5B. Similarly, the differences in mean frequency of reference randomized or original VNUT puncta touching their NN puncta was tested (Fig 3.5C). Significant differences are denoted by an asterisk (*) in Figure 3.5B and C.

The average distances from the perimeter of the original VNUT puncta to the centers of the NN puncta were 162 (± 155) nm for LAMP-1 and 167 (±154) nm for VMAT2. The gap widened when the VNUT puncta were randomly arranged throughout the cells, with the perimeter of the VNUT puncta being an average of 183 (± 155) nm and 196 (± 158) nm away from the centers of LAMP-1 and VMAT2 NN puncta (Fig 3.5A). The fraction of reference puncta containing their LAMP-1 NN puncta within their perimeter was, on average, 11.7% for the original VNUT puncta and 8.0% for the randomized VNUT puncta (Fig 3.5B). Similarly, the average fraction of reference puncta that had their VMAT2 NN puncta within their periphery was 10.3% for the randomized VNUT puncta and 14.0% for the original VNUT puncta (Fig 3.5B). The randomized reference puncta had a lower average frequency of touching their LAMP-1 NN puncta (12.5%) compared to the original VNUT reference puncta (15.6%), Figure 3.5C. For VMAT2, the original reference puncta touched their NN puncta an average of 9.2% of the time, which dropped to 6.3% when the reference puncta were randomized (Fig 3.5C). Tables 3.2 and 3.3 summarize the randomization trial data, with standard deviations in brackets.

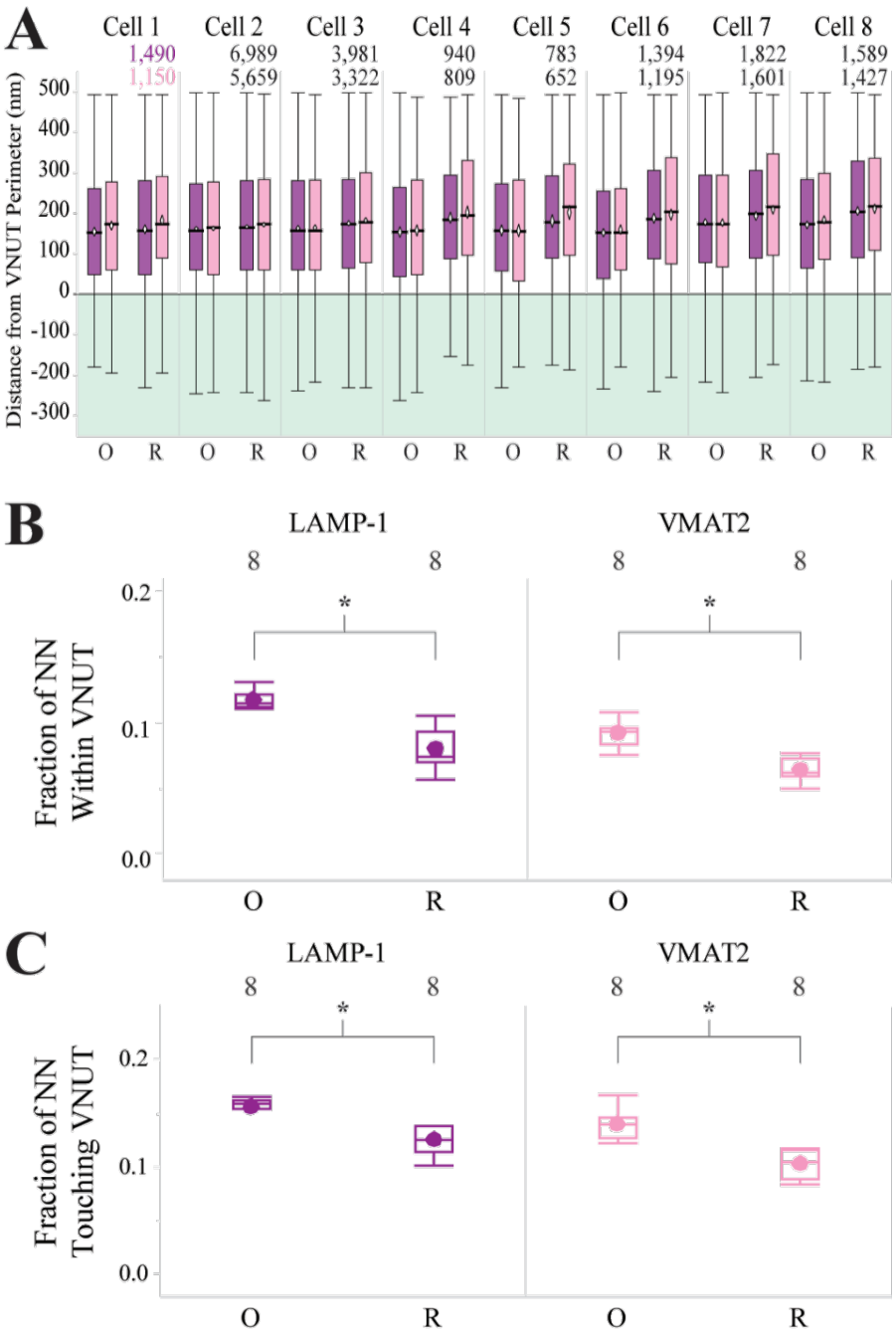

Figure 3.5 Characterization of colocalization between randomized and non-randomized VNUT puncta and LAMP-1 and VMAT2 puncta

A: Top-most numbers refer to cell number; stacked pair of numbers above each set of four boxplots refer to n, number of puncta; diamonds illustrate 95% confidence interval of mean; bar indicates median value. B,C: NN, nearest neighbour (i.e., LAMP-1 or VMAT2); numbers above each boxplot refer to N, number of cells analyzed; dots indicate mean value; bar indicates median value. A-C: O, original arrangement of VNUT puncta as seen in ICC images; R, randomized VNUT puncta that were randomly shuffled within each cell using an ImageJ plugin; LAMP-1 data is shown on the left-hand side of each pairing (A) and on the leftmost graphs (B,C) in purple; VMAT2 data is shown on the right-hand side of each pairing (A) and on the rightmost graphs (B,C) in pink.

Table 3.2 Distance of NN puncta from perimeter of randomized and original VNUT reference puncta

NN Puncta	VNUT Puncta	Cell 1	Cell 2	Cell 3	Cell 4	Cell 5	Cell 6	Cell 7	Cell 8	Average
LAMP-1	Original	155.4 (155.6)	162.9 (152.9)	163.6 (154.2)	154.3 (159.9)	158.4 (151.8)	153 (156.6)	178.3 (155.5)	171.8 (153.8)	162.2 (155)
	Randomized	161.3 (154.7)	167.8 (152.1)	176 (155.6)	189.4 (150.2)	181.7 (155)	188.5 (161.6)	194.3 (156.7)	206 (155.5)	183.1 (155.2)
VMAT2	Original	170.1 (149.2)	163.4 (153.5)	164.5 (154.6)	158.5 (151.3)	157.9 (155.2)	161 (154.6)	177.7 (157.1)	184.5 (156.2)	167.2 (154)
	Randomized	183.5 (150.6)	172.3 (155)	182.9 (158.4)	203.4 (153.9)	202.8 (160.2)	197.1 (168.3)	209.9 (158.5)	211.9 (156.7)	195.5 (157.7)

Table 3.3 Summary of colocalization data from randomization trial

	NN Puncta	VNUT Puncta	Cell 1	Cell 2	Cell 3	Cell 4	Cell 5	Cell 6	Cell 7	Cell 8	Average
Within	LAMP-1	Original	12.2%	11.1%	11.4%	13.0%	11.6%	11.9%	11.4%	11.0%	11.7%
		Randomized	10.6%	9.4%	9.1%	7.0%	7.5%	7.2%	7.2%	5.7%	8.0%
	VMAT2	Original	12.2%	12.9%	14.4%	16.7%	12.7%	14.5%	14.6%	13.7%	14.0%
		Randomized	11.0%	11.7%	11.7%	10.7%	8.5%	8.4%	10.1%	10.0%	10.3%
Touching	LAMP-1	Original	16.1%	15.4%	15.9%	16.5%	16.3%	13.0%	15.8%	15.6%	15.6%
		Randomized	13.5%	13.8%	13.9%	11.1%	12.3%	10.2%	12.3%	12.8%	12.5%
	VMAT2	Original	7.6%	9.1%	9.2%	9.5%	10.8%	8.1%	9.5%	9.5%	9.2%
		Randomized	5.9%	7.5%	7.6%	5.0%	6.1%	6.5%	5.9%	6.1%	6.3%

3.2.2. Analysis of VNUT Colocalization with LAMP-1

To test VNUT localization to lysosomes, I assessed the degree of colocalization between VNUT and LAMP-1. In case of non-specific recongition of off-target proteins by the LAMP-1 or VNUT antibodies, I also assessed the colocalization of VNUT N- or C-terminally-conjugated EGFP construct that was co-transfected with a LAMP-1-RFP construct. Figure 3.6 shows typical, punctate patterning of the immunolabeled LAMP-1 and VNUT as well as the exogenously expressed LAMP-1-RFP and EGFP-conjugated VNUTs alike. In the soma, VNUT puncta are primarily localized to the perinuclear space, while larger and brighter LAMP-1 puncta surround the periphery of the cell body as indicated by the arrow (Fig 3.6C). The neurites and varicosities exhibited some overlap between VNUT and LAMP-1 (arrow), although most of the VNUT-containing puncta appeared to be anti-colocalized with the LAMP-1 puncta (Fig 3.6F). Exogenous expression of LAMP-1-RFP and VNUT-EGFP resulted in punctate fluorescence similar to LAMP-1 and VNUT immunostaining, although the puncta seemed to aggregate at the perinuclear space to a greater extent than the immunostained counterparts (Fig 3.6I). Overlap of the overexpressed VNUT-EGFP and LAMP-1-RFP (arrows) occurred more often than with the immunostaining counterparts, perhaps due to accumulation of the exogenous constructs in the endoplasmic reticulum or Golgi (Fig 3.6J-L).

Across all cell parts, the average distance of LAMP-1 puncta from the perimeter of VNUT reference puncta was 146 nm (Fig 3.6M). On average, LAMP-1-RFP NN puncta were 107 nm from the perimeter of their VNUT-EGFP reference puncta. The whole-cell average frequency of VNUT reference puncta that contained their NN LAMP-1 puncta within their periphery was 12.1%. Statistically significant differences were seen between soma (10.6%), neurites (14.2%), and terminal varicosities (10.7%) (Fig 3.6N). VNUT-EGFP reference puncta contained their LAMP-1-RFP NN puncta slightly more often than their immunolabeled counterparts, with a whole cell average of 15.6%. Significant differences were seen in the means of neurites (10.8%), varicosities (15.1%), and terminal varicosities (23.5%), with the latter housing the highest fraction of NN-containing VNUT-EGFP puncta (Fig 3.6N). The fraction of VNUT reference puncta touching their assigned NN puncta tended to increase from soma to terminal varicosities, but these differences did not reach statistical significance. The average fraction of LAMP-1-adjacent VNUT reference puncta was 16.4%, while the average fraction of

LAMP-1-RFP-touching VNUT-EGFP puncta was 8.7% (Fig 3.6O). The highest fraction of VNUT-EGFP and NN LAMP-1-RFP touching occurred in neurites at 12.3%.

Reversing the MINER analysis such that LAMP-1 or LAMP-1-RFP were the reference channels and VNUT or VNUT-EGFP served as the NN channels resulted in similar distances from perimeter values to VNUT or VNUT-EGFP being the reference. The average distances of LAMP-1 and LAMP-1-RFP to native and exogenous VNUT NN puncta were 139 nm and 101 nm, respectively (Fig 3.6P). Similar to panel N, the differences between the fraction of LAMP-1 or LAMP-1-RFP reference puncta containing their NN pucnta within their perimeter did not reach statistical significance. The average fraction of LAMP-1 and LAMP-1-RFP having the center of an NN VNUT or VNUT-EGFP puncta within their periphery was 15.3% and 12.5%, respectively (Fig 3.6Q). The fraction of NN VNUT-EGFP puncta that touched their reference LAMP-1-RFP puncta averaged out to 7.3% with statistically significant differences in means detected between soma (11.1%) and collectively neurites and terminal varicosities (4.9%) (Fig 3.6R). The average size of LAMP-1 and LAMP-1-RFP puncta were 286 nm and 327 nm, respectively. Across all analyses for VNUT-LAMP-1 colocalization, including the LAMP-1-GFP and immunostained VNUT hybrid experiment shown in Figure 3.7 (below), the average size of VNUT-containing puncta was 255 nm (Fig 3.6S).

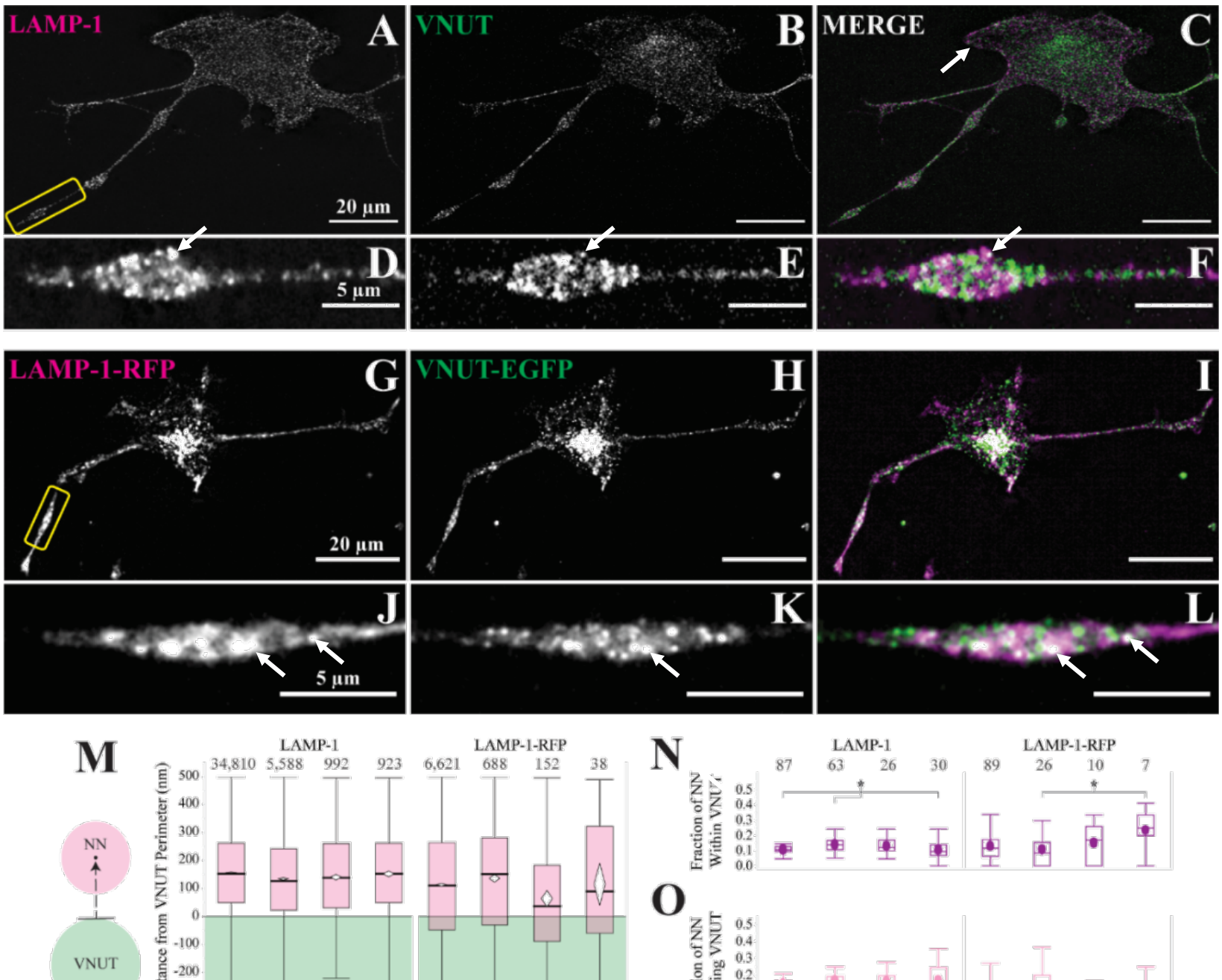

Figure 3.6 Immunostaining for LAMP-1 and exogenously expressed LAMP-1-RFP do not colocalize with VNUT
A-C,G-I: Scale bar = 20 µm. D-F,J-L: Scale bar = 5 µm. M,P,S: Numbers above each boxplot refer to n, number of puncta; diamonds illustrate 95% confidence interval of mean; bar indicates median value. N,O: NN, nearest neighbour (i.e., LAMP-1 or LAMP-1-RFP). Q,R: Ref, refers to reference protein (i.e., LAMP-1 or LAMP-1-RFP). N,O,Q,R: Numbers above each boxplot refer to N, number of cell parts analyzed; dots indicate mean value; bar indicates median value. S: VNUT is represented by the green boxplots on the left of each pairing; LAMP-1 and LAMP-1-RFP are represented by pink boxplots on the right of each pairing. M-S: S, soma; N, neurite; V, varicosity; Vt, terminal varicosity.

An additional assessment of VNUT localization to lysosomes used a LAMP-1-GFP expression construct in conjuction with immunostaining for VNUT, resulting in a hybrid probe experiment (Fig 3.7). The accumulation of LAMP-1-GFP to the perinuclear region, as indicated by the arrow (Fig 3.7A), was similar to LAMP-1-RFP (seen in Figure 3.6G-I). In contrast, VNUT exhibited a consistently punctate pattern of fluorescence throughout the cell. Some LAMP-1-GFP puncta trafficked to neurites and, like LAMP-1-RFP, occaisonal fluorescent overlap was visible with VNUT (Fig 3.7D-F). Similar to the LAMP-1 and LAMP-1-RFP analyses, LAMP-1-GFP puncta were largely anti-colocalized with antibody-labeled VNUT.

Compared to the LAMP-1 and LAMP-1-RFP counterparts, the average distance between the center of LAMP-1-GFP NN puncta and the perimeter of the reference VNUT puncta was slightly larger at 160 nm (Fig 3.7J). An average frequency of 7.9% of VNUT puncta contained their NN LAMP-1-GFP puncta within their periphery and 9.4% of VNUT puncta were touching their NN LAMP-1-GFP puncta (Fig 3.7K,L).

When LAMP-1-GFP served as the reference channel and VNUT as the nearest neighbouring channel in a reverse MINER analysis, the average distance from LAMP-1-GFP perimeter of VNUT puncta was 99 nm (Fig 3.7M). The average fraction of LAMP-1-GFP reference puncta containing their NN VNUT puncta was 24.7%, likely due to the decreased density of LAMP-1-GFP compared to VNUT puncta. An average of 8.7% of LAMP-1-GFP-containing blobs touched their NN VNUT-containing blobs (Fig 3.7N,O). The average size of LAMP-1-GFP puncta was 295 nm (Fig 3.7P), which was comparable to the sizes of the LAMP-1 (286 nm) and LAMP-1-RFP (327 nm) puncta.

The difference in frequency of reference puncta containing their NN puncta in the VNUT reference and reverse MINER experiments indicate that LAMP-1-GFP puncta contained a NN VNUT puncta more often than VNUT puncta reference puncta contained a NN LAMP-1-GFP puncta. This could be due to the size difference between the VNUT and LAMP-1-GFP puncta. Since the LAMP-1-GFP puncta are larger than the VNUT puncta, it is conceivable that the centers of VNUT puncta would be detected within the periphery of the LAMP-1-GFP puncta, but not vice versa. However, the LAMP-1/VNUT and LAMP-1-RFP/VNUT-EGFP colocalization analyses are based on at least three independent replicates. The anti-VNUT/LAMP-1-EGFP colocalization results are based on one replicate; conclusions regarding these experiments should be weighed accordingly.

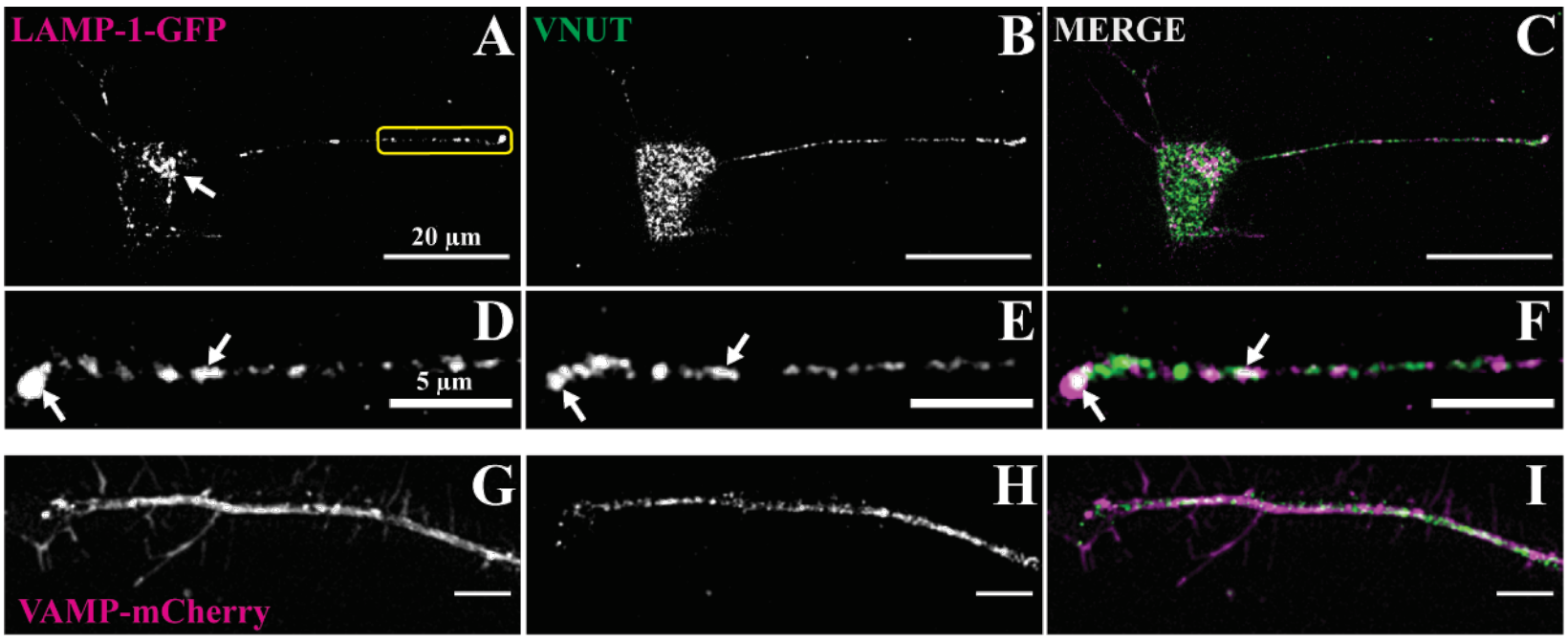

Figure 3.7 Quantification of colocalization between immunolabeled VNUT and exogenously expressed LAMP-1-GFP and VAMP-mCherry

A-C: Scale bar = 20 µm. D-I: Scale bar = 5 µm. J,M,P: Numbers above each boxplot refer to n, number of puncta; diamonds illustrate 95% confidence interval of mean; bar indicates median value. K,L: NN, nearest neighbour (i.e., LAMP-1-GFP or VAMP-mCherry). N,O: Ref, refers to reference protein (i.e., LAMP-1-GFP or VAMP-mCherry). K,L,N,O: Numbers above each boxplot refer to N, number of cell parts analyzed; dots indicate mean value; bar indicates median value. P: VNUT is represented by the green boxplots on the left of each pairing; LAMP-1-GFP and VAMP-mCherry are represented by pink boxplots on the right of each pairing. J-P: S, soma; N, neurite; V, varicosity; Vt, terminal varicosity.

3.2.3. Analysis of VNUT Colocalization with Synaptic Vesicle Markers

VNUT localization to synaptic vesicles was assessed using synaptic vesicle markers synaptobrevin (VAMP2), SV2a, synaptophysin, synaptotagmins, synapsin, and the active zone protein ELKS. Colocalization data for genetically encoded VAMP-mCherry and immunolabeled VNUT is shown in Figure 3.7. Visually, VAMP-mCherry and VNUT exhibited partial overlap (Fig 3.7A-I). The average distance between puncta was 228 nm (Fig 3.7J), which was smaller than the average size of VAMP-mCherry puncta, 326 nm (Fig 3.7P). On average, 2.8% of VNUT puncta contained their NN VAMP-mCherry puncta within their periphery (Fig 3.7K,L). Reference VNUT puncta touched their NN VAMP-mCherry puncta with an average frequency of 5.4%.

In a reversed MINER analysis, the average distance between VAMP-mCherry reference puncta and NN VNUT was 142 nm (Fig 3.7M). On average, 18% of VAMP-mCherry reference puncta contained a NN VNUT puncta within their periphery, while 9.4% were touching their NN VNUT puncta (Fig 3.7N,O). These data indicate that VAMP-mCherry puncta contained or touched a VNUT puncta more often than VNUT puncta contained or touched a VAMP-mCherry puncta, suggesting that a small proportion of VNUT-containing compartments are synaptic vesicles.

Like VNUT, immunostaining for SV2a and synaptophysin resulted in punctate staining (Fig 3.8A-F). Clusters of VNUT and SV2a puncta were observed in neurites and varicosities, with several instances of fluorescent overlap as indicated by the arrows (Fig 3.8A-C). Conversely, synaptophysin puncta did not exhibit many instances of visual overlap with VNUT although the few instances of fluorescence overlap were observed in neurites (Fig 3.8D-F). The average distance between the centers of SV2a and synaptophysin puncta from the VNUT perimeter was 77 nm and 121 nm, respectively (Fig 3.8G). The average frequency of SV2a-containing VNUT puncta was 16.90%, with statistically significant differences in means detected between soma (10.68%) and neurites and varicosities, collectively (19.97%). For synaptophysin, this average was 14.56% (Fig 3.8H). SV2a and synaptophysin puncta touched their VNUT reference puncta with average frequencies of 10.25% and 13.33%, respectively.

In a reversed MINER analysis, the calculated average distance between VNUT NN puncta and their reference SV2a or synaptophysin puncta was 102 nm and 129 nm, respectively (Fig 3.8J). Further, SV2a puncta contained their VNUT NN puncta within their periphery 26.6% of the time, with significant differences reported between the soma (15.4%) and all other cell parts combined (30.3%). Synaptophysin puncta contained their VNUT NN puncta within their perimeter less frequently, with a whole cell average of 15.1% of the time (Fig 3.8K). VNUT NN puncta touched their reference SV2a and synaptophysin puncta more often than they resided within these markers. The average frequency of VNUT-containing puncta touching SV2a and synaptophysin was similar at 20.0% and 20.3%, respectively (Fig 3.8L).

In terms of size, SV2a puncta were 314 nm across while synaptophysin puncta were 267 nm across. The average puncta size for VNUT from all synaptic vesicle protein analyses, including VAMP-mCherry (Fig 3.7), was 258 nm (Fig 3.8M).

Synaptic vesicle-associated synaptotagmin isoforms 1, 2, and 5 (also known as Syt 9 by homology) were used to further assess VNUT localization to synaptic vesicles, Figure 3.9. Some instances of partial fluorescent overlap between VNUT and Syt1 were observed, (Fig 3.9A-C). In contrast to the small puncta of Syt1, Syt2 puncta formed larger clusters that exhibited moderate fluorescent overlap with VNUT. These instances of overlap tended to occur most often in varicosities (Fig 3.9D-F). Visually, fluorescent overlap between Syt5/9 and VNUT was sparse, suggesting Syt5/9 was anti-colocalized to VNUT (Fig 3.9G-I). The average distances of the NN Syt1, 2, and 5 puncta from their VNUT reference puncta were 124 nm, 142 nm, and 136 nm, respectively (Fig 3.9J).

The respective average fractions of Syt1 and Syt5 puncta that resided within their VNUT-containing reference puncta were 15.4% and 11.1%, respectively, but did not significantly differ between the soma and neurites or varicosities. Although the analysis of Syt2 reported a comparable average of 13.0% of VNUT puncta containing their NN puncta, statistically significant differences were detected between varicosities (19.4%) and terminal varicosities (6.3%) (Fig 3.9K). In order, the average frequencies at which Syt1, 2, and 5 touched their VNUT reference puncta were 18.5%, 13.8%, and 10.4% (Fig 3.9L).

In their respective reversed MINER analyses, the average distance from Syt1, 2, or 5 as reference puncta to their NN VNUT puncta was 138 nm, 169 nm, and 173 nm, respectively (Fig 3.9M). The average fraction of reference puncta containing their VNUT NN puncta within their periphery was 9.7% for Syt1, 9.8% for Syt2, and 11.5% for Syt5 (Fig 3.9N), while the average frequency at which VNUT touched these reference puncta was 13.1%, 17.7%, and 17.9% (Fig 3.9O).

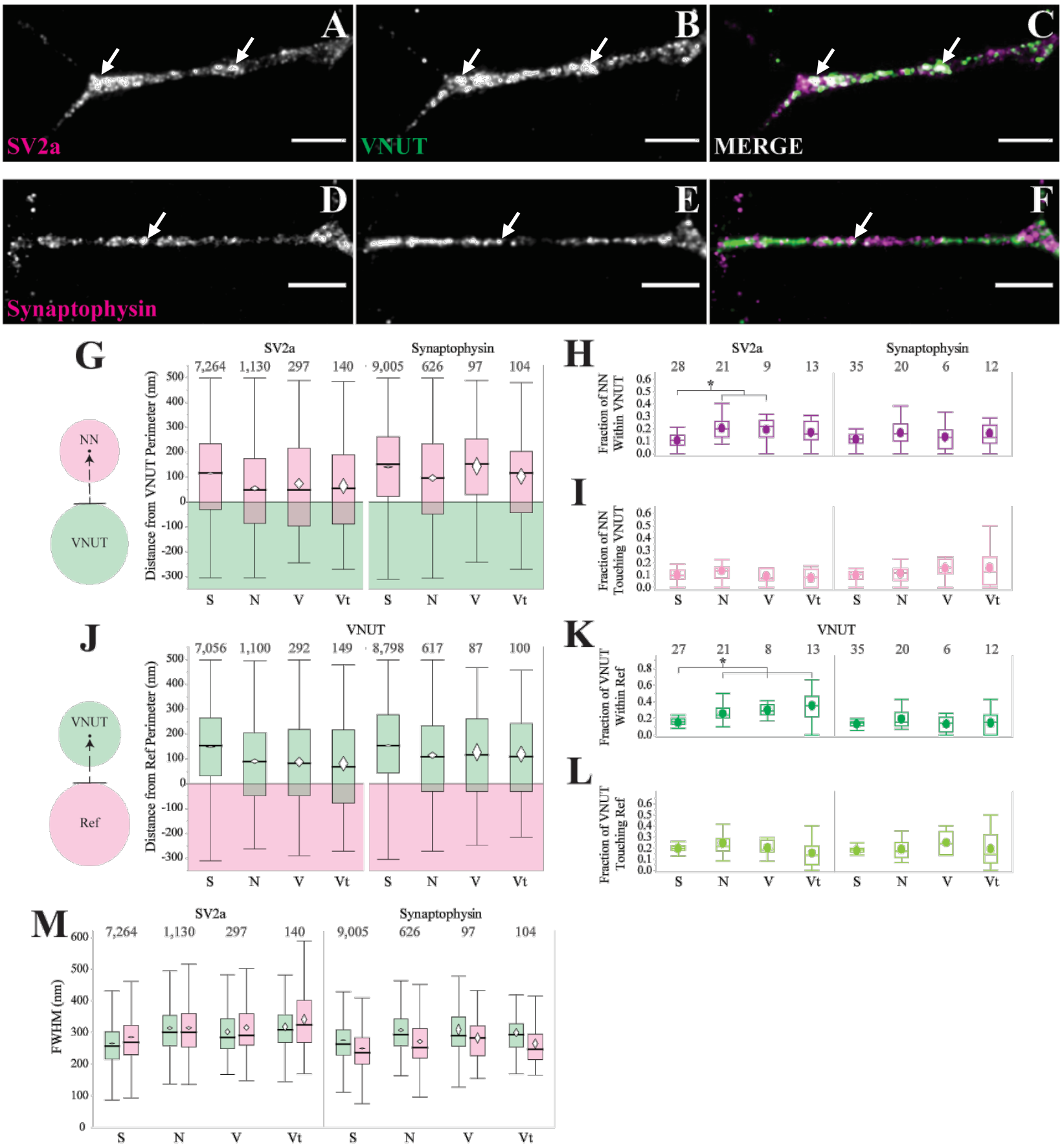

Figure 3.8 Colocalization analysis of synaptic vesicle markers SV2a and synaptophysin with VNUT via ICC
A-F: Scale bar = 5 µm. G,J,M: Numbers above each boxplot refer to n, number of puncta; diamonds illustrate 95% confidence interval of mean; bar indicates median value. H,I: NN, nearest neighbour (i.e., SV2a or synaptophysin). K,L: Ref, refers to reference protein (i.e., SV2a or synaptophysin). H,I,K,L: Numbers above each boxplot refer to N, number of cell parts analyzed; dots indicate mean value; bar indicates median value. M: VNUT is represented by the green boxplots on the left of each pairing; SV2a and synaptophysin are represented by pink boxplots on the right of each pairing. G-M: S, soma; N, neurite; V, varicosity; Vt, terminal varicosity.

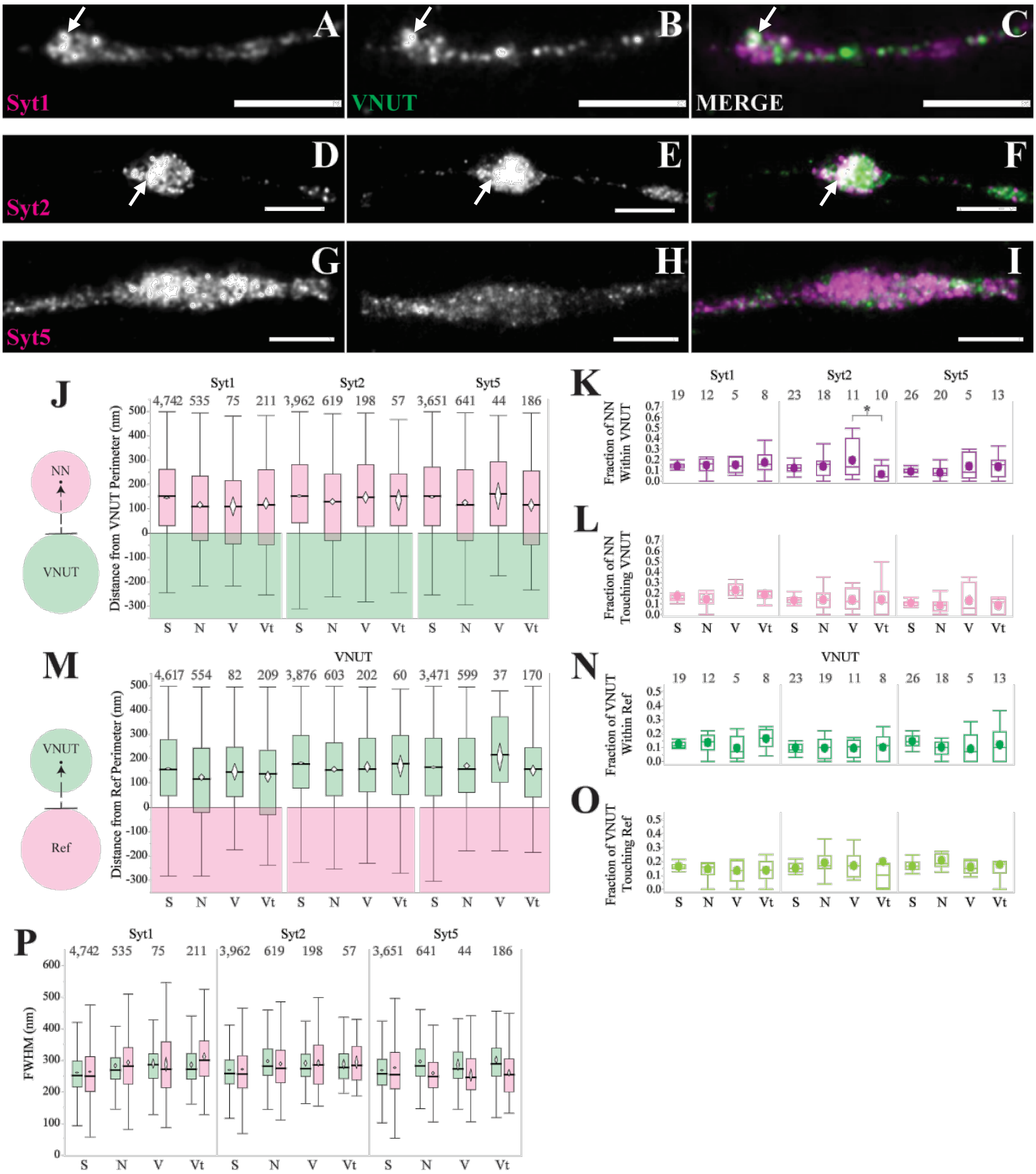

Figure 3.9 Colocalization analysis of immunocytochemical staining for synaptotagmin isoforms 1, 2, 5 and VNUT
A-I: Scale bar = 5 µm. J,M,P: Numbers above each boxplot refer to n, number of puncta; diamonds illustrate 95% confidence interval of mean; bar indicates median value. K,L: NN, nearest neighbour (i.e., Syt1, Syt2, or Syt5). N,O: Ref, refers to reference protein (i.e., Syt1, Syt2, or Syt5). K,L,N,O: Numbers above each boxplot refer to N, number of cell parts analyzed; dots indicate mean value; bar indicates median value. P: VNUT is represented by the green boxplots on the left of each pairing; synaptotagmin isoforms are represented by pink boxplots on the right of each pairing. J-P: S, soma; N, neurite; V, varicosity; Vt, terminal varicosity.

The synaptotagmin-containing puncta were similar in size. Syt1 puncta averaged out to 289 nm, Syt2 to 287 nm, and Syt 5 to 263 nm. Across all synaptotagmin analyses, the average size of VNUT puncta was 285 nm (Fig 3.9P).

The last assessed synaptic vesicle markers were ELKS and synapsin. These proteins participate in vesicle docking. Colocalization of VNUT with ELKS or synapsin would suggest the VNUT-containing vesicle is fusion competent. However, ELKS and VNUT puncta were anti-colocalized (Fig 3.10A-C). Instances of fluorescent overlap was observed only in instances of diffuse ELKS staining (see arrows). Minimal fluorescent overlap was observed between synapsin and VNUT (Fig 3.10D-F). The average distances from the perimeter of VNUT reference puncta to the center of their NN ELKS or synapsin puncta was 135 nm and 153 nm, respectively (Fig 3.10G). Reference puncta contained ELKS NN puncta within their periphery 18.9% of the time on average, with significant differences reported between the soma (15.2%) and neurites (22.5%). VNUT reference puncta had an average of 13.2% of NN synapsin puncta within their periphery (Fig 3.10H). The average fraction of VNUT-touching ELKS or synapsin puncta was 14.6% and 19.6%, respectively (Fig 3.10I).

In their respective reversed MINER analyses in which ELKS and synapsin were the reference channels and VNUT was the NN channel, the average distances from the reference perimeter to the center of the VNUT NN puncta were 129 nm and 146 nm, respectively (Fig 3.10J). Across all cell parts, an average of 11.9% of ELKS reference puncta contained their VNUT NN puncta within their perimeter. Significant differences in mean colocalization between different cell parts were detected between the soma (9.8%), neurites (14.2%), and terminal varicosities (7.0%) as well as between the soma and varicosities (16.6%). The average frequency of synapsin reference puncta containing their VNUT NN puncta was 8.0% (Fig 3.10K). The average frequencies of VNUT puncta touching either ELKS or synapsin puncta were 11.5% and 8.4%, respectively (Fig 3.10L).

ELKS-containing puncta were slightly smaller than synapsin puncta, with an average size of 287 nm, while the average synapsin punctum was 314 nm across. For these analyses, the average size of VNUT-containing puncta was 243 nm.

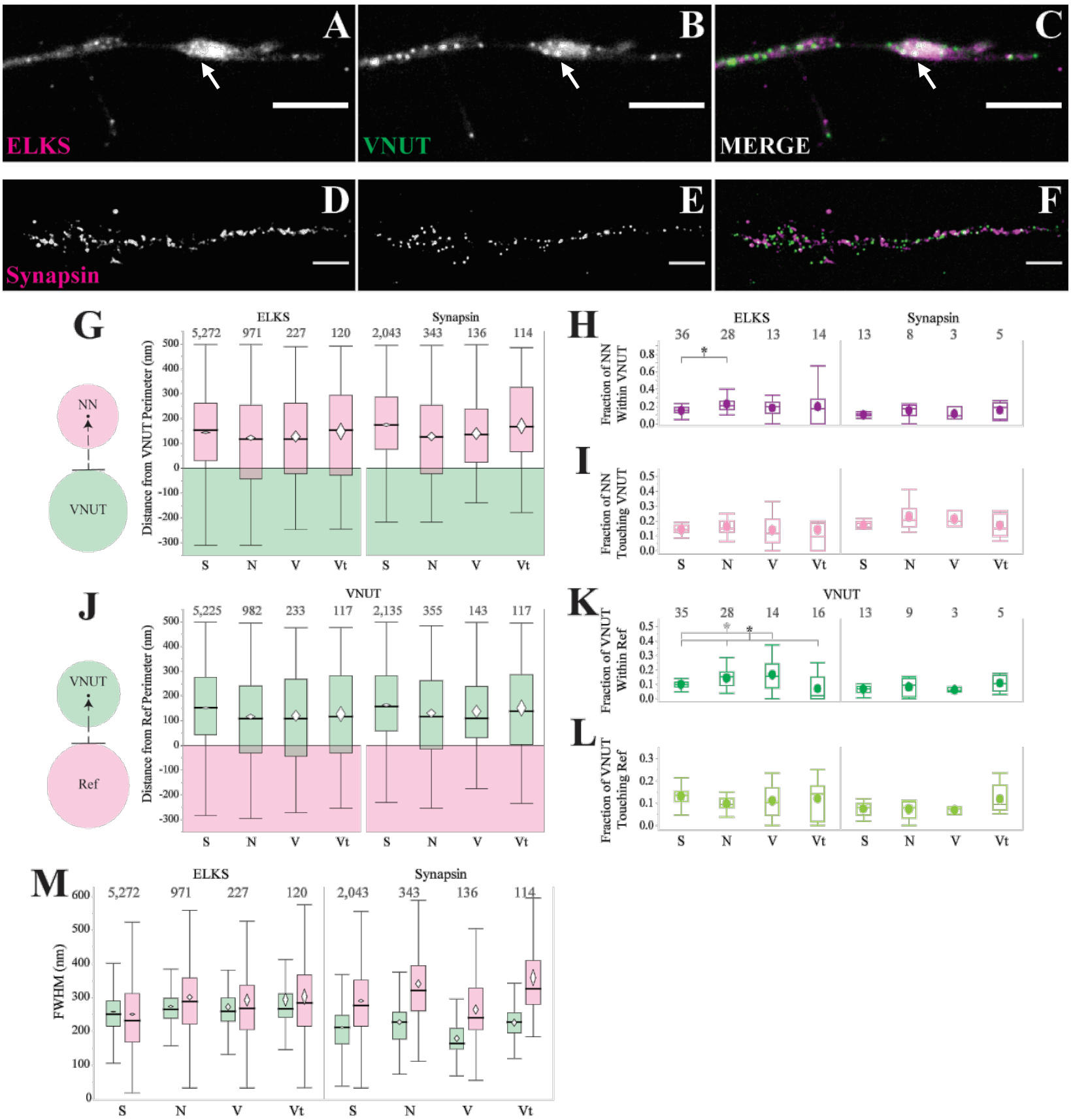

Figure 3.10 Colocalization analysis of synaptic vesicle-associated proteins ELKS nd synapsin with VNUT as visualized with ICC

A-F: Scale bar = 5 µm. G,J,M: Numbers above each boxplot refer to n, number of puncta; diamonds illustrate 95% confidence interval of mean; bar indicates median value. H,I: NN, nearest neighbour (i.e., ELKS or synapsin). K,L: Ref, refers to reference protein (i.e., ELKS or synapsin). H,I,K,L: Numbers above each boxplot refer to N, number of cell parts analyzed; dots indicate mean value; bar indicates median value. M: VNUT is represented by the green boxplots on the left of each pairing; ELKS and synapsin are represented by pink boxplots on the right of each pairing. G-M: S, soma; N, neurite; V, varicosity; Vt, terminal varicosity.

3.2.4. Analyzing VNUT Colocalization with Chromogranin A

VNUT localization to large, secretory vesicles was assessed by measuring the degree and frequency of overlap between VNUT- and chromogranin A-containing puncta. Data collected from this analysis is shown in Figure 3.11. Both immunolabeled CGA and VNUT exhibited a punctate pattern of fluorescence. Visually, some instances of overlap were seen (arrow), but most of the VNUT-containing puncta did not appear to contain a CGA puncta (Fig 3.11A-C). Similar to the immunostaining, CGA-GFP expression resulted in punctate signals (Fig 3.11D-F). The mean distance of immunolabeled CGA puncta from the perimeter of VNUT reference puncta was 143 nm, 94 nm, 115 nm, and 115 nm within soma, neurites, varicosities, and terminal varicosities, respectively. Across all cell parts, the average distance from VNUT perimeter was 117 nm (Fig 3.11G). The whole-cell mean fraction of VNUT reference puncta containing their nearest neighbouring CGA puncta within their periphery was 12.7%. An average of 7.4% of reference puncta contained their NN CGA-GFP puncta within their periphery (Fig 3.11H). The average fraction of CGA puncta touching VNUT blobs was 15.4%, with statistically significant differences detected between neurites (12.7%) and terminal varicosities (17.3%). An average of 9.0% of CGA-GFP puncta touched VNUT-containing blobs across all cell parts (Fig 3.11I).

In their respective reverse MINER analyses, the average distance from perimeter of the CGA or CGA-GFP reference puncta to the center of the VNUT NN puncta was 101 nm and 158 nm, respectively (Fig 3.11J). The average frequency of CGA puncta containing a NN VNUT puncta within their perimeter was 21.0%. Soma and terminal varicosities reported statistically significant differences with 18.9% of CGA blobs containing a VNUT blob in the soma and 26.1% in terminal varicosities. The average fraction of VNUT puncta within CGA-GFP puncta was 15.2% (Fig 3.11K). An average of 14.7% and 22.1% of CGA and CGA-GFP reference puncta were touching their VNUT NN puncta (Fig 3.11L).

The average size of CGA and CGA-GFP puncta were 336 nm and 267 nm, respectively, while the average size of VNUT-containing puncta was 266 nm across both analyses.

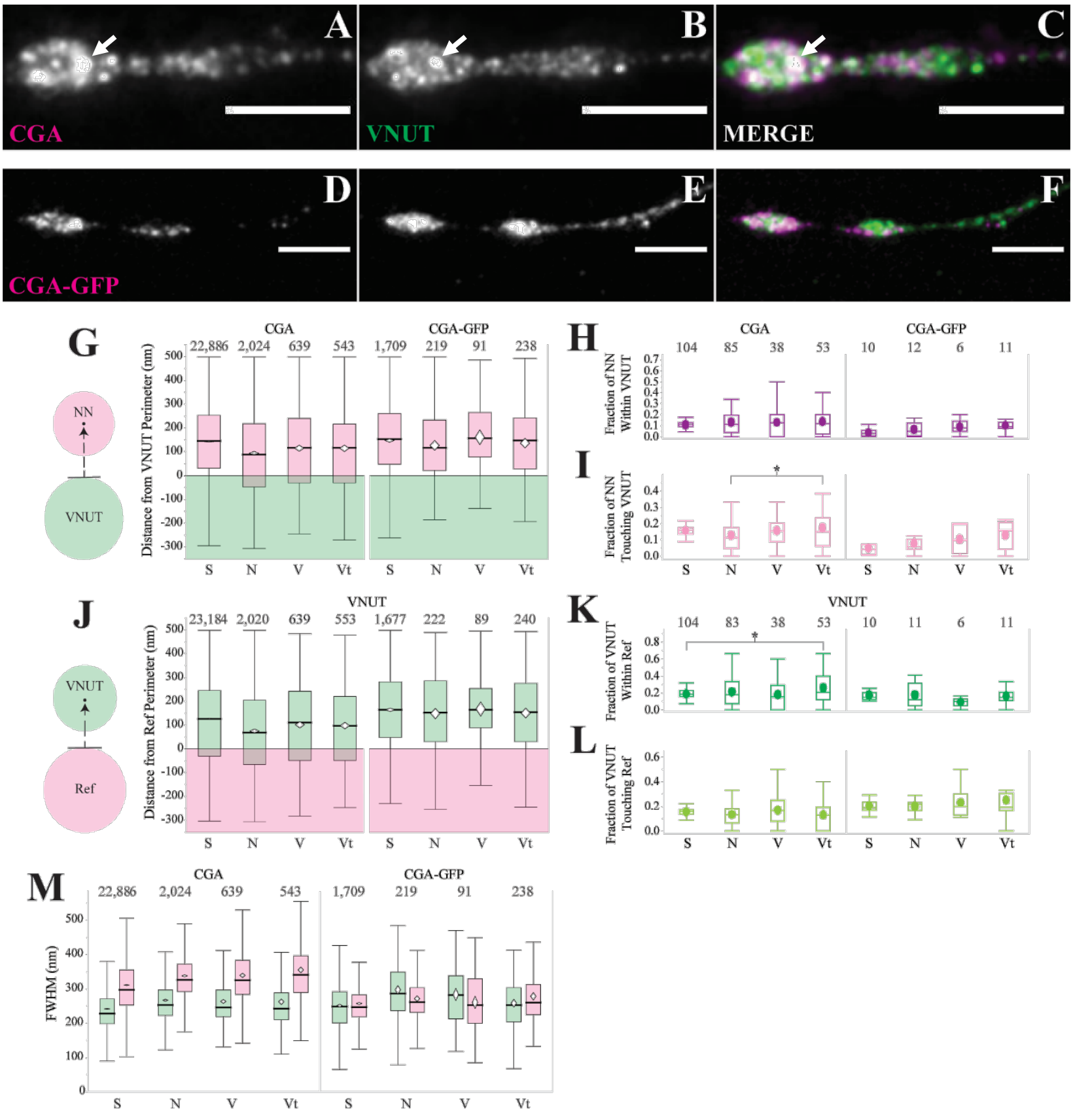

Figure 3.11 Quantification of colocalization between chromogranin A and exogenously expressed chromogranin A-GFP with VNUT

A-F: Scale bar = 5 µm. G,J,M: Numbers above each boxplot refer to n, number of puncta; diamonds illustrate 95% confidence interval of mean; bar indicates median value. H,I: NN, nearest neighbour (i.e., CGA or CGA-GFP). K,L: Ref, refers to reference protein (i.e., CGA or CGA-GFP). H,I,K,L: Numbers above each boxplot refer to N, number of cell parts analyzed; dots indicate mean value; bar indicates median value. M: VNUT is represented by the green boxplots on the left of each pairing; CGA and CGA-GFP are represented by pink boxplots on the right of each pairing. G-M: S, soma; N, neurite; V, varicosity; Vt, terminal varicosity.

3.2.5. VNUT does not Colocalize with the Catechomamine Transporter VMAT2

Previous work in rat tail artery suggested different molecular fingerprints between VNUT-containing purinergic vesicles and VMAT2-containing catecholaminergic vesicles. I tested this hypothesis by measuring the frequency of overlap between VNUT- and VMAT2-containing puncta (Fig 3.12). Immunostaining of VMAT2 and VNUT resulted in small puncta indicative of vesicles or clusters thereof (Fig 3.12A-C). Visually, few instances of overlap were observed, one of which is indicated with an arrow (Fig 3.12D-F). The segregation of VNUT and VMAT2 blobs in the images suggested that these proteins were organized by in an anti-colocalized manner. Averaged across all cell parts, the distance from the perimeter of VNUT reference puncta to the center of nearest neighbouring VMAT2 puncta was 146 nm (Fig 3.12G).

The average fraction of VNUT reference puncta containing their VMAT2 NN puncta within their perimeter was 11.1%, which breaks down to 10.9% for soma, 12.7% for neurites, 9.5% for varicosities, and 11.2% in terminal varicosities. Neurites and varicosities had statistically significant differences in means (Fig 3.12H). The mean frequency of VNUT puncta that touched their VMAT2 NN puncta was 16.1% across all cell parts. Within each cell part, the mean frequency of touching puncta was 15.9% in soma, 17.9% in neurites, 15.9% in varicosities, and 14.7% in terminal varicosities, with statistically significant differences in means between neurites and terminal varicosities (Fig 3.12I).

In a reverse MINER analysis with VMAT2 as the reference channel, the distance from the perimeter of VMAT2 to the center of the nearest neighbouring VNUT puncta was almost double the distance from perimeter for VNUT as the reference, with an average of 289 nm (Fig 3.12J). In order of soma to terminal varicosity, the average fraction of reference VMAT2 puncta containing their VNUT NN puncta within their periphery was 15%, 19.1%, 15.8%, and 16.7%, with an overall average of 16.7% (Fig 3.12K). The average fraction of reference puncta that touched their VNUT NN puncta was 16% for soma, 15.8% in neurites, 15.9% in varicosities, and 14.9% in terminal varicosities (Fig 3.12L). The overall average of VNUT-touching VMAT2 puncta was 15.7%.

The average size of VMAT2 puncta was 305 nm. The average size of VNUT-containing puncta was 266 nm (Fig 3.12 M).

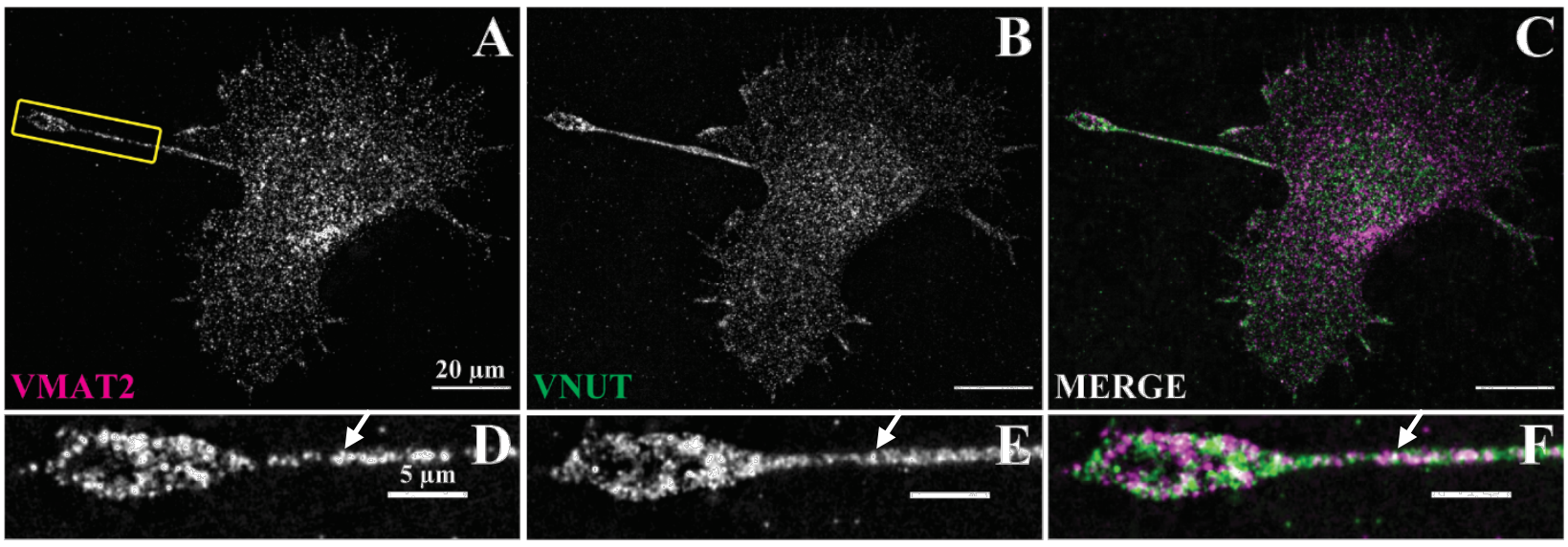

Figure 3.12 Lack of colocalization between VMAT2 and VNUT
A-C: Scale bar = 20 µm. D-F: Scale bar = 5 µm. G,J,M: Numbers above each boxplot refer to n, number of puncta; diamonds illustrate 95% confidence interval of mean; bar indicates median value. H,I: NN, nearest neighbour (i.e., VMAT2). K,L: Ref, refers to reference protein (i.e., VMAT2). H,I,K,L: Numbers above each boxplot refer to N, number of cell parts analyzed; dots indicate mean value; bar indicates median value. M: VNUT is represented by the green boxplots on the left of each pairing; VMAT2 is represented by pink boxplots on the right of each pairing. G-M: S, soma; N, neurite; V, varicosity; Vt, terminal varicosity.

The next four pages summarize all data pertaining to the colocalization analyses of each marker with VNUT in N2a cells. A graphical representation of the data is shown in Figure 3.13, followed by a series of tables (Table 3.4-3.9) that are a numerical summary of the colocalization analyses data. The values in each table are flanked by parentheses, which indicate the standard deviation.

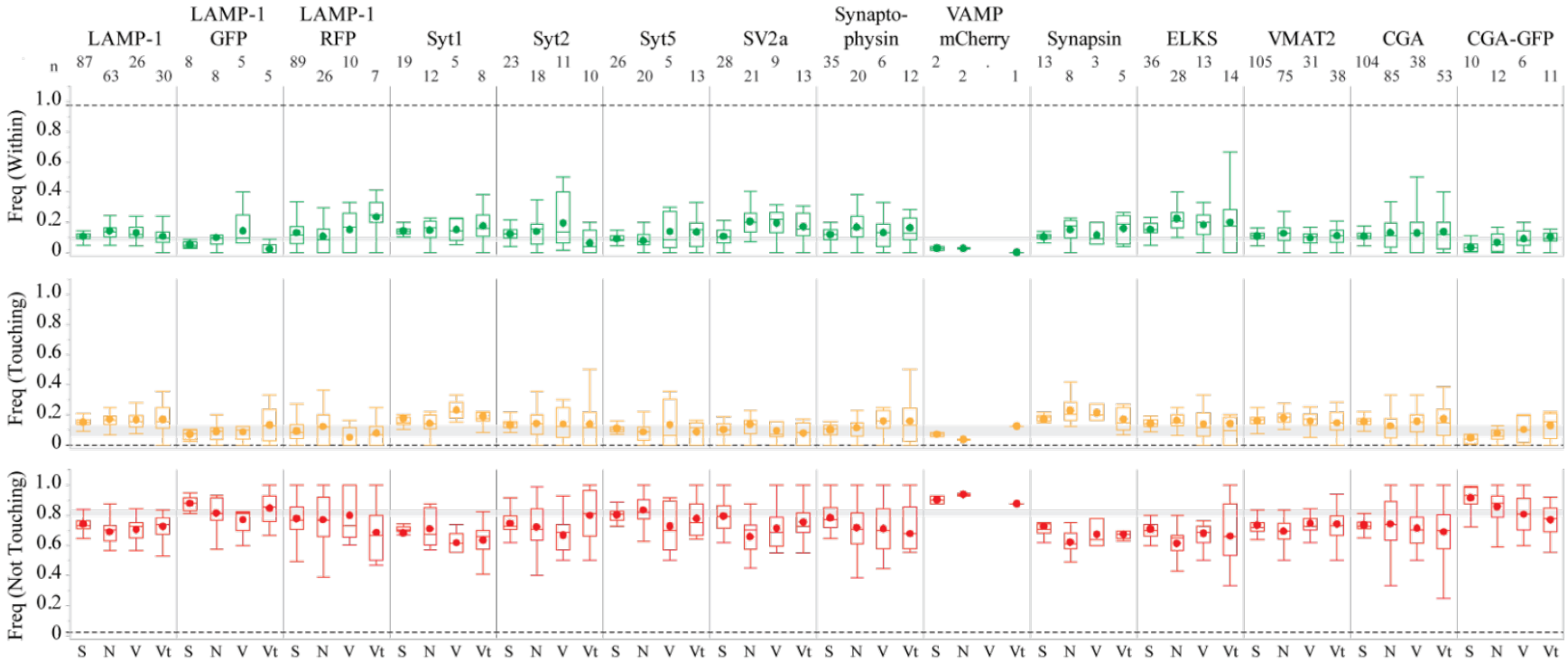

Figure 3.13 Summary of colocalization analyses in N2a cells

Each row of graphs illustrates the frequency of the corresponding degree of colocalization noted on the y-axis. The markers are labeled along the top and are grouped by vesicle population, from left to right: lysosomes (LAMP-1; LAMP-1-GFP; LAMP-1-RFP), synaptic vesicles (Syt1, 2, and5; SV2a; Synaptophysin; VAMP-mCherry; Synapsin; ELKS), catecholaminergic vesicles (VMAT2), and secretory vesicles (CGA; CGA-GFP). The values indicating a high degree of colocalization from the VNUT-self colocalization trial are shown (dotted lines) as well as the range of values that correspond to colocalization of LAMP-1/VMAT2 with VNUT due to random chance (grey bars). The numbers at the top of the graph denote n, number of cell parts. S, soma; N, neurite; V, varicosity; Vt, terminal varicosity.

Table 3.4 Distance from perimeter of VNUT reference puncta to center of NN puncta (in nm)

NN Puncta	Soma	Neurite	Varicosity	Terminal Varicosity	Average
CGA	143.3 (160)	94.3 (169.3)	115.2 (169)	115 (163.6)	117 (165.5)
CGA-GFP	147.4 (156.1)	126.6 (158.8)	161.2 (150.6)	136.7 (155.7)	143 (155.3)
LAMP-1	156.5 (153.3)	134.2 (159)	140.4 (160)	152.4 (156)	145.9 (157)
LAMP-1-GFP	162.1 (162.8)	113.8 (173.6)	166.6 (172.4)	196.4 (161.2)	159.7 (167.5)
LAMP-1-RFP	112.9 (195.6)	136 (183.4)	63.5 (184.5)	115.3 (227.1)	106.9 (197.7)
ELKS	143.5 (165.6)	122.2 (183.2)	127.5 (171.5)	148.2 (189.1)	135.4 (177.3)
Synapsin	174.2 (153.2)	127.8 (169)	139.5 (147.4)	169.8 (173.1)	152.8 (160.7)
SV2a	115.4 (170.5)	54.9 (171.5)	73.6 (190.1)	64.3 (184.3)	77 (179.1)
Synaptophysin	140.3 (169.3)	96.6 (185.1)	143.4 (180)	103.1 (170.2)	120.8 (176.1)
VAMP-mCherry	190.8 (150.7)	246.5 (163.8)	---	245.4 (136.2)	227.6 (150.2)
Syt1	145.8 (162.4)	116.9 (166.7)	110.8 (173.8)	122.2 (180.6)	123.9 (170.9)
Syt2	153 (168.7)	129.9 (169.4)	146.9 (171.8)	136.4 (169.5)	141.6 (169.8)
Syt5	149 (165.9)	125.6 (174.1)	152.8 (183.8)	115.3 (182.4)	135.7 (176.5)
VMAT2	154.1 (154.5)	132.2 (155.9)	153.1 (154.4)	146 (157.1)	146.4 (155.5)

Table 3.5 Distance from reference puncta perimeter to center of NN VNUT puncta from reversed MINER analyses (in nm)

NN Puncta	Reference Puncta	Soma	Neurite	Varicosity	Terminal Varicosity	Average
VNUT	CGA	127.8 (169.5)	75.6 (181.4)	101.4 (176.2)	98.3 (170.6)	100.8 (174.4)
VNUT	CGA-GFP	164.4 (158.8)	148.6 (165.2)	168 (142.7)	150.8 (165.4)	157.9 (158)
VNUT	LAMP-1	147.9 (156.2)	131.2 (162.2)	137.8 (162.7)	137.9 (163.4)	138.7 (161.1)
VNUT	LAMP-1-GFP	199.4 (177.9)	42.1 (180.9)	---	56 (220.3)	99.2 (193.1)
EGFP-N-VNUT	LAMP-1-RFP	131 (188.9)	107.9 (187.1)	136.7 (187.3)	71.7 (217.5)	111.8 (195.2)
VNUT-C-EGFP	LAMP-1-RFP	123.9 (190)	100.7 (187.7)	69.7 (198)	64.6 (190.2)	89.7 (191.5)
VNUT	ELKS	151.9 (162.5)	117.2 (168.8)	119.8 (176.1)	127.1 (172.9)	129 (170.1)
VNUT	Synapsin	163.8 (155.2)	130.7 (166.1)	138 (155.2)	151.3 (183.6)	145.9 (165)
VNUT	SV2a	148.8 (161.1)	90.9 (163)	87.9 (174.2)	80.8 (184)	102.1 (170.6)
VNUT	Synaptophysin	153.5 (161.6)	114.7 (169)	126.9 (168.7)	119.4 (168.6)	128.6 (167)
VNUT	VAMP-mCherry	136.7 (173.4)	153.2 (184.8)	---	136.6 (180.5)	142.2 (179.6)
VNUT	Syt1	158.9 (157.9)	123.7 (162.2)	146.1 (159)	125.3 (175.3)	138.5 (163.6)
VNUT	Syt2	182.3 (155.2)	156.1 (155.3)	166.8 (160.1)	170.2 (175.8)	168.9 (161.6)
VNUT	Syt5	165.2 (165)	170.7 (157.3)	206.5 (175.1)	151.1 (153.1)	173.4 (162.6)
VNUT	VMAT2	136 (164.7)	112.2 (178.3)	139 (171.4)	119 (166.8)	126.5 (170.3)

Table 3.6 Fraction of VNUT reference puncta with NN puncta within their periphery

NN Puncta	Soma	Neurite	Varicosity	Terminal Varicosity	Average
CGA	10.8 (3.1)	13.1 (11.6)	12.9 (11.4)	13.7 (12.5)	12.7 (9.7)
CGA-GFP	3.6 (3.4)	6.5 (6)	9.2 (6.7)	10.2 (5.8)	7.4 (5.5)
LAMP-1	10.6 (3.1)	14.2 (7.4)	13 (5.4)	10.7 (7.1)	12.1 (5.8)
LAMP-1-GFP	5.3 (2.1)	9.8 (6.5)	14.4 (14.4)	2.1 (3.8)	7.9 (6.7)
LAMP-1-RFP	13.1 (9.3)	10.8 (11.8)	15.1 (12.5)	23.5 (12.8)	15.6 (11.6)
ELKS	15.2 (4.5)	22.5 (9.1)	18.3 (8.6)	19.8 (20.3)	18.9 (10.6)
Synapsin	10.4 (3.9)	15.2 (7.7)	11.5 (7.5)	15.8 (9.8)	13.2 (7.2)
SV2a	10.7 (5.3)	20.5 (9.2)	19.4 (9.6)	17 (9.6)	16.9 (8.4)
Synaptophysin	11.8 (4.5)	16.8 (9.8)	13.2 (11.4)	16.4 (13.7)	14.6 (9.8)
VAMP-mCherry	2.9 (1.6)	2.8 (0.4)	---	---	2.8 (1)
Syt1	14.1 (2.3)	14.8 (7.3)	15.2 (7.5)	17.6 (11.7)	15.4 (7.2)
Syt2	12.3 (4.9)	13.9 (8.8)	19.4 (16.8)	6.3 (7.5)	13 (9.5)
Syt5	9.1 (3.2)	8 (5.5)	13.9 (12.9)	13.5 (9.8)	11.1 (7.8)
VMAT2	10.9 (3.3)	12.7 (7.1)	9.5 (4.4)	11.2 (7.2)	11.1 (5.5)

Table 3.7 Fraction of reference puncta with NN VNUT puncta within their perimeter from reverse MINER analysis

Reference Puncta	Soma	Neurite	Varicosity	Terminal Varicosity	Average
CGA	18.9 (5.4)	21.2 (16.8)	18 (16.8)	26.1 (21.3)	21 (15.1)
CGA-GFP	17.5 (8.1)	17.6 (15.4)	9.3 (5.6)	16.5 (9.9)	15.2 (9.7)
LAMP-1	13 (3.5)	16.7 (8.2)	16 (6.8)	15.4 (10.8)	15.3 (7.3)
LAMP-1-GFP	6.4 (8.4)	17.6 (25)	---	50 (70.7)	24.7 (34.7)
LAMP-1-RFP	12.8 (13.8)	10.2 (16.2)	14.4 (24.7)	12.7 (15.2)	12.5 (17.5)
ELKS	9.8 (2.3)	14.2 (6.3)	16.6 (11.3)	7 (8.6)	11.9 (7.1)
Synapsin	6.6 (2.8)	8.3 (6.2)	6.2 (1.7)	10.8 (5.8)	8 (4.1)
SV2a	15.4 (5.9)	25.8 (11.6)	30 (7.8)	35.2 (17.9)	26.6 (10.8)
Synaptophysin	13.3 (3.9)	19.2 (11.6)	13.4 (9.5)	14.5 (13.6)	15.1 (9.7)
VAMP-mCherry	20.9 (2)	16.7 (1.6)	---	16.7 (0)	18.1 (1.8)
Syt1	9.8 (4.6)	9.9 (8.2)	7.3 (8.1)	12 (7.7)	9.7 (7.1)
Syt2	9.8 (4.8)	9.6 (7.1)	9.7 (6.5)	10.2 (9.6)	9.8 (7)
Syt5	14.6 (4.1)	10.1 (6.9)	9.1 (11.7)	11.9 (11.4)	11.5 (8.5)
VMAT2	15 (3.5)	19.1 (8.5)	15.8 (7.2)	16.7 (9.2)	16.7 (7.1)

Table 3.8 Average puncta size, FWHM, of NN puncta (in nm)

NN Puncta	Soma	Neurite	Varicosity	Terminal Varicosity	Average
CGA	311.6 (96.4)	338.5 (75.6)	339.9 (84.4)	355.7 (102.1)	336.4 (89.6)
CGA-GFP	257.9 (66.4)	271.9 (62.2)	261 (87.2)	278.9 (87.8)	267.4 (75.9)
LAMP-1	272 (93.6)	293.8 (94.9)	287.8 (91.7)	289.5 (94.4)	285.8 (93.6)
LAMP-1-GFP	297.5 (130.2)	313.8 (114.7)	291.6 (120.5)	276 (89.5)	294.7 (113.7)
LAMP-1-RFP	306.7 (150)	346 (135.3)	324.7 (126.7)	331.6 (147.8)	327.3 (139.9)
ELKS	251 (126.2)	301 (135.2)	292.8 (145.3)	302.7 (131.8)	286.9 (134.6)
Synapsin	290.4 (113)	341.2 (114.7)	264.8 (84.7)	359 (130.7)	313.8 (110.8)
SV2a	285.3 (88.2)	314.3 (82.2)	315.2 (81.7)	340.9 (98.8)	313.9 (87.7)
Synaptophysin	249.6 (82.4)	271.7 (86.7)	282.6 (84.3)	264.6 (77.2)	267.1 (82.7)
VAMP-mCherry	301.8 (120.3)	322 (119.9)	---	354 (101.7)	326 (114)
Syt1	264 (94.2)	293.5 (96.1)	287.3 (101.2)	311.9 (91.3)	289.2 (95.7)
Syt2	272 (88.5)	288.7 (85.5)	292.1 (82.7)	294.4 (77.9)	286.8 (83.7)
Syt5	276.7 (102.4)	259.5 (71.2)	253.4 (67.7)	261 (73.3)	262.7 (78.7)
VMAT2	293 (97)	317.7 (96.8)	309.7 (87.8)	301.1 (84.1)	305.4 (91.4)

Table 3.9 Average puncta size, FWHM, of VNUT puncta (in nm)

NN Puncta	Soma	Neurite	Varicosity	Terminal Varicosity	Average
CGA	242.3 (72.7)	267.3 (68.3)	263.8 (70.4)	263 (98.2)	259.1 (77.4)
CGA-GFP	251.3 (91.3)	297.6 (94.1)	284.2 (86.2)	258.6 (90.9)	272.9 (90.6)
LAMP-1	249.7 (88.8)	271.4 (82.2)	263.4 (83.7)	262.2 (88.3)	261.7 (85.7)
LAMP-1-GFP	225.8 (86.8)	246.1 (96.3)	249.4 (127.8)	254.9 (79.8)	244.1 (97.7)
LAMP-1-RFP	278.8 (122.1)	245.4 (89.5)	276.4 (106.7)	231.5 (85.5)	258 (101)
ELKS	258.4 (73.7)	273.7 (57.5)	272.5 (74.9)	294.1 (112)	274.7 (79.5)
Synapsin	211.3 (69.8)	227.6 (72.8)	179.2 (58)	225.9 (59.6)	211 (65)
SV2a	265.5 (85.2)	313.3 (86.1)	302.1 (87.3)	317.7 (77.4)	299.7 (84)
Synaptophysin	275.2 (79.3)	307 (70.7)	308.5 (92.2)	299 (69.1)	297.5 (77.8)
VAMP-mCherry	178.2 (101.8)	168.6 (98.2)	---	183.5 (71.3)	176.8 (90.4)
Syt1	261.5 (80.9)	283.3 (89.7)	289.9 (66)	286.4 (72.4)	280.3 (77.2)
Syt2	269.6 (74.7)	297.3 (71.8)	291 (68.2)	288.2 (60.4)	286.5 (68.8)
Syt5	268.8 (75.8)	296.9 (72.9)	286.6 (59.4)	301.4 (86.8)	288.4 (73.7)
VMAT2	252.9 (87.7)	273.5 (82.2)	266.1 (80.3)	269.9 (85.7)	265.6 (83.9)

3.3. VNUT does not Colocalize with LAMP-1 in HEK293 and HeLa Epithelial Cell Lines

After observing infrequent colocalization between VNUT and LAMP-1 in N2a cells, I assessed whether the N2a cells were an ideal model for VNUT colocalization analysis. Since several researchers have reported lysosomal localization of VNUT, perhaps VNUT localization to lysosomes is characteristic of epithelial cells. I used human epithelial kidney 293 (HEK293) cells and HeLa human cervical cancer cells to test this working theory. The cells were gifted from SFU researchers T. Claydon and J. Guttman, respectively, and were given to me ready for fixing. Immunostaining, imaging, and analysis was performed in the same manner as for the N2a cells, described in Section 2.2.1. To distinguish epithelial cell extensions and swellings from N2a neurites and varicosities, I named these cell parts projections and nodes, respectively, Figure 3.14. Representative images and data pertaining to HEK- and HeLa-based experiments are shown in Figure 3.15.

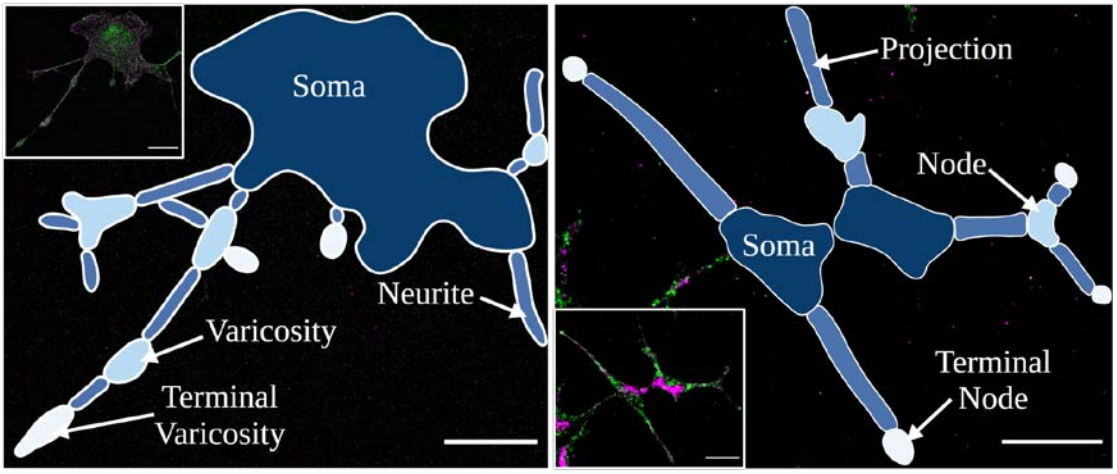

Figure 3.14 Annotated N2a and epithelial cell parts
The N2a cell (left) and HEK cell (right) have been annotated with their respective cell parts. HeLa cell parts were identified using the same method shown for HEK cells. Scale bar = 20 µm. Insets show original images without overlaid cell part tracings. N2a cell darkest to lightest blue: Soma, neurite, varicosity, terminal varicosity. HEK cell darkest to lightest blue: Soma, projection, node, terminal node. Created with BioRender.com.

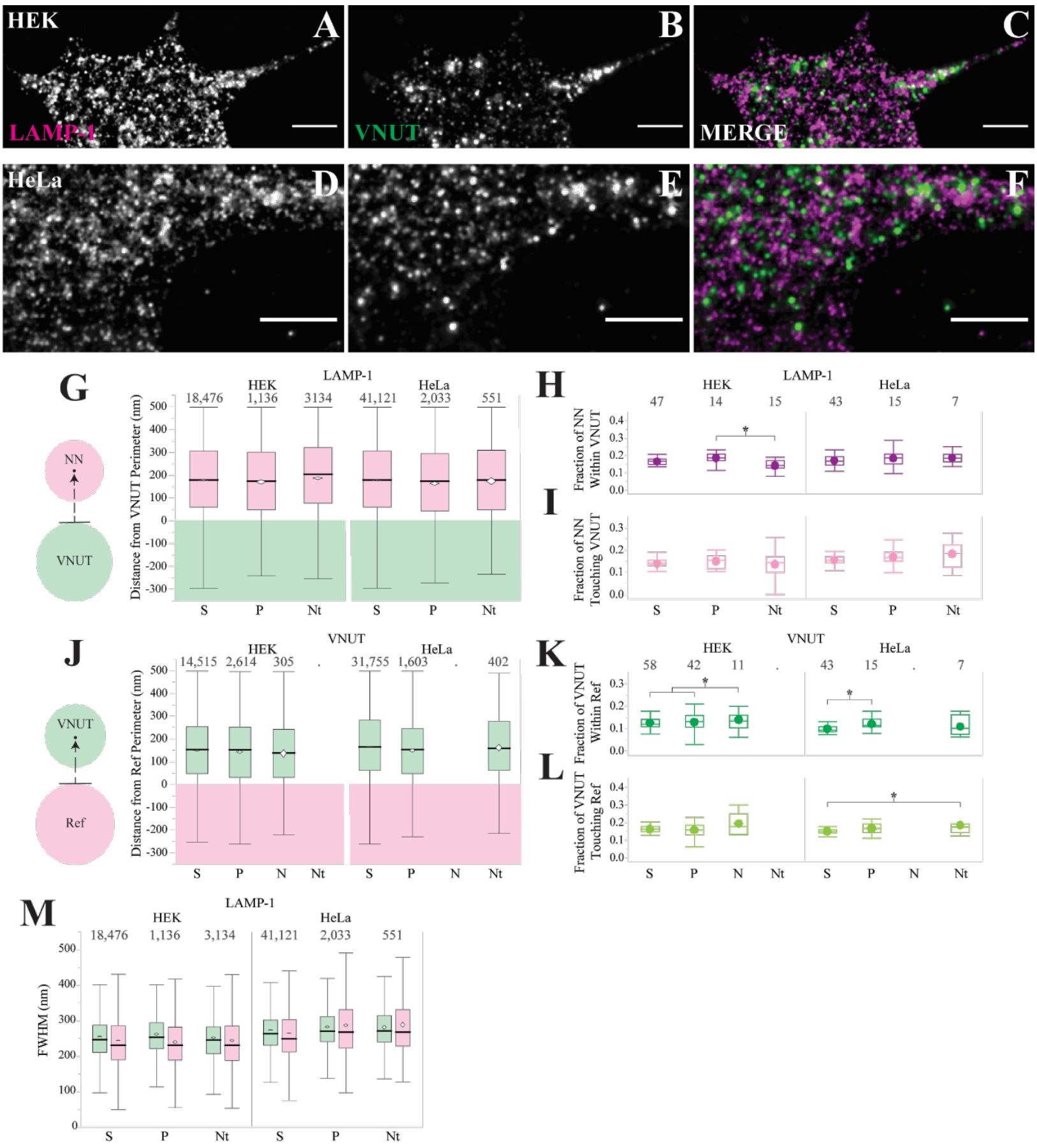

Figure 3.15 LAMP-1 and VNUT are anti-colocalized in epithelial cells

A-F: Scale bar = 5 µm. G,J,M: Numbers above each boxplot refer to n, number of puncta; diamonds illustrate 95% confidence interval of mean; bar indicates median value. H,I: NN, nearest neighbour (i.e., LAMP-1). K,L: Ref, refers to reference protein (i.e., LAMP-1). H,I,K,L: Numbers above each boxplot refer to N, number of cell parts analyzed; dots indicate mean value; bar indicates median value. M: VNUT is represented by the green boxplots on the left of each pairing; LAMP-1 is represented by pink boxplots on the right of each pairing. G-M: S, soma; P, projection; N, node; Nt, terminal node.

Like the N2a cells, immunolabeling VNUT and LAMP-1 resulted in punctate staining in both epithelial cell lines. Unlike the N2a cells in which LAMP-1 puncta were concentrated at the cell periphery and VNUT aggregated in the soma, the puncta were evenly distributed throughout the cell (Fig 3.15A-F). HEK cells exhibited infrequent overlap between LAMP-1 and VNUT fluorescent probes, as indicated by the arrow (Fig 3.15C). HeLa cells also exhibited minimal fluorescent overlap between VNUT and LAMP-1 (Fig 3.15F).

The average distance between the VNUT reference puncta perimeter to the center of their LAMP-1 NN puncta was 179 nm in HEK cells and 172 nm in HeLa cells (Fig 3.15G). VNUT-containing blobs had a LAMP-1 NN blob within their perimeter at similar average frequencies of 16.4% in HEK cells and 17.9% in HeLa cells. Statistically significant differences in means were detected between the projections (18.4%) and terminal nodes (14.2%) of HEK cells (Fig 3.15H). VNUT puncta touched their LAMP-1 NN puncta with an average frequency of 14.2% and 16.9% in HEK and HeLa cells, respectively (Fig 3.15I).

Reversing the MINER analysis such that LAMP-1 was the reference channel and VNUT was the NN channel reduced the average distance between puncta to 143 nm in HEK cells and 160 nm in HeLa cells. In HEK and HeLa cells, the average frequency of LAMP-1 puncta containing their VNUT NN puncta residing within their periphery was 13.1% and 10.9%, respectively. Statistically significant differences were reported between nodes (13.9%) and combined soma and projections (12.7%) in HEK cells, while HeLa cells reported a significant difference between soma (9.7%) and projections (12.1%) (Fig 3.15K). The average fraction of LAMP-1 puncta that touched their assigned NN VNUT puncta was 17.2% and 16.8% in HEK and HeLa cells, respectively. The soma and terminal nodes of HeLa cells reported statistically significant differences in means with an average of 15.1% puncta touching in soma and 18.6% in terminal nodes (Fig 3.15L).

The average size of LAMP-1 puncta was 243 nm in HEK cells and 281 nm in HeLa cells. The epithelial LAMP-1 puncta were slightly smaller than their N2a counterparts, which had an average size of 303 nm. In comparison, the average size of VNUT-containing puncta in both epithelial cell lines were similar to N2a cells. HEK cells reported an average VNUT puncta size of 257 nm and HeLa cells 280 nm (Fig 3.15M), while the collective average size of VNUT puncta in N2a-based LAMP-1 analyses was 255 nm.

Tables 3.10-3.13 summarize the data I analyzed during my colocalization analyses in HEK and HeLa cells, with standard deviations in parentheses.

Table 3.10 Summary of physical data from HEK and HeLa colocalization analysis

Distance from VNUT Perimeter (nm)	Cell Type	Soma	Projection	Terminal Node	Average
	HEK	177.9 (172.5)	170.6 (173.3)	187.1 (171.2)	178.5 (172.3)
	HeLa	177.5 (173.4)	164.2 (176.7)	174.2 (178.2)	171.9 (176.1)
LAMP-1 FWHM (nm)	Cell Type				
	HEK	244.9 (85.9)	240.4 (76.8)	244.4 (97.5)	243.3 (86.7)
	HeLa	265.3 (80.1)	287.4 (92)	289 (87.2)	280.6 (86.4)
VNUT FWHM (nm)	Cell Type				
	HEK	255.4 (77.5)	262.3 (72.5)	252.2 (75.7)	256.6 (75.2)
	HeLa	274 (72.6)	282.9 (71.2)	281.7 (68)	279.5 (70.6)

Table 3.11 Summary of physical data from HEK and HeLa reverse MINER colocalization analysis

Distance from Ref Perimeter (nm)	Cell Type	Soma	Projection	Node	Terminal Node	Average
	HEK	150 (153.3)	143.4 (155.9)	136.3 (156.5)	---	143.2 (155.2)
	HeLa	166.8 (155.2)	149.6 (151)	---	162.1 (152.8)	159.5 (153)
LAMP-1 FWHM (nm)	Cell Type					
	HEK	272.6 (88.2)	284.9 (77.6)	275.5 (72.9)	---	277.6 (79.6)
	HeLa	286.1 (79.4)	297.6 (87)	---	295.4 (77.4)	293 (81.3)
VNUT FWHM (nm)	Cell Type					
	HEK	215.7 (77.1)	224.1 (73.9)	221.7 (76.7)	---	220.5 (75.9)
	HeLa	251.8 (72.8)	271 (82.9)	---	272.5 (83.8)	265.1 (79.8)

Table 3.12 Degree of colocalization between VNUT reference puncta and LAMP-1 NN puncta in HEK and HeLa cells

	Cell Type	Soma	Projection	Terminal Node	Average
Within	HEK	16.5 (3.3)	18.4 (3.3)	14.2 (5.2)	16.4 (3.9)
	HeLa	16.9 (3)	18.3 (4.8)	18.5 (3.6)	17.9 (3.8)
Touching	HEK	13.8 (3.1)	15.1 (3.2)	13.7 (5.9)	14.2 (4.1)
	HeLa	15.5 (1.9)	16.9 (3.8)	18.4 (6.4)	16.9 (4)

Table 3.13 Degree of colocalization between LAMP-1 reference puncta and VNUT NN puncta in reverse MINER analysis in HEK and HeLa cells

	Cell Type	Soma	Projection	Node	Terminal Node	Average
Within	HEK	12.6 (2.6)	12.7 (4.1)	13.9 (5.3)	---	13.1 (4)
	HeLa	9.7 (1.4)	12.1 (3.5)	---	10.8 (4.4)	10.9 (3.1)
Touching	HEK	16.4 (2)	15.9 (4.6)	19.4 (6.1)	---	17.2 (4.2)
	HeLa	15.1 (1.7)	16.6 (3)	---	18.6 (7.2)	16.8 (4)

3.4. Possible VNUT Localization to the ER-Golgi Complex

Despite VNUT failing to colocalize with the tested markers, a distinct pattern of localization was observed. Puncta containing immunolabeled and genetically encoded VNUT were capable of trafficking out to neurites and varicosities. However, large clusters of high-intensity VNUT signal were consistently seen in the perinuclear region of the soma, Figure 3.16. Similar localization patterns were also observed in other experiments in the Poburko lab. Experiments validating pH sensitive fluorescent probes VMAT2-pHuji and VNUT-pHluorin for visualizing the release of catecholaminergic- and ATP-containing vesicles, respectively, were tested in N2a cells, shown in Figure 3.17.

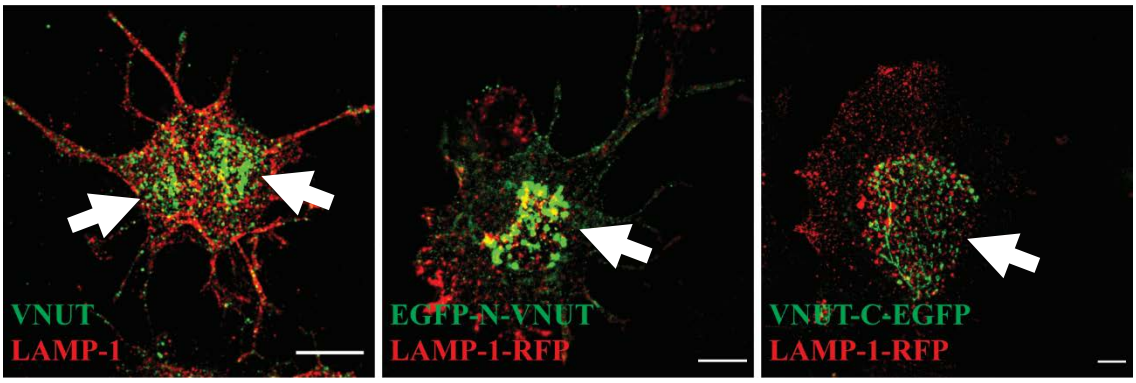

Figure 3.16 Perinuclear localization of VNUT in N2a cells
Images were taken at 100X oil magnification. The leftmost image shows immunolabeled VNUT and LAMP-1, while the center and rightmost images show exogenous N-terminal and C-terminal conjugated VNUT-EGFP expression vectors, respectively. The VNUT-EGFP vectors were co-transfected with LAMP-1-RFP. In all three images, the VNUT probe is shown in green. The LAMP-1 probes are shown in red. Perinuclear regions are indicated by arrows. Scale bar = 10 µm.

These constructs are similar in composition and function. The cartoon in Figure 3.17 demonstrates the conditions required for quenching and dequenching the pHluorin construct. Although not shown, the pHuji construct works in a similar manner for catecholaminergic vesicles. Conjugation of the fluorescent proteins on a luminal loop of each transporter causes the pH sensitive fluorescent proteins to be quenched in acidic compartments, such as synaptic vesicles, lysosomes, and endosomes. Exposure to less acidic pH levels, like the extracellular space during a vesicle fusion event, dequenches the probes. The resulting fluorescent signal is maintained for the duration of exposure of externalization. These genetically encoded transporters were conjugated to red (pHuji) and green (pHluorin) fluorescent proteins to allow simultaneous imaging of VMAT2 and VNUT, respectively (Fig 3.17B).

The pH sensitive VNUT and VMAT2 constructs illustrate the different release kinetics and pH responses of their respective compartments, illustrated by manipulating extracellular and intracellular pH using saline solutions buffered with 2-(N-morpholino)ethanesulfonic acid (MES), sodium butyrate (Na.butyrate), or ammonium chloride (NH_4Cl) (Sankaranarayanan, De Angelis, Rothman, & Ryan, 2000). Reminiscent of my own experiments, compartments labeled with the VNUT-pHluorin probe were primarily clustered in the perinuclear space. Based on the pH dependent excitation and emission spectra of pHluorin (Miesenböck, De Angelis, & Rothman, 1998), these puncta appear to have a slightly acidic or near-neutral pH (Fig 3.17B). VNUT-pHluorin was not

quenched in response to MES buffered saline (pH 5.5) but was quenched in the presence of 20 mM sodium butyrate (Fig 3.17B). This membrane permeable, weak acid decreases the cytosolic pH of rat crypt cells (Diener, Helmle-Kolb, Murer, & Scharrer, 1993) and was used to reversibly decrease luminal pH. The VNUT-pHluorin probe exhibited moderately increased fluorescence in response to NH_4Cl solution (Fig 3.17B). NH_4Cl dissociates into the weak base NH_4^+, followed by the membrane permeable gas NH_3 (Lazarenko, DelBove, Strothman, & Zhang, 2017) that increases cytosolic and luminal pH. These results indicate the VNUT-pHluorin-containing compartments are not readily externalized, are localized to the perinuclear space, and have a pH that is not compatible with synaptic vesicles. Conversely, the VMAT2-pHuji construct was localized to highly acidic compartments that were capable of externalization. Externalized VMAT2-pHuji probe fluoresced when exposed to HEPES buffered saline solution (pH 7.4). Extracellular acidification using MES buffered saline quenched the VMAT2-pHuji probe. Further, the VMAT2-pHuji probe experienced a robust response to NH_4Cl, while intracellular acidification with sodium butyrate did not cause further quenching (Fig 3.17B). These results are indicative of VMAT2 localization to synaptic vesicles, while VNUT seems to localize to perinuclear organelles bearing similar pH and morphologies to the ER/Golgi complex.

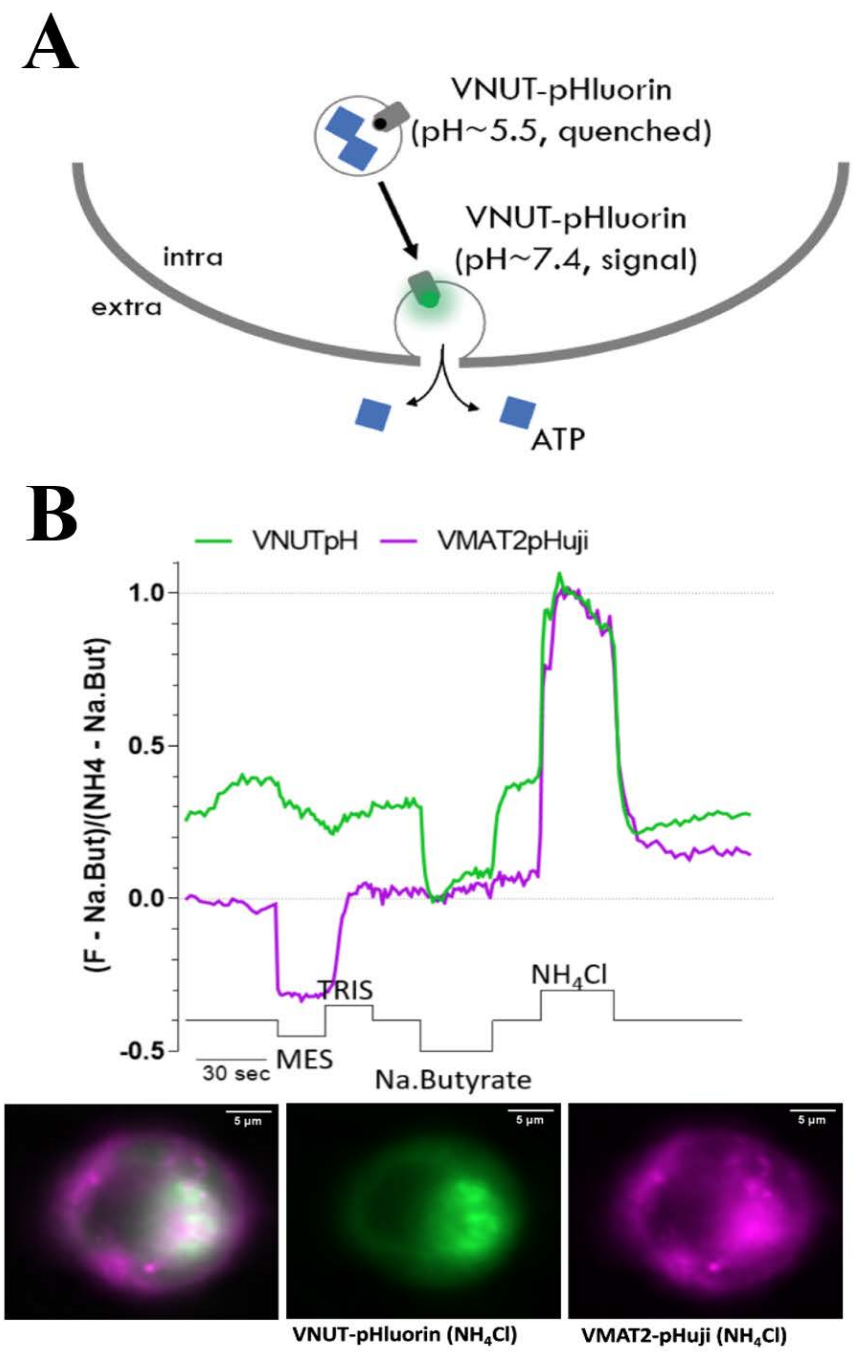

Figure 3.17 VNUT-pHluorin construct localizes to ER/Golgi complex
A: In the cartoon, ATP molecules are represented by blue squares, VNUT-pHluorin is shown by the grey bar (VNUT) with the black or green circle representing quenched and unquenched pHluorin, respectively. The thick grey curve is the plasma membrane while the thin grey circles are synaptic vesicles. B: Traces are normalized to the fluorescence change of the pH-sensitive probes relative to the range of intensity. The response of VMAT2-pHuiji is shown in purple while the response of VNUT-pHluorin is shown in green. The stimuli and duration of exposure are noted by the black trace along the x-axis. From left to right, the images below the traces show the 2-channel merge of VNUT-pHluorin and VMAT2-pHuiji, the isolate channel for VNUT-pHluorin, and the isolated channel for VMAT2-pHuji. Scale bar = 5 µm. Traces and images were provided courtesy of Lara Gastaldello and Damon Poburko from the Poburko lab (unpublished data).

Chapter 4.

Bioinformatic Study of VNUT and SLC17 and SLC18 Transporter Families

4.1. Structural Comparison of VNUT and other Solute Carrier Transporters

4.1.1. Studying VNUT Structure

This chapter describes my comparative study of the VNUT C-terminus with the C-termini of other solute carriers of the 17 and 18 families. The study began by corroborating the secondary structure of VNUT, which allowed the identification of the predicted transmembrane domains. The predicted C-terminal domain of VNUT was assessed for common targeting motifs, which could hint to the subcellular localization of VNUT. Figure 4.1 illustrates some of the motifs for which VNUT was assessed.

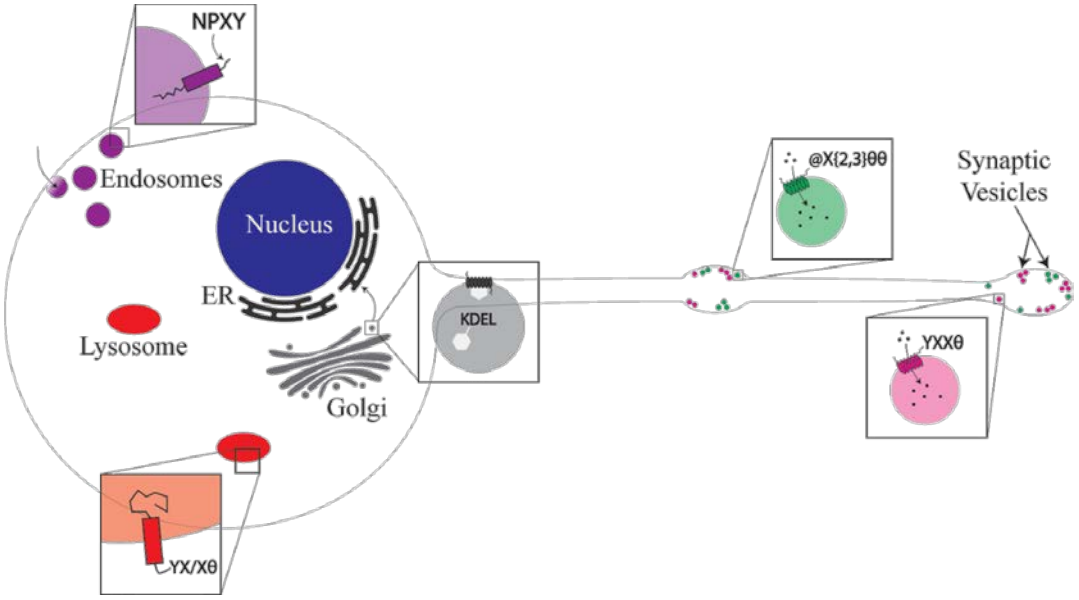

Figure 4.1 An overview of common C-terminal targeting motifs
Purple: low density lipoprotein receptor with NPXY internalization motif. Red: LAMP-1 with YXXθ lysosome targeting sequence. Grey: ER resident with KDEL receptor recognition motif. Green: Solute carrier with dileucine-like internalization and/or synaptic vesicle targeting motif (@X{2,3}θ). Pink: VAChT with tyrosine motif (YXXθ). Partially created with BioRender.com.

In addition to discovering that VNUT is encoded by the *SLC17A9* gene, Sawada and colleagues analyzed homologies between members of the SLC17A family to identify possible transmembrane domains (Sawada et al., 2008). I sought to validate their prediction to provide an updated prediction of C-terminal domain length from the last predicted transmembrane domain. Additionally, our lab was interested in comparing the cytosolic loops of the SLC17A family members to guide optimal insertion of pH sensitive probes into VNUT without impeding function or trafficking. Finally, the structural data acquired via this thesis can be used as a foundation to future bioinformatics-based studies of the conservation, or lack thereof, in the cytosolic domains of VNUT.

I first sought to assess the online constrained topology prediction software (CCTOP). CCTOP provides a consensus of ten topology prediction methods to provide a best guess estimate of the transmembrane domains within a protein (Dobson, Reményi, & Tusnády, 2015a, 2015b). I compared the predicted secondary structure of VNUT with the homology-based predictions made by Sawada (Sawada et al., 2008) and SWISS-MODEL, an interactive modeling server that predicts secondary structures based on homology to solved protein structures within the repository. The SWISS-MODEL method used the VGLUT2 transporter of *Rattus norvegicus* (SWISS-MODEL ID: Q9JI12) as the reference model for homology-based predictions of the VNUT secondary structure. Figure 4.2 illustrates the VNUT transmembrane domains as predicted by Sawada, CCTOP, and SWISS-MODEL.

The CCTOP prediction corroborates the initial SLC17-based homology performed by Sawada and colleagues (Sawada et al., 2008). Unexpectedly, the VGLUT2-based SWISS-MODEL method predicted ten transmembrane domains in VNUT. This is odd given there are 12 transmembrane domains in the related SLC17A family member VGLUT2. However, the ten transmembrane domains in the unsolved VNUT structure correspond to CCTOP-predicted domains within a few amino acid residues (Fig 4.3). The protein sequences of human VNUT (NCBI accession Q9BYT1.2) and *R. norvegicus* VGLUT2 (NCBI accession Q9JI12.1) were also aligned using CLC Genomics Workbench. The alignment showed 21.53% sequence identity in CLC whereas the SWISS-MODEL repository reports 26.20% sequence identity. This discrepancy can be explained by ten C-terminal residues in the VNUT sequence (VDLSSTHEDL) that are ignored by the VGLUT-based model. Conversely, entering the VGLUT2 Fasta sequence into CCTOP resulted in twelve transmembrane domains that closely coincide with the

solved secondary structure in the SWISS-MODEL repository (Fig 4.3). Further, the CCTOP topology prediction method was validated using 170 test sequences with predictions as accurate as 95% (Dobson et al., 2015a). Of the two independent methods of assessing topology, the CCTOP method was chosen to predict and compare the secondary structure of VNUT and other solute carriers of the 17A and 18A families.

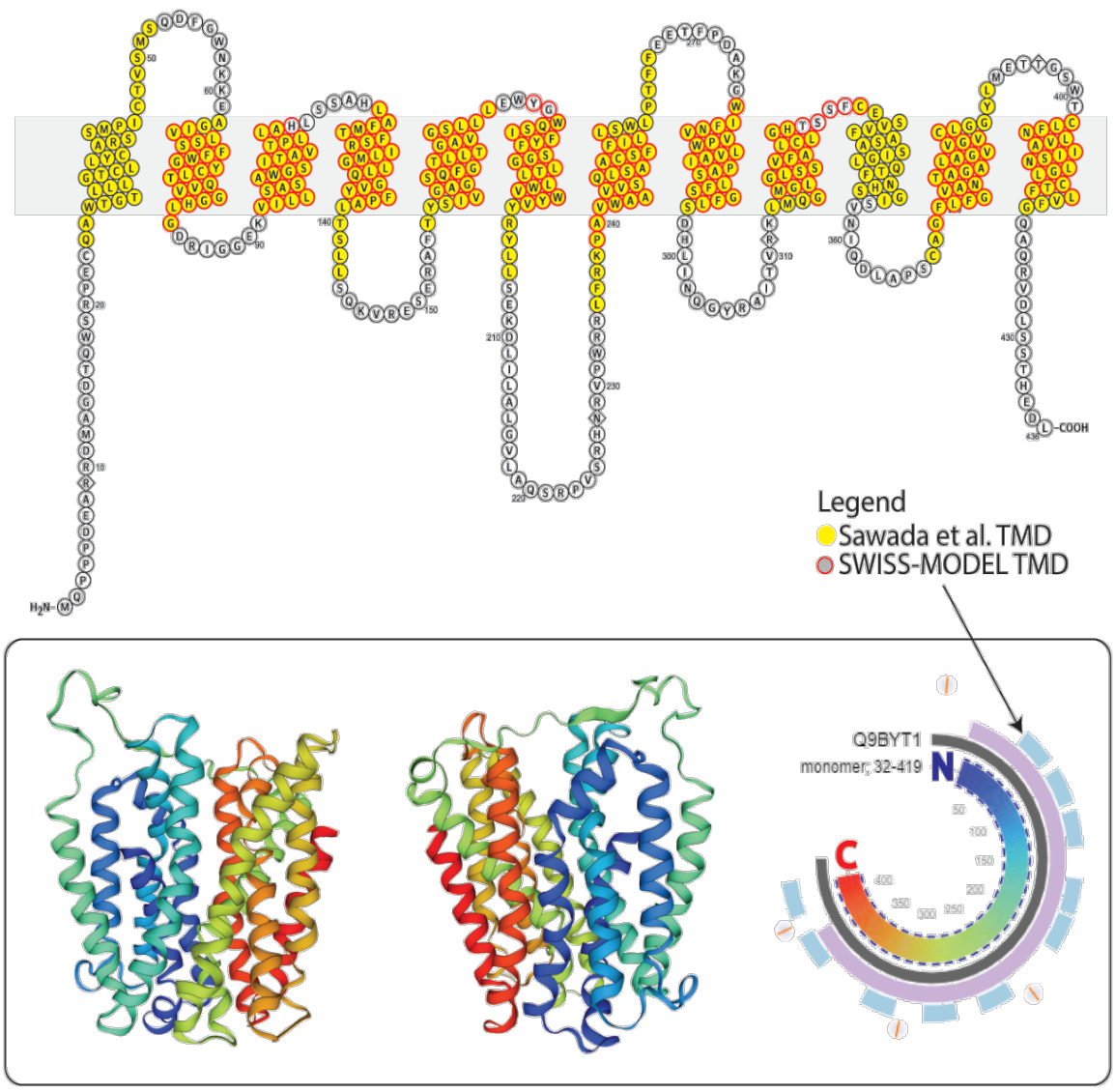

Figure 4.2 Predicting VNUT structure
Top: Transmembrane domains as predicted by Sawada are shown with yellow fill. SWISS-MODEL homology model-based TMDs are outlined in red. Physical arrangement as shown was predicted by CCTOP software. Bottom: Structural illustration of VNUT from SWISS-MODEL prediction. The N-terminus is shown in blue. The C-terminus shown in red.

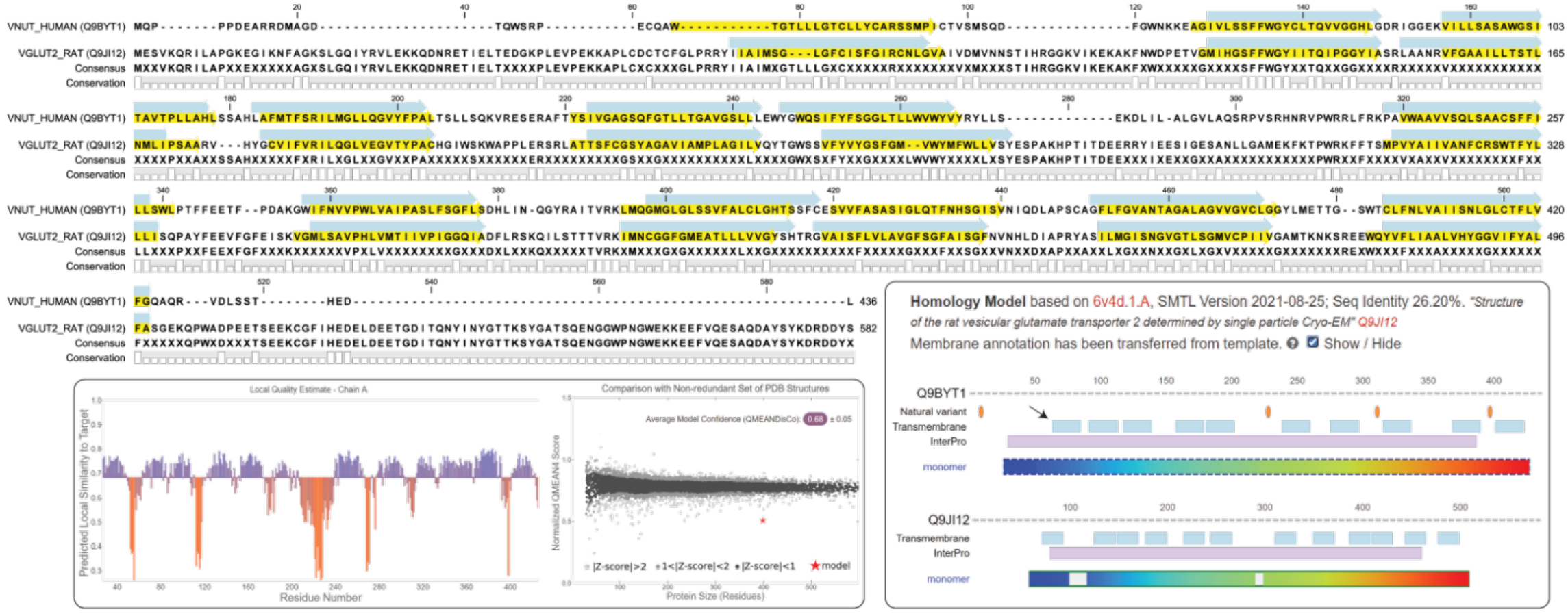

Figure 4.3 Structural prediction of human VNUT based on the VGLUT2 transporter of the Norway rat
Top: Alignment shows VGLUT2 and VNUT protein sequences. The transmembrane domains as predicted by CCTOP are highlighted in yellow. Transmembrane domains predicted by the SWISS-MODEL are highlighted in blue. The first and tenth CCTOP-predicted domains are missing from the SWISS-MODEL prediction. Bottom left: SWISS-MODEL quality estimate information illustrates poor model quality. The star at far right shows how the model performs compared to the repository. Bottom right: Human VNUT (Q9BYT1) and rat VGLUT2 (Q9JI12) schematics with transmembrane domains shown in blue blocks (arrow, correspond to blue highlighting in alignment).

When comparing primary amino acid sequences of VNUT, SLC17A, and SLC18A transporters, the VNUT sequence is consistently shorter regardless of organism Class, Figure 4.4. In Class Mammalia, the N-terminus varies greatly in length, from 15 amino acids in White-throated Capuchin monkeys to 132 amino acids in Bison (Fig 4.5A). Conversely, the C-terminal domain is consistently comprised of 13 amino acids after the last predicted transmembrane domain (Fig 4.5A). These 13 amino acids are highly conserved in mammals (Fig 4.5B).

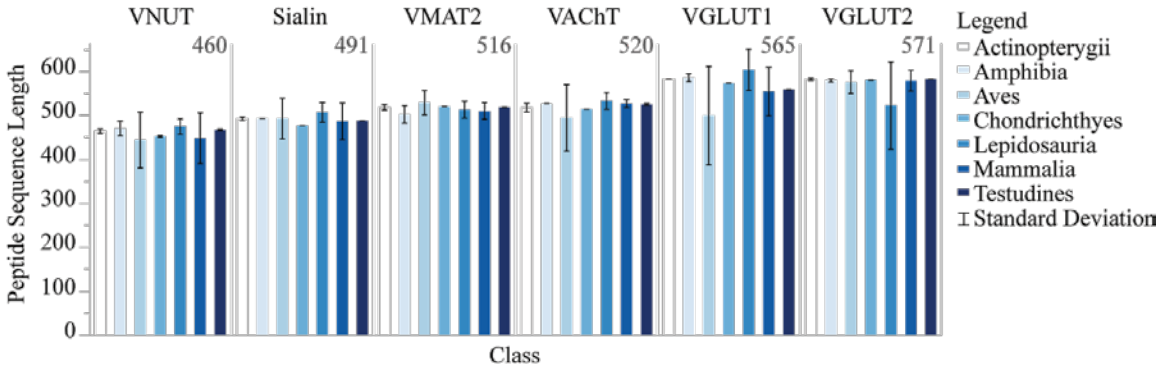

Figure 4.4 Comparison of transporter sequence lengths
The numbers under the common names of each transporter reports the average sequence length across 7 analyzed Classes of chordate animals. Error bars indicate the standard deviation between accession numbers within each Class.

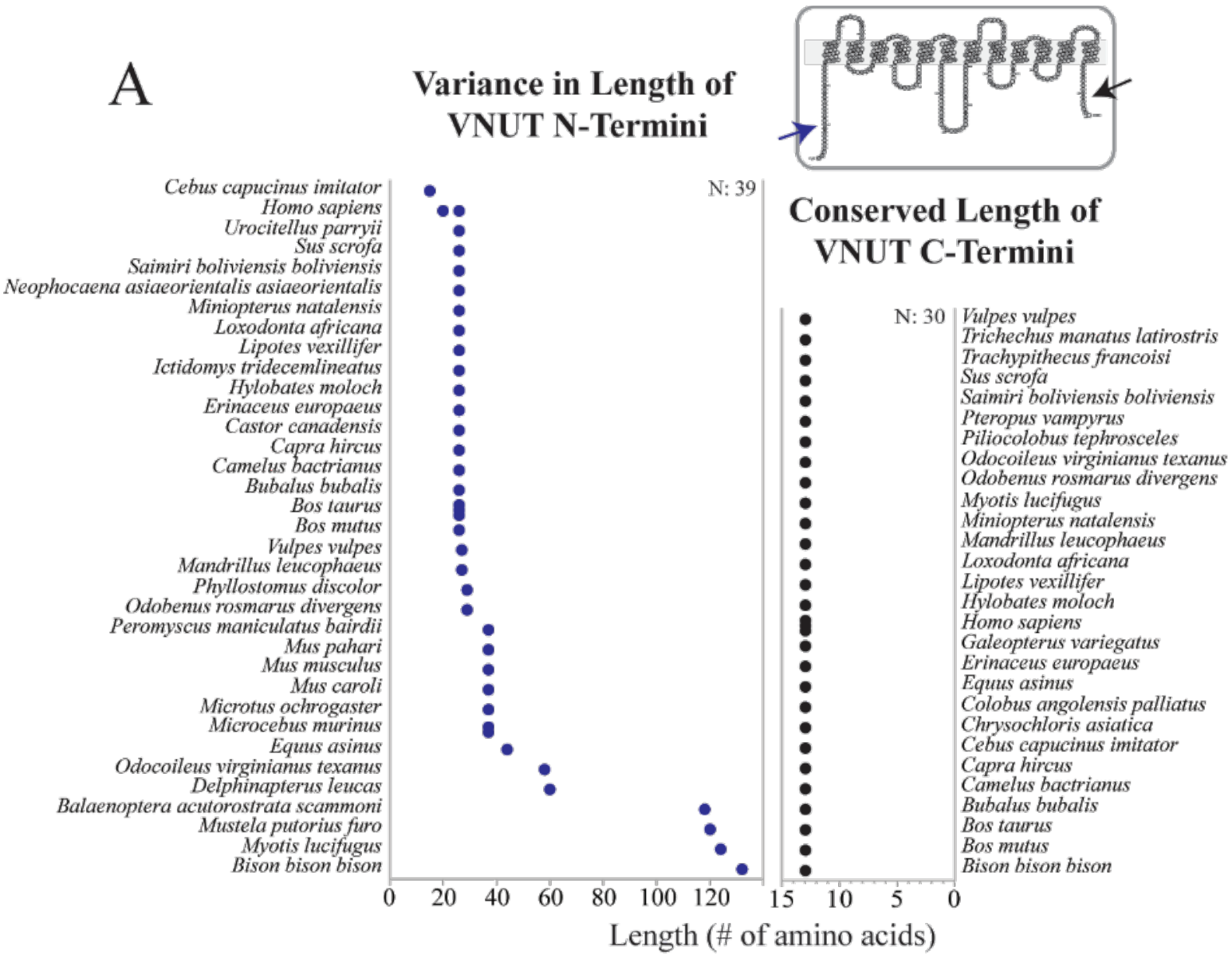

B

Conserved Sequence of VNUT C-Termini

```
human (NP_071365)                          ETTGSWTCLFNLVAIISNLGLCTFLVFGQAQRVDLSSTHEDL 42
dog (XP_543091)                            .......SM.....A..G.......L..E.......P..... 42
red fox (XP_025870919)                     .......SM.....A..G.......L..E.......P..... 42
Grizzly Bear (XP_026359667)                .......SM.....AV.S.......L..E.......P..... 42
Pacific walrus (XP_012421261)              .......SM.....AV.S.......L..E.......P..... 42
Hawaiian monk seal (XP_021533457)          .......SM.....AV.S.......LL.E.......P.R... 42
harbor seal (XP_032243559)                 .......SM.....AV.S.......LL.E.......P.R... 42
Steller sea lion (XP_027946961)            .......SV.....AV.S.......L..E.......P..... 42
domestic cat (XP_023106779)                .......SM.S...A..S....I..L..E.......P..... 42
puma (XP_025787896)                        .......SM.S...A..S....I..L..E.......P..... 42
Bison (XP_010834955)                       .......SV.....A..S..........K.......PA.... 42
cattle (NP_001093848 XP_596244)            .......SV.....A..S..........K.......PA.... 42
water buffalo (XP_006068912)               .......SV.....A..S..........K.......PA.... 42
pig (XP_020933896)                         ......ASV.....AV.S....I.....K.......PA.... 42
Yangtze River dolphin (XP_007462313)       .......SV.....A..S..........K..Q....PA.... 42
Common Minke Whale (XP_007185485)          .......SV...A.A..S........L.K.......P..... 42
domestic ferret (XP_012915577)             ......ASM.....AVGS.......L..E.......PA.... 42
ass (XP_014704638)                         .......SV.....A..S............K.....PA.... 42
western European hedgehog (XP_016042416)   .......SV.....A..S....N..L..K.....Q.AS..N. 42
Bolivian squirrel monkey (XP_003932711)    ..............................PSR.E. 42
house mouse (NP_898984)                    ........V.H..........G......K......VP..... 42
Norway rat (NP_001102083 XP_001059811 XP_342602) ........V.H....V.....G......K......VP..... 42
Chinese hamster (EGW11064)                 .A.......I............G......K......AP..... 42
American beaver (XP_020029313)             .A.......V............G.............IPA.... 42
degu (XP_023560125)                        .A...................G..............P.R... 42
Bactrian camel (XP_010952673)              .......SV.....A..S..........K.......P..... 42
gray mouse lemur (XP_020137329)            .......Y.......T....................P..... 42
small-eared galago (XP_012659420)          .......S..Y....V....................P..... 42
African savanna elephant (XP_023396611)    .......S......VV..........K.......PA.... 42
Florida manatee (XP_004370244)             .I.....S......VV...........K.H.L...PA.... 42
Philippine tarsier (XP_008067736)          ......A...Q...V................R....NPS.Q.. 42
koala (XP_020837214)                       .A.....SV............M.....E.....F..AY... 42
Consensus                                  ETTGSWTSVFNLVAAISSLGLCTFLVFGKAQRVDLSPTHEDL
Conservation
```

Figure 4.5 Comparison of N- and C-terminal lengths of VNUT in mammals
A. Blue dots in the left graph shows the variation of sequence length across 39 mammals. The N-terminus is indicated in the schematic (blue arrow). The right graph shows high level of sequence length conservation in C-terminus (black dots), which is indicated in the protein structure schematic by a black arrow. N refers to the number of accession numbers. Some species had multiple accession numbers. For example, there are 28 species listed for the C-terminal analysis, yet 30 sequences were analyzed. *Homo sapiens* had three separate accession numbers that were analyzed. B. The C-terminal domain is highly conserved at the amino acid level. To the left of each sequence is the common name of the animal, followed by the accession number(s). The last transmembrane domain is highlighted within several sequences. The numbers at the end of each sequence denotes the total number of amino acids shown for each sequence.

In addition to identifying general structural differences in VNUT and the other transporters, I wanted to assess possible targeting motifs within VNUT. Chapter 1, Sections 1.3.2 and 1.3.3 explain in greater detail some of the known targeting motifs for synaptic vesicles, lysosomes, Golgi, ER, and nucleus. Known targeting motifs of other transporters and synaptic vesicle proteins are typically found in the C-terminal domain. For example, the C-terminal domain of VAChT is necessary and sufficient for targeting to synaptic vesicles. In PC12 cells, a chimera protein consisting of the plasmalemmal Tac protein conjugated with the VAChT C-terminus is redirected to synaptic vesicle-like vesicles (Colgan et al., 2007). VAChT and VMAT2 chimeras in which the C-terminal tails were swapped resulted in each recombinant protein being targeted as dictated by the C-terminus (Varoqui & Erickson, 1998). In the VGLUT transporters, C-terminal dileucine-like motifs are important for targeting to synaptic vesicles (Haiyan Li et al., 2017). Similarly, synaptic vesicle proteins synaptotagmin, synaptophysin, and synaptobrevin contain dileucine-like motifs in their C-termini (Prado & Prado, 2002). Due to the importance of the C-terminus for other transporters and synaptic vesicle proteins, as well as the high degree of conservation amongst mammalian VNUT C-termini, the motif analysis was focused on the C-terminal domain.

4.1.2. Comparison of Targeting Motifs in SLC Transporter Proteins

I assessed 295 chordate VNUT sequences for targeting motifs identified from primary literature. I compared the motifs in the C-terminus of VNUT to 493 chordate sequences for SLC17A5-8 and SLC18A1-3. Figure 4.6 illustrates the workflow for assessing the presence of targeting motifs within these transporters. SLC17A1-4 were excluded from the motif analysis for two reasons. One, topology predictions suggest SLC17A2 and SLC17A3 have 11 transmembrane domains, while SLC17A4 has eight. Comparing VNUT to transporters with 12 transmembrane regions allows more direct comparisons to be made when interpreting the importance of each motif. Further, biochemical properties like transport dynamics, localization, function and inhibition of SLC17A1-4 are less well-known compared to sialin, the VGLUTs, VAChT, and VMAT2 (Omote & Moriyama, 2013; Reimer, 2013; Wimalasena, 2011).

Although I hypothesized that VNUT is localized to synaptic vesicles, I examined the C-terminus for additional motifs such as those that target proteins to lysosomes, peroxisomes, endosomes, internalization at the plasma membrane, the Golgi apparatus,

the endoplasmic reticulum (ER), and the nucleus. Since the three- and two-wild card dileucine-like motifs may be involved in synaptic vesicle and/or internalization trafficking (Pandey, 2009; Prado & Prado, 2002), both motifs were combined into a shared @X{2,3}θθ motif. Residue labeling is based on normalized nomenclature (Aasland et al., 2002). For example, the θ symbol represents a hydrophobic reside. An exception was made for acidic residues, which are represented by the @ symbol. The { } brackets denote a variable number of the preceding letter. In the @X{2,3}θ motif, the minimum and maximum number of wild card residues is two and three, respectively. A compiled list of motifs and target membranes can be found in Tables 4.1 and 4.2, where the former lists motifs found within the C-terminal tail of VNUT and the latter lists absent motifs.

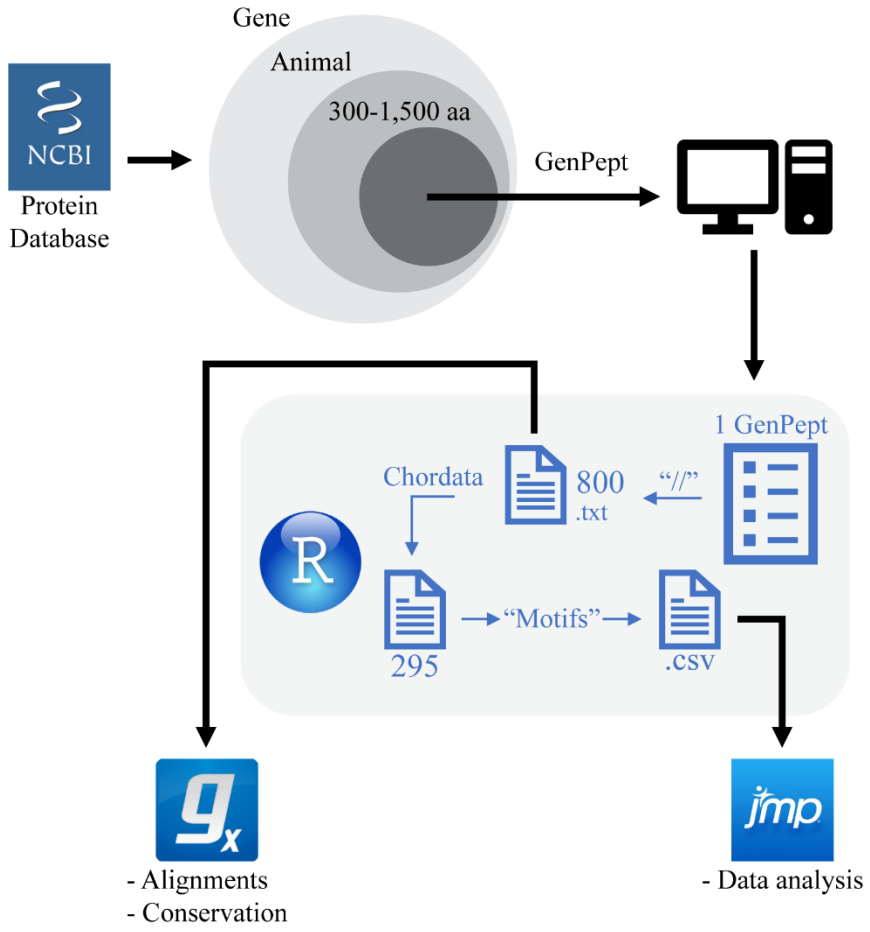

Figure 4.6 Method for acquiring and analyzing SLC 17 and 18 transporter sequences for targeting motifs
The VNUT Genpept files of 800 animals were downloaded *en masse* into one file from NCBI. This file was separated into a separate .txt file per accession number. These .txt files were used for alignment analysis. Since most animal models in which VNUT might be studied are chordate

animals, the chordate .txt files were selected for motif analysis. This was done using an R script to scan the taxonomy data of each .txt file. All motif searches were compiled into a JMP spreadsheet. The separation of the original Genpept file containing 800 accession numbers into .txt files and the regex-based motif searching were both performed using R scripts.

VNUT does not have a peroxisome, trans-Golgi network (TGN), NPXY internalization, or nuclear targeting motifs in the C-terminus of 16 Classes of animals (Fig 4.7). For most of the Classes except Mammalia, VNUT has a YXXθ motif that is associated with internalization and/or targeting to synaptic vesicles or lysosomes, depending on post-translational modification (Bonifacino & Traub, 2003; Guarnieri et al., 1993; Prado & Prado, 2002). In most Classes of organisms, sialin, the VGLUTs, VAChT, and VMAT2 have a @X{2,3}θθ motif in their C-terminus. This is in stark contrast to the mammalian VNUT C-terminus, which is conspicuously lacking any common vesicle-associated targeting motifs. Note that while VNUT does contain dileucine-like motifs, these positions are likely embedded within transmembrane domains.

The C-terminus of mammalian VNUT does have a KDEL receptor-like endoplasmic reticulum (ER) retention motif (Fig 4.7). Note that the motifs in Table 4.1 correspond to the motifs shown in Figure 4.7, in which only motifs present within the C-termini are shown. The motifs shown in Table 4.2 were not commonly present in the C-termini of the assessed transporters. Differences in the length of the C-termini for each transporter was accounted for by using an average number of amino acids from the end of the sequence.

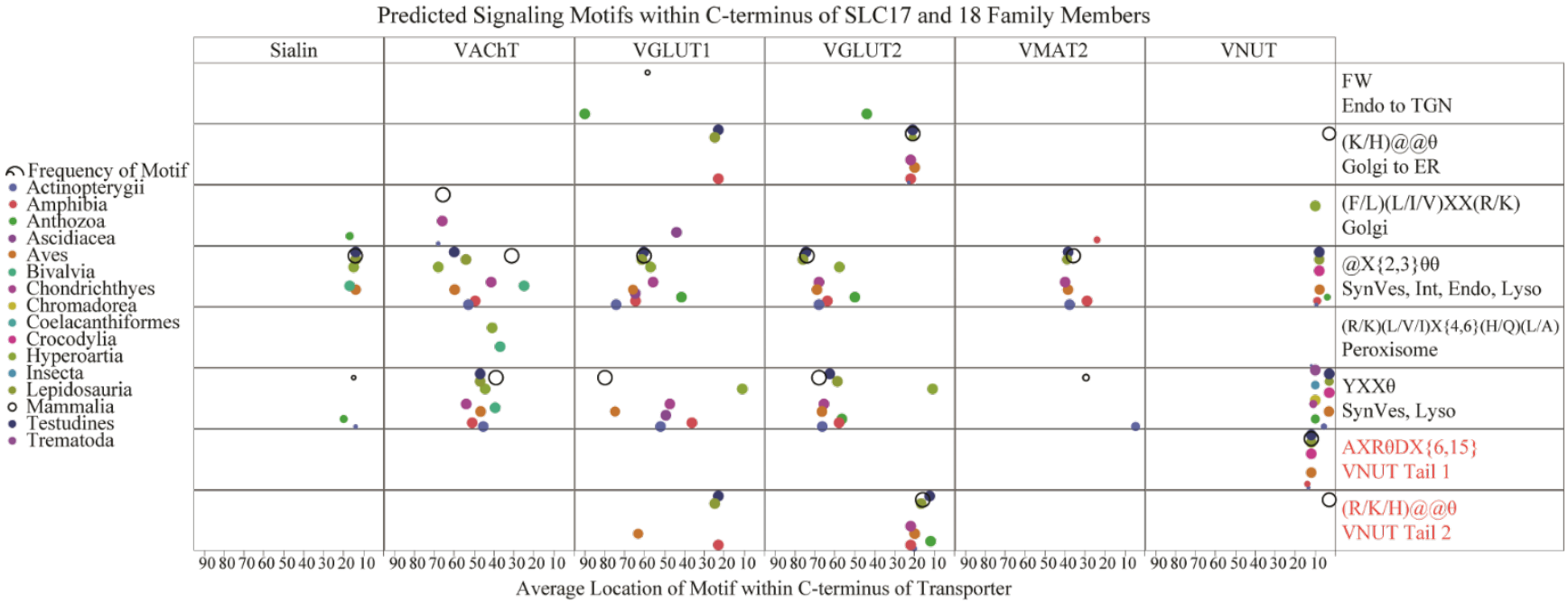

Figure 4.7 Signaling motifs in the C-terminus of SLC17 and 18 family members

The presence of a variety of targeting sequences, denoted by the right-hand Y-axis, are noted by a dot. Each dot is colour-coordinated with a Class of animals as listed in the legend on the left. The size of the dot or circle corresponds to the frequency of the motif within the species of that Class. The location of the motif is shown on the x-axis, which shows the amino acid position relative to the C-terminal end of the amino acid sequence. The two red motifs were identified as being unique to VNUT. Motifs from Table 4.1 not listed here were either rarely found or not found at all in any of the C-termini or Classes. Abbreviations: Endo, endosome; TGN, trans-Golgi network; ER, endoplasmic reticulum; SynVes, synaptic vesicle; Int, internalization (endocytosis); Lyso, lysosome.

Table 4.1 Targeting motifs found in the literature and C-termini of VNUT, sialin, VGLUT1, VGLUT2, VAChT, and VMAT2

Motif	Common Name	Target	Protein(s)	References
FW	Diaromatic motif	Endosome to TGN	CD-MPR	Bonifacino, J.S, & Traub, L.M., 2003.
(K/H)@@θ	KDEL motif	Golgi to ER	Calreticulin, Ubiquitin	Teasdale, R.D. & Jackson, M.R., 1996; Raykhel, I., *et al,* 2007.
(F/L)(L/I/V)XX(R/K)	FLIXR motif	Golgi	Glycosyltransferases	Banfield, D.K., 2011; Pandey, K.N., 2009.
@X{2,3}θθ	Dileucine-like motif			
@XXXθθ		Synaptic Vesicle, Internalization, Endosome, Lysosome	VMAT2, VGLUT1-3, VAChT	Colgan, L., *et al*, 2007; Li, H., et al, 2017; Prado, V.F, & Prado, M.A.M., 2002; Bonifacino, J.S, & Traub, L.M., 2003; Varoqui, H., & Erickson, J.D., 1998; Pandey, K.N., 2009.
@XXθθ		TGN to Endosome	Sortilin	Prado, V.F, & Prado, M.A.M., 2002; Bonifacino, J.S, & Traub, L.M., 2003; Pandey, K.N., 2009.
(R/K)(L/V/I)X{4,6}(H/Q)(L/A)	Peroxisome localization sequence (PLS)	Peroxisome	Thiolase I	Kiel, J.A.K.W., *et al*, 2004.
YXXθ	Tyrosine motif	Synaptic Vesicle, Lysosome	VAChT, LAMP-1	Colgan, L., et al, 2007; Guarnieri, F.G., *et al*, 1992; Varoqui, H., & Erickson, J.D., 1998; Bonifacino, J.S, & Traub, L.M., 2003; Pandey, K.N., 2009.

Table 4.2 Targeting motifs found in the literature but not in C-termini of VNUT, sialin, VGLUT1, VGLUT2, VAChT, and VMAT2

Motif	Common Name	Target	Protein(s)	References
YθYYθX	Non-classical tyrosine motif	Synaptic Vesicle	VAChT	Colgan, L., et al, 2007; Varoqui, H., & Erickson, J.D., 1998.
NPXY	NPXY motif	Internalization	LCL receptor	Bonifacino, J.S, & Traub, L.M., 2003; Pandey, K.N., 2009.
@@{6,9}	Acidic cluster motif	Endosome to TGN	VMAT2	Bonifacino, J.S, & Traub, L.M., 2003.
Y{3,7}	Y-rich motif	Endosome to TGN	CD-MPR	Bonifacino, J.S, & Traub, L.M., 2003.
P-rich	P-rich motif	Endosome to TGN	CD-MPR	Bonifacino, J.S, & Traub, L.M., 2003.
(K/R)X{7,13}K{3,4}	Nuclear localization sequence (NLS)	Nucleus (Bipartite)	Nucleoplasmin	Lange, A., et al, 2007.
K(K/R)X(K/R)		Nucleus (Monopartite)	SV40 Large T-antigen, C-Myc	Lange, A., *et al*, 2007.
LIKAKKGGKSKL	Peroxisome localization sequence (PLS)	Peroxisome	Firefly Luciferase	Gould, S.J., Keller, G-A., & Subramani, S., 1987.

4.2. Evolutionary Changes to VNUT

VNUT has undergone major evolutionary changes from fish to birds. Figure 4.8 is a segment of the tree of life, which illustrates the widespread expression of *SLC17A9* (stars). A brief note about Class Ascidiacea: the protein sequence for *Phallusia mammillata* (NBI accession number CAB3266123) is the only sequence of this Class that has been submitted to the NCBI library. Further, this sequence has not been validated, thus the sea squirts were not denoted as having *SLC17A9* in their genome (Fig 4.8), but other sea squirts may express *SLC17A9*.

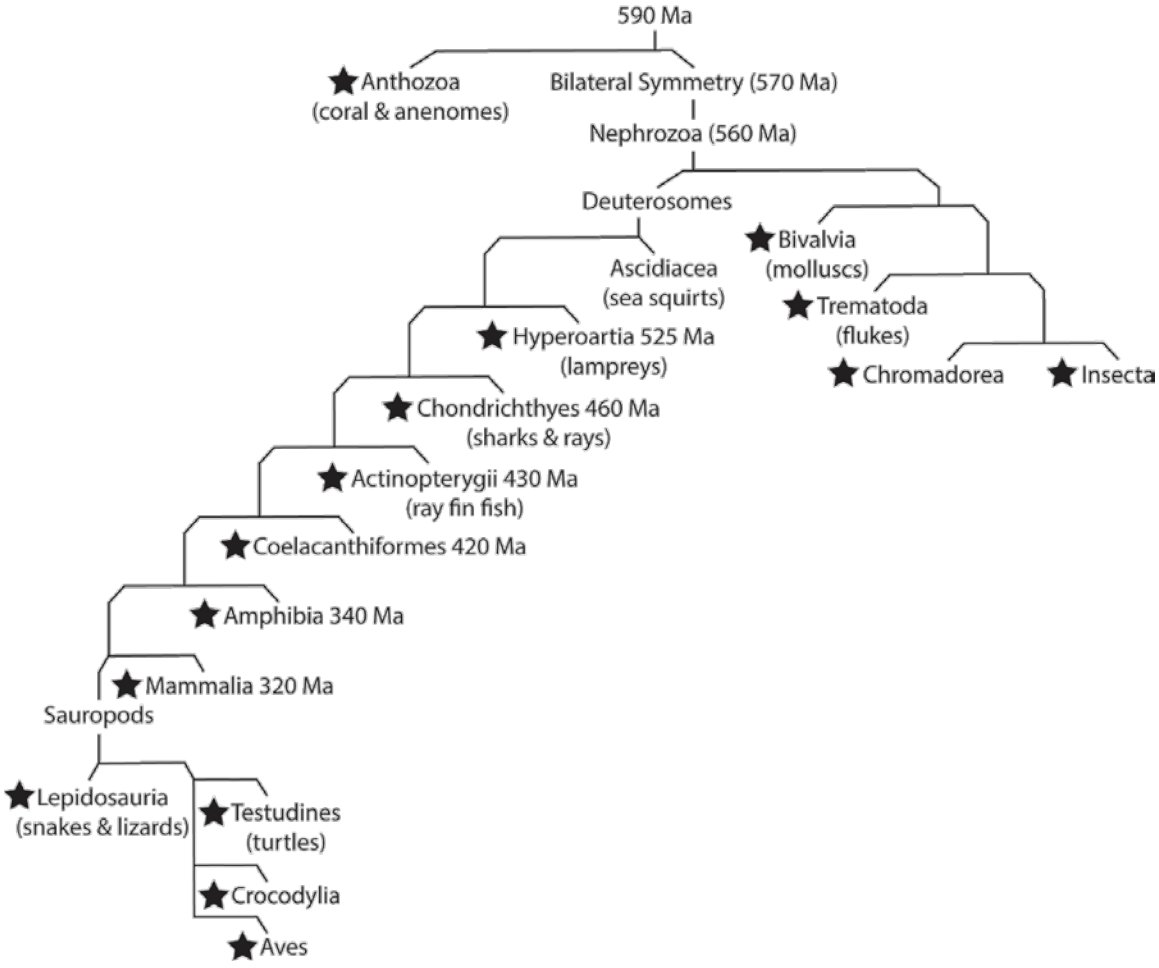

Figure 4.8 Evolutionary tree of Kingdom Animalia
This tree is set up in dichotomous fashion to make evolutionary relationships between Classes of animals easier to trace. Where known, the timepoint of divergence is indicated ("OneZoom Tree of Life Explorer," n.d.). Starred Classes have *SLC17A9*. Abbreviations: Ma, millions of years ago.

The alignment analysis in Figure 4.9 shows a charged residue-rich motif of @AβRVDI@-XXKXR(Y/H)HNIHI that is present in fish (β represents a positively-charged, polar amino acid), with some exceptions such as Arctic char, croaker, and zebrafish. This conserved sequence, which contains a possible YXXθ motif (blue highlighting in Fig 4.9), changes as VNUT likely experiences a deletion event between Actinopterygii and Classes Amphibia, Mammalia, Reptilia, and Aves, approximately 430 million years ago. The DNA nucleotides that were likely deleted are highlighted in Figure 4.10. As a result, the C-terminus length changes from ~19 amino acids in bony fish to ~14 amino acids in the other Classes. The deletion of these nucleotides may have resulted in a dileucine-like motif that is not present in fish (Chondrichthyes and most Actinopterygii), while an alternative tyrosine motif appears to have been retained in amphibians, reptiles, and birds (Fig 4.9).

The 14 amino acid length of the C-terminal domain was unchanged in mammals, yet different mutations occurred. Of particular interest are the last four residues, which seem to undergo an evolutionary change from the tyrosine (YXXθ) motif found in analyzed representatives of the other Classes to a predominant HEDL sequence in mammals (Fig 4.9). This HEDL motif bears strong resemblance to the KDEL receptor recognition motif.

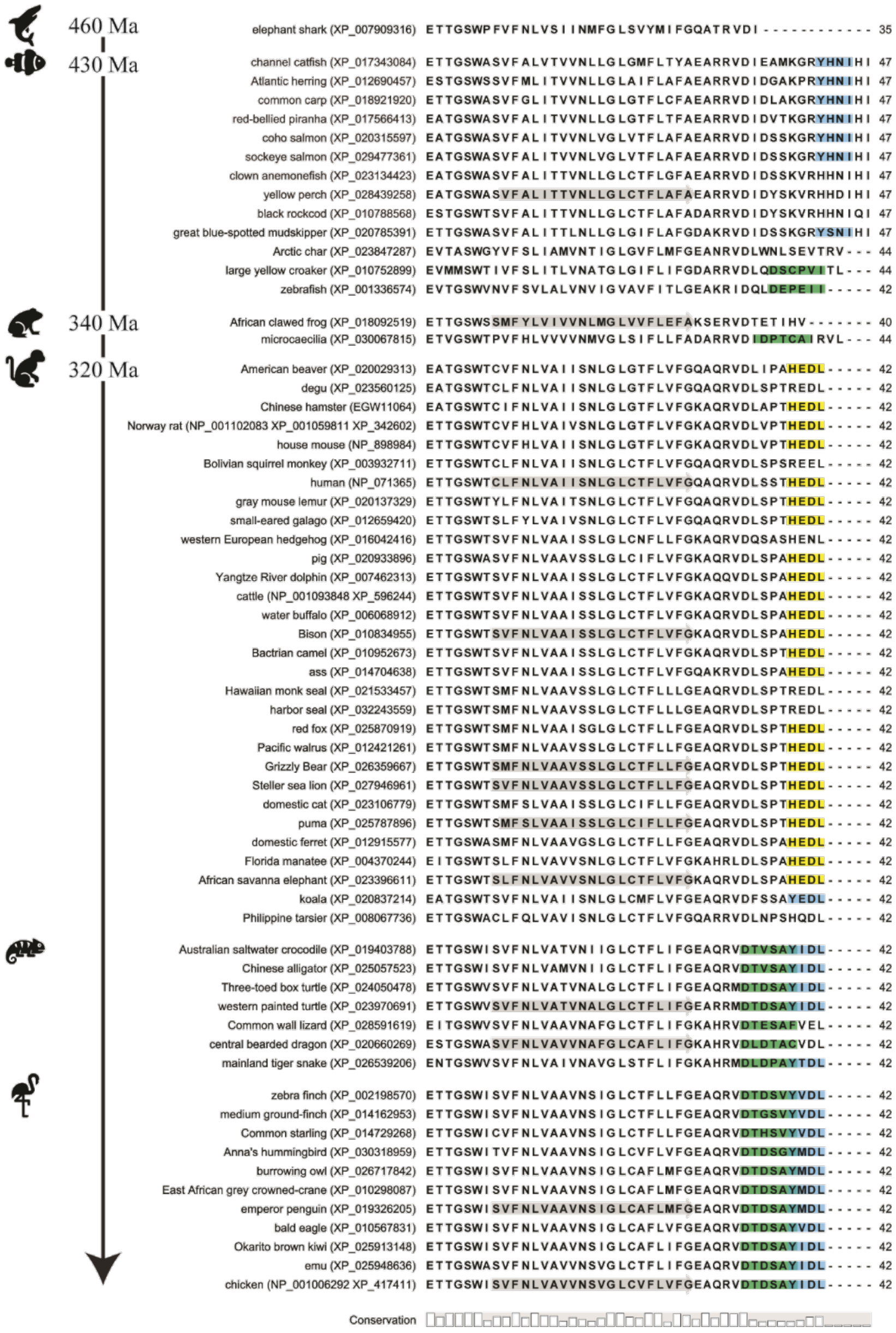

Figure 4.9 Conservation of VNUT C-termini across Kingdom Animalia
The C-terminus of VNUT is shown for one cartilaginous fish, eleven bony fish, two amphibians, 30 mammals, seven reptiles, and eleven birds, from top to bottom. Grey: the last transmembrane domain in selected species. Green: dileucine-like motif where present in the C-terminal domain of each sequence. Blue: Tyrosine motifs were present within the C-terminal domains of each sequence. The numbers to the right of each sequence denote the number of amino acids shown. To the left of each sequence is the common name of the animal followed by NCBI accession number(s) for traceability. At the far left is a simplified evolutionary tree of Kingdom Animalia.

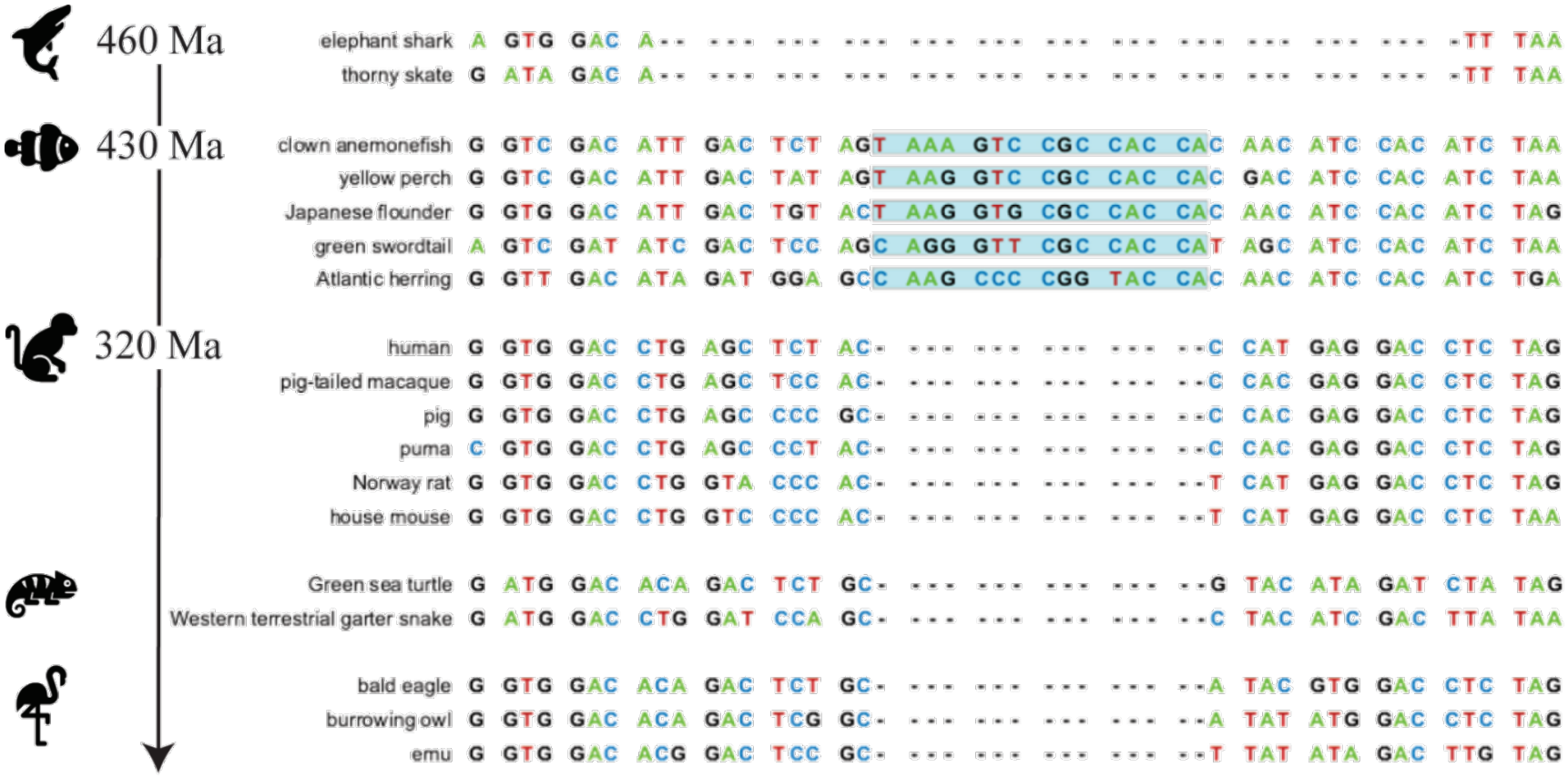

Figure 4.10 C-terminal deletion of VNUT in reptiles, aves, amphibians and mammals
Nucleotide alignment of mammalian, avian, amphibian, and fish VNUT. Nucleotides are coloured such that thymine is red, guanine is black, adenine is green, and cytosine is blue. The blue highlighting indicates the predicted deletion, based on homology alignment.

4.3. Possible Golgi-Targeting Motif in the C-terminal Domain of Mammalian VNUT

A comparison of human SLC17 family members further illustrates the uniqueness of the C-terminal domain of a representative mammalian VNUT, Figure 4.11. All other twelve transmembrane domain SLC17A transporters have a dileucine-like motif in their C-terminal domains, indicated in green in Figure 4.11. An important note is that the dileucine-like motifs alone do not dictate the subcellular location of these transporters, which is varied. For example, the VGLUTs traffic to vesicles (Haiyan Li et al., 2017), NPT1 is mainly found on the plasma membrane (Reimer, 2013) and sialin sorts to lysosomes (Wreden, Wlizla, & Reimer, 2005). Where VNUT lacks a synaptic vesicle targeting dileucine-like motif, it bears a KDEL-like HEDL motif at the very end of the C-terminus, shown in yellow (Fig 4.11). The KDEL motif is specifically responsible for Golgi-to-ER cycling of ER resident proteins. The resemblance of the HEDL motif to the KDEL receptor motif and the flexible recognition ability of KDEL receptors (Raykhel et al., 2007) jointly point to the HEDL motif being a functional KDEL receptor ligand. Further, the YθDL motif seen in reptiles and birds (Fig 4.9) might be a moderately functional ligand for the reptilian and avian equivalent of the KDEL receptor, suggesting possible divergent evolution of VNUT into an ER/Golgi ATP transporter.

A comparison of VNUT to human SLC18A family members VAChT and the VMATs also hints to the importance of the C-terminus in determining the subcellar location of VNUT. Figure 4.12 shows the monoamine transporters having acidic cluster motifs in addition to a dileucine-like motif. Acidic cluster motifs target prohormone processing enzymes to the TGN when phosphorylated (Bonifacino & Traub, 2003). The acetylcholine transporter also has a secondary motif in addition to the dileucine-like motif seen in both SLC17 and 18 transporters. Two tyrosine motifs are critical for targeting VAChT to synaptic vesicles (Colgan et al., 2007). Using CLC Genomics Workbench, the C-termini of the transporters shown in Figures 4.11 and 4.12 were aligned in Figure 4.13.

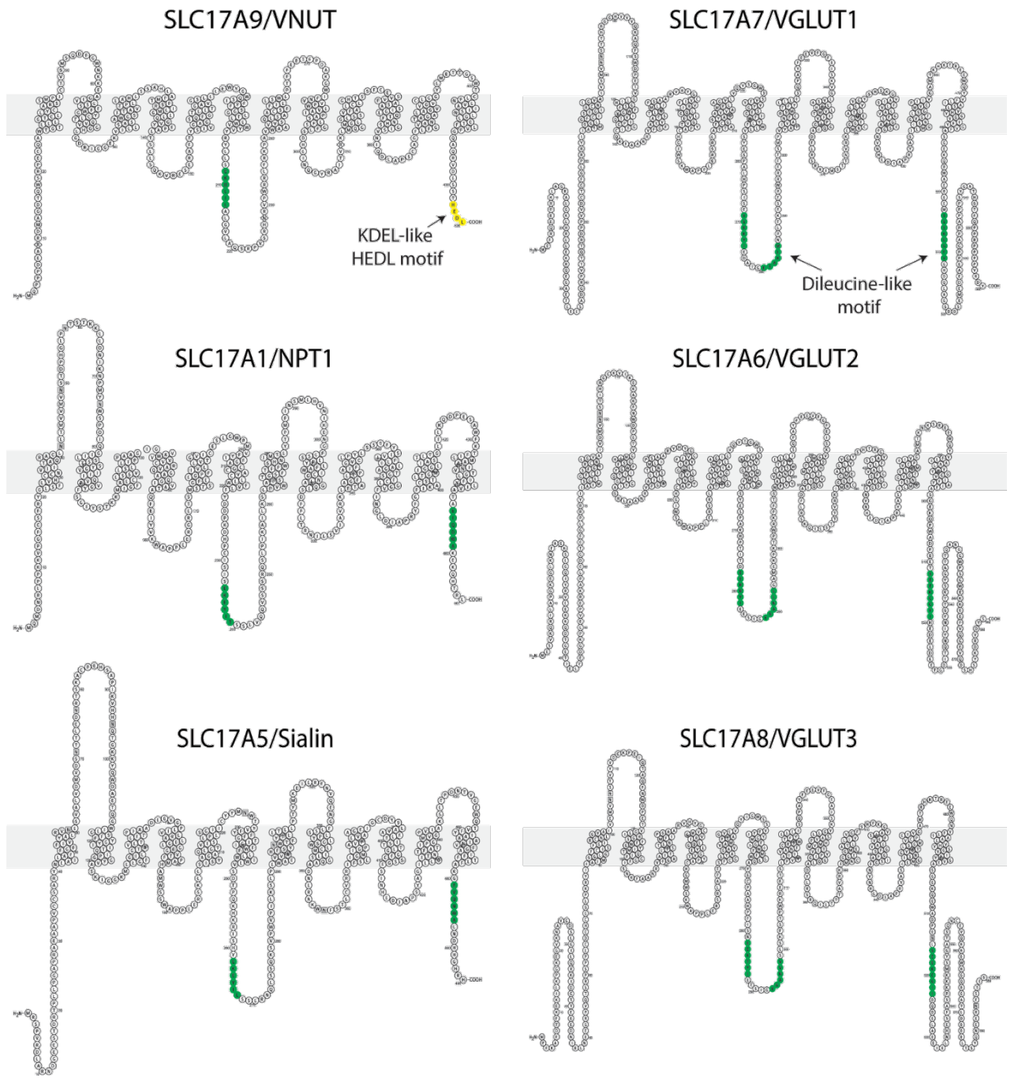

Figure 4.11 Predicted structures of human SLC17A transporters
The grey rectangles represent lipid bilayers. Green represents dileucine-like motifs, yellow shows predicted ER retention motifs.

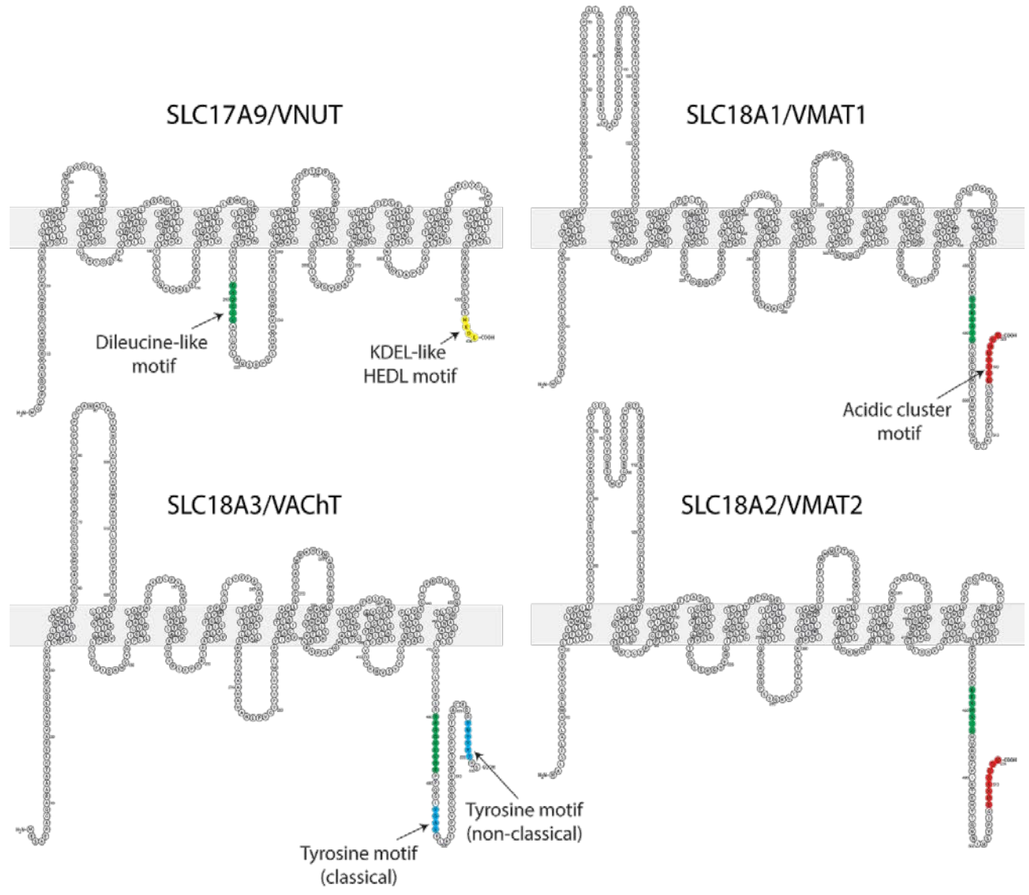

Figure 4.12 Comparison of VNUT with the monoamine and acetylcholine transporters
The grey rectangles represent lipid bilayers. Green represents dileucine-like motifs, red represents acidic cluster motifs, while blue indicates tyrosine motifs. Yellow shows predicted ER retention motifs

.

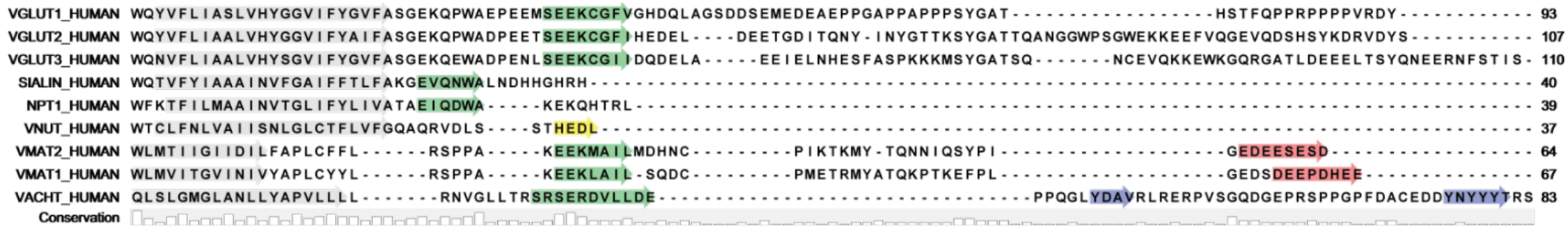

Figure 4.13 Alignment of 12-transmembrane domain transporters of the SLC17A and SLC18A families
The common name of each transporter is shown on the right side of each sequence. The twelfth transmembrane domains of each transporter is highlighted in grey. Dileucine-like motifs are highlighted in green, acidic cluster motifs in red, and tyrosine motifs in blue. The KDEL-like motif is highlight in yellow. The numbers on the right correspond to the number of amino acids in each sequence. The NCBI accession numbers for each sequence, in descending order, are: Q9P2U7, Q9P2U8, Q8NDX2, Q9NRA2, Q14916, Q9BYT1, Q05940, P54219, and Q16572.

In the electric organ of the Pacific Ray, the VAChT colocalizes with VNUT, VGLUT1, and VGLUT2 to synaptic vesicles (Huinan Li & Harlow, 2014). *California torpedo* is a member of Class Chondrichthyes. Figure 4.14, a simplified version of Figure 4.7, compares the mammalian and cartilaginous fish transporters that colocalized in the Pacific Ray. The VNUT sequence of the Pacific Ray is not available on NCBI. Two Chondrichthyes representatives were available, the elephant shark (XP_007909316) and the thorny skate (XP_032897284). A total of two VNUT and one of each VGLUT1, VGLUT2, and VAChT Chondrichthyes sequences were analyzed. Due to a lack of cartilaginous fish representatives, the bony fish (Actinopterygii) were included in the comparison. For Class Actinopterygii, 58 VNUT sequences were analyzed alongside one VGLUT1 sequence, 18 VGLUT2 sequences, and 10 VAChT sequences. Similarly, 63 mammalian VNUT sequences were compared to their fish counterparts (cartilaginous and bony), in addition to 56 sequences of VGLUT1, 44 sequences of VGLUT2, and 57 VAChT sequences.

The tyrosine and dileucine-like motifs are present in the C-terminus of fish and mammalian VAChT, VGLUT1, and VGLUT2. Of the 58 species of Actinopterygii for which VNUT sequences could be found, only one had a dileucine-like motif in the C-terminal domain of VNUT (Fig 4.14). The dileucine-like motif was absent from all other sequences. Neither of the Chondrichthyes representatives had a tyrosine motif, but 15 Actinopterygii species did have a C-terminal tyrosine motif. No mammalian VNUT sequence contained a tyrosine motif in the C-terminal domain (Fig 4.14). These data further highlight the unique and conspicuous absence of a C-terminal targeting motif in mammalian VNUT.

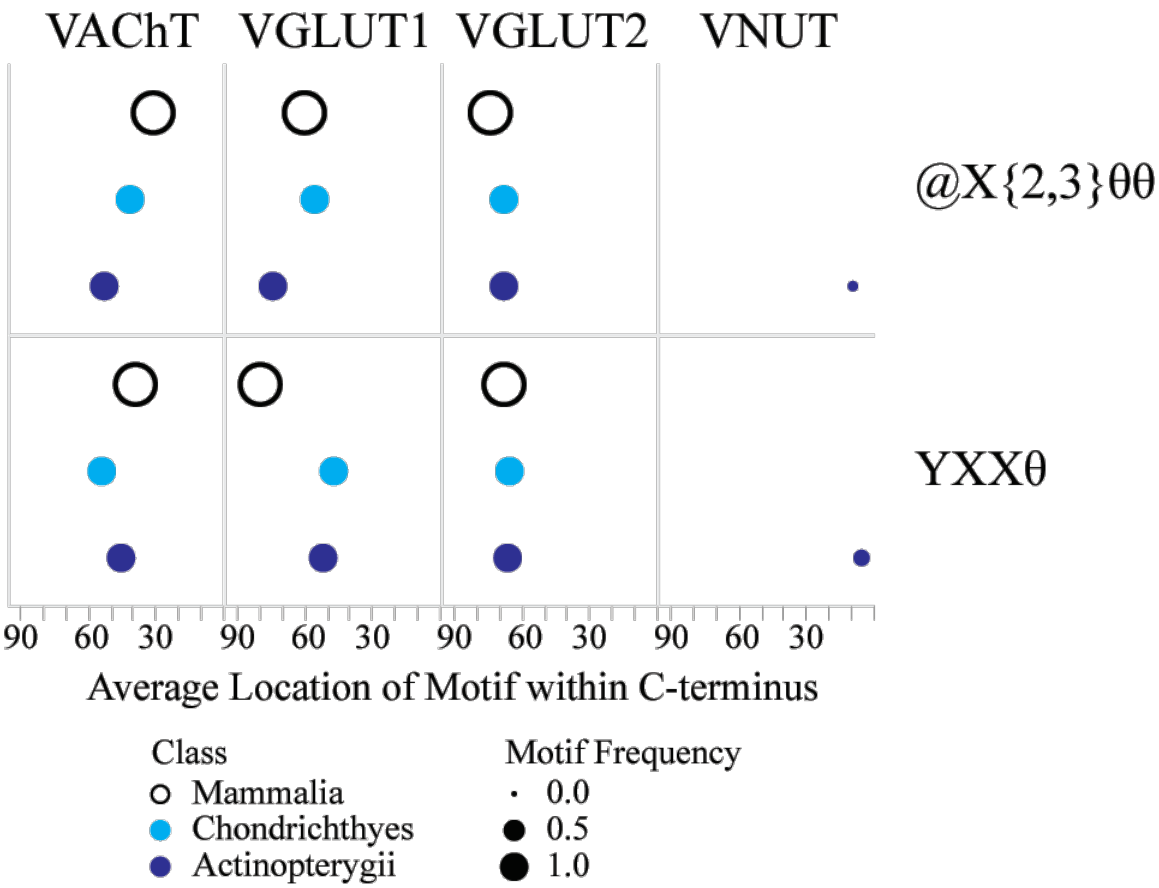

Figure 4.14 Comparison of Classes Chondrichthyes and Mammalia
The presence of each motif is indicated by dots or circles, with the symbol size illustrating the frequency of the motif within each class. Light blue, Chondrichthyes. Dark blue, Actinopterygii. Black, Mammalia. Note that the size of the dot indicating the presence of a dileucine-like motif in Actinopterygii corresponds to a single species.

4.4. Unique Regions of Mouse, Rat, and Human VNUT

Having noticed the unique lack of targeting motifs in the C-terminal domain of VNUT, I checked for homology between the C-terminal sequence of human, rat, and mouse VNUT and the proteome corresponding to each species using NCBI's Protein BLAST. My goal was to identify any transporters or receptors to which the VNUT C-terminal domain bore resemblance, hinting to possible trafficking locations. For each BLAST, unverified sequences such as models (XM/XP), non-redundant RefSeq proteins (WP), and uncultured or environmental sample sequences were excluded. In each proteome, VNUT self-matched with no other hits. The C-terminal tails of each VGLUT isoform only returned hits for the other isoforms of VGLUT. In contrast, the C-terminal sequences of sialin and the NPTs returned a variety of non-specific hits such as mitochondrial inner

membrane protease subunit 2, dual specificity protein kinase CLK4, plasma membrane calcium transporting ATPase, epidermal growth factor receptor substrate 15, and echinoderm microtubule-associated protein-like 2. The lack of specificity of sialin and the NPT C-termini is not surprising considering their lengths of 7 amino acids (SLC17A2/NPT3) and 16 amino acids (SLC17A4/NPT2, SLC17A3/NPT4, SLC17A1/NPT1, and SLC17A5/sialin). Amongst the SLC18A family, the C-termini are specific for each protein, with VAChT self-matching and the VMAT isoforms matching themselves and each other. These results indicate that transporter C-terminal domains are highly specific, except when the C-terminal length is short.

I analyzed the remaining cytosolic regions of VNUT, which were non-specific except for the loop between the sixth and seventh transmembrane domains (S6-7 loop). Some off-target hits included proteins like RUFY3, general transcription factor 3C, syntaxin 6, dynein heavy chain 5, 8, and 9, myosin 15, angiopoietin 1, and Timeless. Appendix C shows supplemental data that summarizes some of the results from the Protein BLAST analysis of mouse VNUT (NCBI accession Q8VCL5). The S6-7 loop appeared to be highly specific to VNUT. The mouse S6-7 loop did not have any significant homology to other mouse proteins. The S6-7 loops of the other SLC17 transporters were also specific. For example, the VGLUT isoforms only showed homology with each other, while sialin was homologous to itself and the sodium-dependent phosphate transporter isoforms 1-4 (*SLC17A1-4*). Additionally, the adjacent sixth and seventh transmembrane domains were highly conserved amongst all SLC17 transporters, Figure 4.15.

In comparison, the SLC18 transporters do not have unique S6-7 loops, likely due to their short lengths. VAChT and VMAT1-2 returned numerous non-specific hits that included proteins like sickle tail protein, apolipoprotein L3, endothelial transcription factor GATA-2, cadherin 23, and dystonin. The alignment shown in Figure 4.15 illustrates the variation of the S6-7 cytosolic loops of SLC17 and 18 transporters. The specificity of the S6-7 loop was characteristic of the SLC17 but not the SLC18 transporters. The C-termini of the VMATs and VAChT have additional targeting motifs, such as acidic cluster and tyrosine motifs, that are not present in the C-termini of the SLC17A family members. The specificity of the S6-7 loop in conjunction with the increase in size (and perhaps accessibility for regulatory proteins) present a possible secondary location for targeting motifs for the SLC17A family members.

An example of a secondary targeting motif can be found in the S6-7 loop of sialin. The five amino acid residues SSL(R/K)N at positions 268-272 are important for targeting to lysosomes (Wreden et al., 2005). These residues are highlighted in orange in Figure 4.15. Further, mutational analysis of a dileucine motif in the cytoplasmic amino (N) terminal domain of sialin also disrupts lysosomal targeting by preventing interactions with other lysosomal proteins (Wreden et al., 2005). Figure 4.15 also shows the NPTs having a motif similar to the SSL(R/K)N motif found in sialin, although it is not clear if these motifs target the NPTs to lysosomes. These data illustrate the role of secondary targeting motifs in cytoplasmic domains other than the C-terminus in protein trafficking. It would be interesting to test what role, if any, the S6-7 loop has on VNUT targeting. Assessing additional cytosolic domains other than the C-terminus could provide insight into targeting motifs, like those seen in sialin. While mutational studies are needed to assess the importance of the S6-7 loop in VNUT trafficking, a conserved dileucine-like motif might explain why a small portion of VNUT is sorted to vesicles.

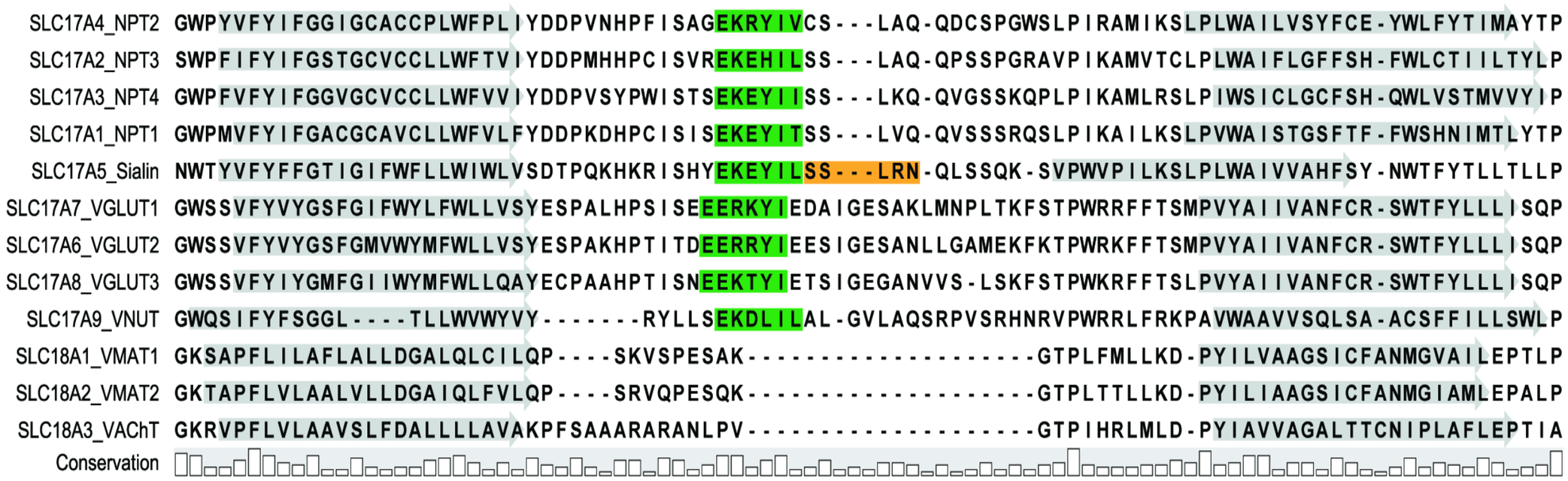

Figure 4.15 Alignment of the cytosolic 6-7 loop sequences
Transmembrane domains are indicated by grey arrows overlaid on each sequence. The sequence in between each of the transmembrane domains is the 6-7 loop, which is considerably shorter in the SLC18 transporters compared to the SLC17 transporter loops. The VNUT 6-7 loop is shorter than those of other SLC17 family members and lacks the level of homology seen between all other SLC17A family members. There is a conserved @X{2,3}θθ motif amongst the SLC17A family (green). Sialin also contains an SSLRN motif (orange).

.

Chapter 5.

Discussion

5.1. Subcellular Localization of VNUT in N2a Cells Inconclusive Based on Immunostaining Results

5.1.1. VNUT does not Localize to Synaptic Vesicles

Purinergic Synaptic Vesicles

I originally predicted that VNUT would localize to purinergic synaptic vesicles. Previous research in the Poburko lab demonstrated a correlation between synaptic vesicle proteins SV2a, synaptophysin, and synaptotagmin 1 (Syt1) with the monoamine transporter VMAT2 in rat tail artery. On the contrary, VNUT-containing blobs did not associate with these proteins in rat tail artery (Kalkhoran et al., 2019). Colocalization analyses in hippocampal neurons support a lack of colocalization between immunoreactive VNUT with Syt1 and synaptophysin (Larsson et al., 2012). A similar lack of colocalization between synaptophysin and VNUT was seen in cerebellar granule neurons (Menéndez-Méndez et al., 2017). VNUT, synaptophysin, and VGLUT were co-expressed in murine retinal tissue, but the tissue-scale staining does not lend insight to subcellular colocalization of these proteins (S. Moriyama & Hiasa, 2016).

The subcellular localization of VNUT may differ between cell types, in which there seems to be varying levels of colocalization between VNUT and synaptic vesicle proteins. A separate study using N2a cells found partial overlap of fluorescent signals corresponding to synaptophysin and Myc-tagged VNUT (Menéndez-Méndez et al., 2015). I argue that the density of the synaptophysin and Myc-tagged VNUT puncta overestimated the true extent to which these proteins colocalized, especially in the soma. Based on the predicted functional relationship of facilitating neurotransmitter release, these proteins should show a high degree of colocalization in the parts of the cell associated with vesicular release. For this reason, VNUT colocalization was assessed by cell part.

In the studies of this thesis, VNUT did not colocalize with markers of synaptic vesicles, secretory vesicles, catecholaminergic vesicles, or lysosomes with any degree of consistency, as summarized in Figure 5.1. The randomization trial of VNUT, LAMP-1, and VMAT2 colocalization calculated the frequency of NN puncta randomly residing within their reference VNUT puncta to be 8-10% (Table 3.12). The analysis of VNUT with LAMP-1 (Fig 3.6) and VMAT2 (Fig 3.10) resulted in marginal colocalization, illustrated by the NN puncta residing within VNUT at a slightly higher-than-random frequency of about 11-12% (Table 3.13). After subtracting the rate of randomness, the frequency of NN within reference was further reduced to 2-4%. Considering the rate of random colocalization of VNUT with LAMP-2 and VMAT2, we assume that synaptotagmin isoforms 1 (5-7%), 2 (3-5%), and 5/9 (1-3%), synaptophysin (5-7%), synaptobrevin (0%), and the synaptic vesicle-associated protein synapsin (3-5%) exhibit sparse colocalization with VNUT.

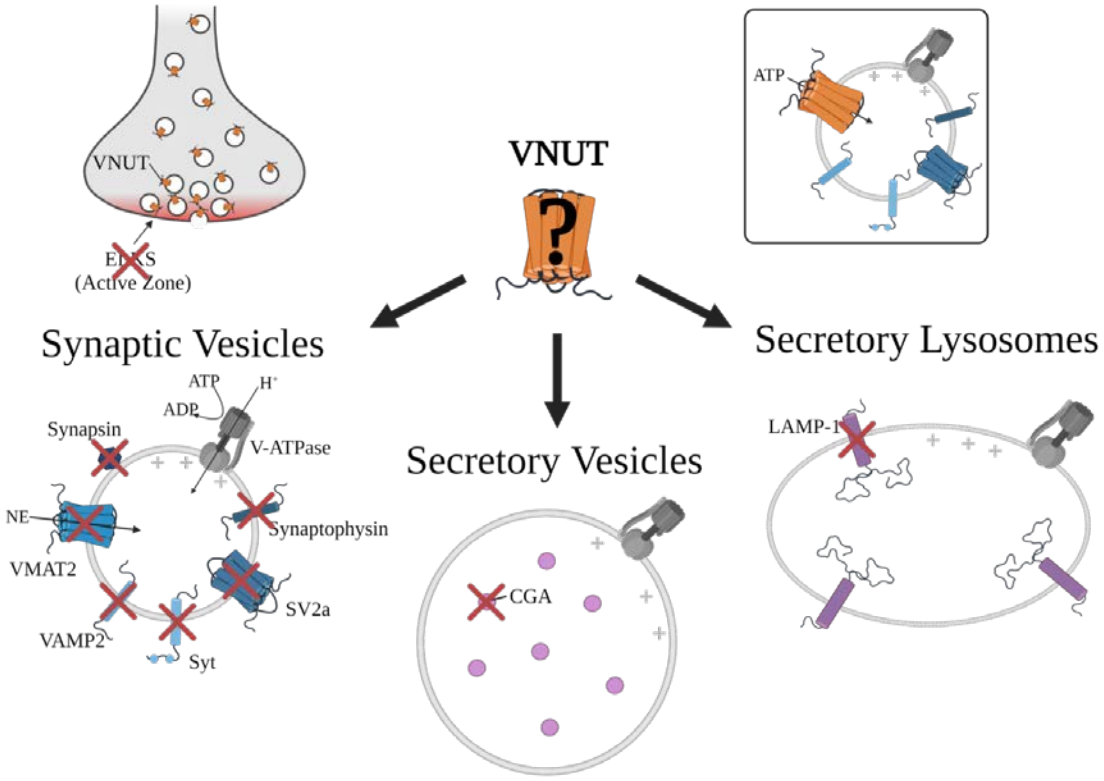

Figure 5.1 Graphical summary of colocalization analyses
Markers are described in Figure 3.1. Red crosses denote proteins that were not consistent markers of VNUT-containing compartments. Created with Biorender.com.

Of the tested markers, the best candidates for colocalization based on NN within reference VNUT puncta frequencies were ELKS and SV2a. ELKS puncta coincided with VNUT at a frequency of 22.5% in neurites and 19.8% in terminal varicosities (Table 3.3), with a collective average of 20.2% in neurites and all varicosities. ELKS localizes to active zones, where it serves as a scaffold within a multiprotein apparatus that helps tether readily releasable vesicles to sites of calcium entry (Held & Kaeser, 2018). An influx of calcium triggers vesicle fusion and subsequent neurotransmitter release. While ELKS was not a definitive molecular marker of VNUT-containing organelles, 1 in 5 VNUT-containing puncta contained an ELKS-labeled puncta in the cell parts that are most likely to contain active zones. ELKS tethering suggests that these VNUT-containing puncta could represent a form of releasable vesicle.

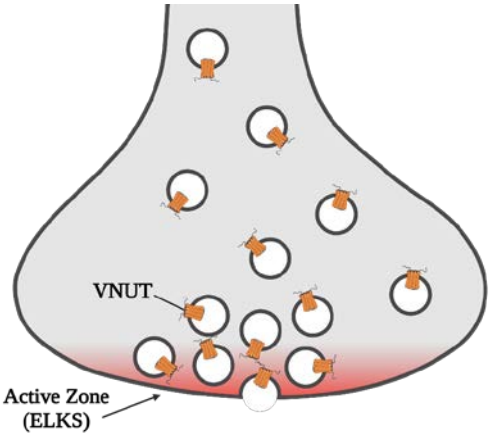

Figure 5.2 ELKS and associated proteins are diffuse throughout the active zone
VNUT localization is constrained to the vesicle membrane, resulting in punctate staining patterns. ELKS is found throughout the cytosol in active zones. Created with BioRender.com.

Since ELKS is not an integral transmembrane protein like VNUT, VMAT2, or LAMP-1, its subplasmalemmal dynamics are not confined to the circumference of a vesicle membrane. ELKS interacts with cytoskeletal elements and is present within the cytosol throughout the active zone, Figure 5.2. Of the numerous vesicle populations, ELKS would mostly interact with the readily releasable pool, which is the closest to the plasma membrane. Due to differences in localization and dynamics, extrapolating the VNUT-VMAT2-LAMP-1 randomization frequency of 8-10% is likely not as application to ELKS as it is for other markers that exhibit punctate staining and density similar to VNUT. Instead, colocalization analyses using VMAT2 and ELKS would provide better statistical comparisons. Further, ELKS-associated proteins such as Rab3-interacting molecules, Munc13 proteins, and bassoon also participate in temporary tethering (Held & Kaeser, 2018). Future studies could test the colocalization of these active zone proteins with VNUT.

SV2a is a 12 transmembrane domain protein that is thought to have a role in vesicle priming and/or fusion competency (Bartholome et al., 2017). The exact role of SV2a is

not known, but hypotheses include regulating the recruitment of Syt1 and/or the assembly polypeptide adaptor complex 2 (AP-2) (Bartholome et al., 2017). In addition to recruiting clathrin to the vesicle coat, adaptor proteins are cargo-specific, loading specific substrates into vesicles by recognizing acidic cluster/dileucine and tyrosine motifs (Kelly et al., 2014). The recruited clathrin helps shape vesicles during endocytosis and, in coordination with the adaptor protein complexes, participates in vesicle targeting. In mice pups, SV2a knockout was lethal within 1-2 weeks of birth, although the brain physiology remained unchanged (Bartholome et al., 2017). Thus, SV2a was not important for development in utero but its function was critical to post-birth survival. Its role in neurotransmission was established by knockout studies, in that spontaneous and evoked postsynaptic currents are reduced in the absence of SV2a (Bartholome et al., 2017). If VNUT localizes to synaptic vesicles, SV2a should be a consistent marker of VNUT-containing vesicles. However, the majority of VNUT puncta do not have SV2a puncta within their borders, and vice versa (Fig 3.6H and K). ELKS and SV2a were not consistent markers of VNUT-containing organelles despite having the highest frequencies of NN puncta within the perimeter of VNUT reference puncta of the synaptic vesicle markers.

Catecholaminergic Synaptic Vesicles

ATP is co-released from sympathetic nerves that release norepinephrine. ATP release is rapid with short-term post-junctional effects (i.e., twitch contractions). Conversely, norepinephrine is primarily released in response to stronger stimuli. In addition to its release being sustained during longer periods of stimulation, norepinephrine induces post-junctional responses of greater amplitude and duration than ATP (Todorov et al., 1999; Westfall et al., 1996). ATP and norepinephrine also have different, yet co-dependent, pre-junctional regulatory mechanisms (Todorov et al., 1999). These differences in release kinetics suggest different populations of ATP- and norepinephrine-containing vesicles. Immunohistochemical staining of rat tail artery identified anti-colocalization of VNUT-containing puncta from puncta stained for the catecholamine transporter VMAT2 (Kalkhoran et al., 2019). I predicted that VNUT-containing vesicles were responsible for quantal release of ATP in N2a cells and further hypothesized that these quanta were molecularly distinct from catecholaminergic vesicles.

Accounting for the random likelihood of VMAT2 NN puncta residing within their reference VNUT of 10.3% (Table 3.13) and the assessed frequency of 11.1% (Table 3.3), VMAT2 colocalization was negligible with frequency of NN within VNUT of 0.8%. I was not expecting VNUT to co-reside with VMAT2, based on my colleagues' observations in rat tail artery (Kalkhoran et al., 2019) and the differences in ATP and NE release reported in sympathetic nerves (Kennedy, McLaren, Westfall, & Sneddon, 1996; Todorov et al., 1996). This N2a cell-based research corroborates previous findings in rat tail sympathetic nerves that VNUT is not localized to catecholaminergic synaptic vesicles. The localization of VNUT may be cell line or tissue specific. Immunoelectron microscopy illustrates VNUT localization in a minority of secretory vesicle-like chromaffin granules in PC12 cells (Sawada et al., 2008).

5.1.2. Chromogranin A is not a Marker of VNUT-Containing Organelles

In bovine chromaffin cells, ATP is thought to be an important component of dense cored secretory vesicles (Estévez-Herrera et al., 2016). In sympathetic neurons, ATP is co-released with NE, which is typically released from small dense cored vesicles. The electron density of these organelles is due to the presence of chromogranins (Hearn, 1987; Hoon Huh, Hoo Jeon, & Hyun Yoo, 2003), which are also present in large dense cored secretory vesicles that typically release neuropeptides (Merighi, 2018). To rule out VNUT localization to peptidergic secretory vesicles, I assessed VNUT colocalization with chromogranin A (CGA). Immunolabeled CGA and genetically encoded CGA-GFP did not colocalize with VNUT in N2a cells. The NN puncta for each marker resided within their assigned VNUT reference puncta with an average frequency of 12.7% and 7.4% (Table 3.3). Assuming the random colocalization frequency of 8-10% results in non-random frequencies of approximately 3-5% and 1-3% for CGA and CGA-GFP, respectively. I did not expect CGA to be a consistent constituent of VNUT-containing vesicles due to the lack of colocalization with catecholaminergic vesicles, some which also contain CGA (Kloukina-Pantazidou et al., 2013).

5.1.3. VNUT does not Localize to Lysosomes in N2a Cells

VNUT localization to lysosomes might be dependent on cell line. Reports studying kidney epithelial cells, myocytes, astrocytes, and glial cells suggested some degree of colocalization between VNUT and LAMP-1 (Cao et al., 2014; Oya et al., 2013; Zhong et

al., 2016). Studies of s*tria vascular* marginal cells of rat cochlea also suggest VNUT localization to lysosomes (J. Liu et al., 2016). It is worth noting that ATP release from lysosomes has been identified in the central nervous system. Cerebellar granule neurons and primary cultures of dorsal root ganglion neurons exhibit calcium-induced lysosomal ATP release (Menéndez-Méndez et al., 2017; Miras-Portugal et al., 2019). VNUT localization to lysosomes and lysosomal ATP release have not been assessed in sympathetic nerves.

I hypothesized that VNUT would not localize to lysosomes in N2a cells. The degree of colocalization between immunoreactive LAMP-1 and exogenously expressed LAMP-1-RFP constructs with immunolabeled VNUT and N- and C-terminal EGFP-conjugated VNUT was comparable. The punctate pattern of VNUT and LAMP-1 immunofluorescence is the N2a cells was consistent with their localization to small, membrane bound organelles. The observation that localization of LAMP-1 NN puncta fell within the bounds of VNUT ROIs and vice versa was only 4-7% above that seen for randomly distributed puncta suggests that these two markers are not colocalized in N2a cells. Although shRNA or isolation of primary cell culture from *SLC17A9* deficient mice are the gold standard of assessing antibody specificity, the former technique could not be completed due to time constraints (Appendix B). However, the exogenously expressed constructs produced the same punctate patterns of fluorescence as the immunostaining, which was promising evidence of antibody specificity. Further, the degree of colocalization between the fluorophore-conjugated LAMP-1 and VNUT was similar to the immunolabeled counterparts. For overexpressed and native VNUT, fluorescence imaging data indicate that VNUT is not consistently localized to lysosomes.

The reader might ask why I did not use LysoTracker, a common molecular probe for lysosomes. As discussed in Chapter 3, this fluorescent probe stains lysosomes based on the principle of pH-trapping lipophilic weak bases in acidic compartments. However, synaptic vesicles, endosomes, and multivesicular bodies are also acidic organelles that range in pH from 4 to 5.5 (Ahdut-Hacohen, Duridanova, Meiri, & Rahamimoff, 2004; Vacca, Scott, & Gruenberg, 2016). Due to pH-dependent accumulation, LysoTracker is unable to differentiate between lysosomes and other acidic organelles. Conversely, LAMP-1 is a canonical marker of lysosomes that is less likely to falsely label non-lysosomal compartments. However, LysoTracker Red staining of cells that express EGFP-VNUT could provide information about the proportion of VNUT that is localized to

acidic compartments. For example, if VNUT is primarily localized to the ER/Golgi but also resides in synaptic vesicles or lysosomes, this would be observed by a greater proportion of VNUT reference puncta not containing a LysoTracker Red NN puncta within their perimeter.

5.1.4. VNUT Might be a Golgi/ER Protein

My data point to two possible configurations for the subcellular location of VNUT. A very small portion of VNUT-containing organelles might be synaptic vesicles, indicated by the range of frequencies of NN puncta within VNUT puncta of 2-20% for all synaptic vesicle proteins (not accounting for random colocalization). This theory does not account for the greater fraction of VNUT puncta that do not associate with canonical synaptic vesicle proteins or indeed the differences in puncta size and clustering in the soma compared to the neurites. A second explanation that accounts for the larger proportion of VNUT blobs in the soma is VNUT localization to a synaptic vesicle-adjacent compartment, but not synaptic vesicles themselves. These compartments may be trafficking compartments containing enzymes that hydrolyze ATP to metabolize their substrates. These organelles may include fragments of ER or Golgi, such as endoplasmic-reticulum-Golgi intermediate compartments (ERGICs), Golgi outposts and smaller satellites.

Unlike the typical imagery shown in textbooks, the ER forms continuous tubular networks that extend into axons (Öztürk, O'Kane, & Pérez-Moreno, 2020) and dendrites (Mikhaylova, Bera, Kobler, Frischknecht, & Kreutz, 2016). Segments of the Golgi, called Golgi outposts tend to reside at the base of dendrites while smaller satellite segments interact with the ERGICs and endosomes (Mikhaylova et al., 2016). Like the main body of the ER and Golgi, the smaller counterparts are thought to allow protein modifications, lipid synthesis, and protein sorting. These compartments allow faster protein recycling and export to the plasma membrane by reducing the trafficking distance, although they are not fully functional like the major organelles (Mikhaylova et al., 2016; Ori-McKenney, Jan, & Jan, 2012; Öztürk et al., 2020). The ERGICs, Golgi outposts, and satellites all share membrane components with endosomes through the close cycling of proteins. Endosomes also participate in phagocytic processes involving fusion with multivesicular bodies and lysosomes. The recycling of membrane components of the endocytic recycling and phagocytosis processes would explain weak partial colocalization of VNUT

with synaptic vesicle proteins, VMAT2, secretory vesicle proteins, and lysosomes. In this theory, VNUT is vital in recruiting ATP for enzyme function in addition to vesicle loading.

5.1.5. Limitations

Antibody Specificity

Due to the heavy reliance on antibodies throughout my research, the most obvious limitation is antibody specificity. The gold standard techniques for assessing antibody specificity are interfering RNA or a knockout animal model. I designed short hairpin RNA (shRNA) constructs that would knock down VNUT and firefly luciferase (FFL), shown in Appendix B. The FFL construct would have been the negative control, as there is no luciferase in mouse N2a cells. Unfortunately, time constraints due to the COVID-19 pandemic prevented my undergraduate assistant and me from building and validating these constructs. Our lab is currently working on validating commercially produced shRNA constructs, but these constructs are failing to knock down VNUT mRNA expression. Our lab continues to work on VNUT knock down studies, however we are reasonably confident in our anti-VNUT antibody for two reasons. First, a second anti-VNUT antibody was purchased from Alomone Labs to replenish our dwindling supply of Santa Cruz rabbit polyclonal antibody, which can no longer be purchased due to Santa Cruz having lost their license to use animals. The Alomone antibody exhibits a similar staining pattern as the Santa Cruz antibody (data not shown). Secondly, the EGFP-conjugated VNUT probe also presents a similar pattern of fluorescence to the Santa Cruz antibody. Other than stronger perinuclear staining, the over-expressed EGFP-VNUT fusion proteins stained the neurites and varicosities in a similarly punctate manner as the immunolabeled native proteins.

Randomization of ROIs

The regions of interest (ROIs) outlining each VNUT puncta were randomly re-located within the confines of 8 cells using the Poburko Lab's Randomization macro in ImageJ/Fiji. This method uses an algorithm to assign each VNUT ROI a new x and y coordinate that cannot exceed the boundary of the cell outline. Although the random number generator does result in a random distribution of the VNUT ROIs, the ROIs were not homogenously distributed across the area of the cell. Small clusters of randomized ROIs may artificially increase the frequency of nearest neighbour colocalization within

VNUT ROIs. Analyzing multiple randomization replicates would help average out such an effect of small clusters, improving the evenness in the distribution of VNUT ROIs. The resultant mean frequencies of colocalization across all replicates would be a more statistically robust measure of random colocalization. One round of VNUT ROI randomization was completed for the LAMP-1 and VMAT2 colocalization analysis, the results of which were extrapolated to the colocalization analyses of the other markers. Ideally, multiple replicates of VNUT ROI randomization would have been performed for each marker. Due to time constraints, this was not possible. However, the analyzed images were typical of the N2a cells in which these markers were consistently labelled with a high degree of density throughout the cells.

The constrained volume of neurites and varicosities and density facilitates the proximity of the markers and VNUT such that the greatest probability of colocalization should happen in these cell parts. Of all assessed markers, VNUT-EGFP/LAMP-1-RFP had the highest proportion of VNUT reference puncta containing a NN LAMP-1-RFP puncta (~24% in terminal varicosities, before considering the randomized colocalization frequency; Table 3.6) along with some of the highest density of puncta throughout the cells. Conversely, most markers with low frequencies of colocalization exhibited marginally higher NN colocalization indices within the confines of the neurites and varicosities. Since the volume of these cell parts is limited, the high density of puncta likely results in an overestimation of colocalization. This suggests that most of the colocalization seen is random. Further, the images were acquired using z-stacks which were compressed into a single z-plane, resulting in a best-focus image. This compression would flatten two puncta that were separated along the z-plane into a single image, resulting in false colocalization. If a marker was physiologically associated with VNUT such that the proteins consistently shared that same geographical space, this phenomenon should result in highly colocalized puncta that should be particularly apparent in the neurites and varicosities. However, inferences from the density of the ROIs for each marker suggests that most of the observed colocalization was random and that none of the markers tested are consistent markers of VNUT-containing compartments.

5.2. Understanding VNUT through Bioinformatics

The C-terminus of mammalian VNUT is unique compared to the other SLC17A and 18A transporters. The VNUT tail lacks a dileucine-like motif that is shared between NPT1, sialin, the VGLUTs, the VMATs, and VAChT. Further, VAChT and VMAT2 have additional tyrosine-based and acidic cluster motifs, respectively, that likely allow differential localization of these co-expressed proteins (Varoqui & Erickson, 1998). While these transporters contain vesicle-associated targeting motifs, the C-terminus of VNUT lacks common vesicle targeting motifs, such as dileucine-like and tyrosine motifs.

I identified a potentially evolutionary loss of a C-terminal tyrosine motif that is present in bony fish, reptiles, and avians but is not present in mammals. Further, reptiles have a dileucine-like motif also not present in the C-terminal domain of mammalian VNUT (Figure 4.9). I sought to compare the C-terminus of VNUT with those of the other solute carriers that colocalize in synaptic vesicles of the Pacific Ray, Figure 4.14 (Huinan Li & Harlow, 2014).

The electric organ of *Torpedo californica* expresses VAChT and VNUT, as well as VGLUT1 and VGLUT2, resulting in a promising model for studying transporter localization. Immunocytochemical analyses identified colocalization between VAChT, VGLUT1, VGLUT2, and VNUT in the cholinergic neurons of the electric organ of the Pacific Ray (Huinan Li & Harlow, 2014). In addition to releasing acetylcholine, these neurons are capable of releasing ATP. Corelease of these neurotransmitters occurs as a result of shared vesicles, with 69% of VAChT-labeled vesicles being co-labeled for VNUT in isolated vesicles (Huinan Li & Harlow, 2014). In addition to colocalizing with VNUT, the 59% of VAChT vesicles co-labeled for VGLUT1 and 61% co-labeled for VGLUT2 (Huinan Li & Harlow, 2014). The shared localization of these neurotransmitter transporters suggested that they might share a common targeting motif in *T. californica*, a member of Class Chondrichthyes. The C-terminal tail of the VAChT is necessary and sufficient for targeting to synaptic vesicles, containing a dileucine-like motif and a YXXθ tyrosine motif (Colgan et al., 2007; Varoqui & Erickson, 1998). The C-termini of the VGLUTs contain a dileucine-like motif that drives synaptic vesicle targeting and recycling (Haiyan Li et al., 2017). I wondered which motifs were present in the Pacific ray VNUT sequence. Although the VNUT peptide sequence of *T. californica* was not available in the NCBI database, I analyzed a total of 60 VNUT, 2 VGLUT1, 19 VGLUT2, and 11

VAChT sequences from fish alongside 63 mammalian VNUT, 56 VGLUT1, 44 VGLUT2, and 57 VAChT sequences. I compared the presence of the dileucine-like and tyrosine motifs in the C-termini of these transporters (Fig 4.14). The VNUT C-termini of some bony fish contained a tyrosine motif that might play a role in vesicular targeting, like the VAChT tyrosine motif. Although the Chondrichthyes representatives did not have synaptic vesicle targeting motifs in the C-terminus, it would be premature to suggest that this Class does not have any C-terminal signaling motifs based on a small sample size of two representatives. Future research would benefit from acquiring the VNUT sequence for *T. californica* and additional Chondrichthyes to assess for motifs that drive synaptic vesicle targeting. The comparison between fish and mammalian VNUT C-termini further illustrates the lack of synaptic vesicle targeting motifs in mammals. These results suggest that the motif(s) responsible for targeting VNUT to synaptic vesicles in mammals may reside on a different cytosolic domain other than the C-terminus, such as the S6-7 loop.

It would be interesting to test if the pattern of VNUT staining and colocalization with VGLUT1-2 and VAChT is corroborated in reptiles and birds. Future studies could investigate changes in VNUT localization by removing the C-terminus and comparing the frequency of colocalization with VAChT in *T. californica*. Another experiment uses a mammalian-fish VNUT chimera in a mammalian cell model. The C-terminus of the mammalian VNUT would be swapped for the fish tail, like the VAChT and VMAT2 chimera experiment (Varoqui & Erickson, 1998). The results of these experiments would clarify if the VNUT C-terminus is required for trafficking to synaptic vesicles in the Pacific Ray. If so, a previously unknown targeting motif may be present, or VNUT trafficking could be regulated by an alternative regulatory mechanism (e.g., the pH-sensitive ER-Golgi cycling of the KDEL receptor). Conversely, continued sorting of the truncated VNUT to vesicles would support a trafficking motif in another cytosolic domain.

5.3. VNUT Localization to the ER-Golgi Complex

In my mammalian cell line, colocalization between VNUT and synaptic vesicle markers, large secretory vesicle markers, and lysosomes (some of which may participate in secretion) was weak. Some possible reasons for the lack of consistent localization include VNUT being cycled between compartments, VNUT localization to certain compartments in a development- and tissue-dependent manner, or VNUT having a

versatile, multifunctional role. The immunocytochemical and bioinformatic evidence presented in this thesis point to VNUT possibly localizing to the ER-Golgi complex, two organelles that require future analysis. Two main observations drive this hypothesis. Firstly, VNUT immunolabeling produces larger blobs in the nuclear and perinuclear space, which bears morphological resemblance to the ERGIC and Golgi. Secondly, the extreme end of the VNUT C-terminus possesses a KDEL-like HEDL motif in mammals. The HEDL motif will be examined in detail in Section 5.3.1.

Immunocytochemistry studies in rat epithelial kidney cells identified pre-Golgi structures using immunolabeled p58, a marker of intermediate compartments between the ER and Golgi apparatus (Ying, Flatmark, & Saraste, 2000). The rat p58 is homologous to the human ERGIC marker, ERGIC53. The immunoreactive p58 resulted in punctate perinuclear staining to which the VNUT immunolabeling bears resemblance. A GFP-conjugated ERGIC53 as well as antibody stained ERGIC53 and GM120, and Golgi marker, also exhibit punctate staining with enriched signal in the perinuclear space of HEK293 cells (Farhan et al., 2008). It is worth noting that the ERGIC53 fluorescence looked more similar to the VNUT immunofluorescence and VNUT-EGFP signal than GM130. This marker is particularly localized to the proximal areas of the perinuclear space (Davids et al., 2016; Farhan et al., 2008).

A more widespread staining pattern that is most concentrated to around the nucleus, like I observed in my colocalization experiments, appears to be characteristic of the ERGIC. Indeed, this observation was confirmed by looking at immunofluorescent images of anti-ERGIC53 antibodies, such as Santa Cruz (SC-365158), Sigma Aldrich (E1031), and ProteinTech (13364-1-AP). A study using primary rat hippocampal neurons demonstrates the presence of ER exit sites and Golgi outposts in dendrites (Horton & Ehlers, 2003). ER exit sites are discrete locations on the ER membrane where cargo is concentrated for secretion. This study supports ER and Golgi functionality in dendrites, although Golgi functionality was absent from axons. If VNUT primarily localizes to the ER-Golgi complex, it would conceivably cycle between the ER, ERGIC, and Golgi outposts of the N2a neurites.

5.3.1. Bioinformatic Evidence of ER-Golgi Localization of VNUT

My bioinformatics research identified dileucine-like motifs and tyrosine motifs in non-mammalian VNUT C-termini, but no such localization motifs in the mammalian counterpart. Mammals appeared to be unique in that they lost the dileucine-like and tyrosine motifs and instead contain a C-terminal HEDL sequence. While the driving force behind the evolution of this change is not clear, the presence of the HEDL motif suggests a shift in VNUT localization from primarily synaptic vesicles (as seen in *T. californica*) to the ER-Golgi complex. Experimental observations show VNUT localization to the perinuclear space. Without conducting C-terminal mutation experiments, it is unclear if the HEDL sequence is responsible for targeting VNUT to this region of the cell. Thus, the question is whether the HEDL sequence could reasonably retain VNUT in the ER-Golgi complex.

In HeLa cells, the KDEL receptor was capable of recognizing conservative mutations in the KDEL motif, such as HDEL, KEEL, HADL, HEEL, and KEDL (Raykhel et al., 2007). The recognition rates of these variants were on par with the original KDEL sequence with ~80% ER localization and ~20% remaining in the Golgi (Raykhel et al., 2007). Although the HEDL sequence seen in the C-terminal tail of mammalian VNUT was not strictly included in this mutation study, based on the flexibility of the KDEL receptor recognition, I postulate that the KDEL receptor should be able to recognize the HEDL variant. Specifically, recognition of the KEDL and HDEL variants support the likelihood of the HEDL motif being a functional ligand for the KDEL receptor.

Studies in N2a, COS7 and HEK293 cells provide evidence for HEDL-driven ER-Golgi localization of novel ER resident cysteine-rich with EGF-like domains 2 (CRELD2) (Oh-hashi et al., 2009; Oh-hashi, Kunieda, Hirata, & Kiuchi, 2011). N2a cells stably expressing a Myc-tagged CRELD2 construct exhibit perinuclear staining (Oh-hashi et al., 2009) that looks similar to what I observed in the immunolabeled and EGFP-conjugated VNUT colocalization analyses. Modifications to the C-terminal HEDL motif, such as a deletion of all four residues or the addition of tags like hemagglutinin or Myc/His, altered the localization of CRELD2. Instead of primarily residing within the ER-Golgi complex with occasional spontaneous secretion, C-terminal alterations to CRELD2 significantly increased secretion (Oh-hashi et al., 2011). The four C-terminal residues (R/H)EDL in the CRELD2 C-terminus are highly conserved amongst human, bovine, murine, rat,

chicken, xenopus, and zebrafish (Oh-hashi et al., 2011). The (R/H) variation of the -4 position was also seen in mammalian VNUT (Fig 4.9). In COS7 cells, immunoreactive CRELD2 colocalized with ER and Golgi markers calnexin and GM130, respectively, although colocalization with the latter was partial (Oh-hashi et al., 2011). In N2a cells, the ER-Golgi complex marker BODIPY-conjugated brefeldin A colocalized with Myc-tagged or EGFP-conjugated CRELD2 (Oh-hashi et al., 2009). These results further support ER-Golgi localization of this HEDL motif-bearing protein.

The flexibility of KDEL receptor recognition (Raykhel et al., 2007) seems to allow various permutations of the KDEL motif in the four terminal residues of ER residents, such EDEL, KVEL, KEEL, and QEDL (Oh-hashi et al., 2011). Even greater permutations of the KDEL motif may be functional. For example, ER resident mesencephalic astrocyte-derived neurotrophic factor (MANF) has a C-terminal R(T/S)(DE)L sequence, although KDEL motif variants are not as efficient as the KDEL motif itself (Gerondopoulos et al., 2021; Oh-Hashi, Norisada, Hirata, & Kiuchi, 2015). When the REDL sequence of mouse CRELD2 was replaced with RTDL, CRELD2 secretion was dramatically increased. In comparison, replacing the HEDL sequence with the canonical KDEL motif largely eliminated secretion of CRELD2 (Oh-Hashi et al., 2015). The KDEL motif greatly improves the efficacy of the KDEL receptor retention of ER residents, yet the HDEL motif variant has greater affinity for the KDEL receptor than the KDEL motif (Gerondopoulos et al., 2021). An explanation for the KDEL receptor recognition flexibility might be explained by the sheer abundance of some proteins and the relative scarcity of others.

The sheer amount of KDEL-bearing proteins, about 5-10 μM, results in competition for available KDEL2 receptors, the concentration of which is approximately 0.2-0.3 μM in HeLa cells (Gerondopoulos et al., 2021). With a five-fold greater concentration of proteins compared to the HDEL and RDEL variants, less abundant ER proteins can better compete with the KDEL-bearers by bearing a motif with a greater affinity for KDEL receptors, HEDL (Gerondopoulos et al., 2021). Differences in receptor affinity did not change the localization of the receptors. As long as ligands bore the HDEL, KDEL, or RDEL motif variations (ordered from highest affinity to lowest), the KDEL receptors were largely localized to the ER (Gerondopoulos et al., 2021). However, the flexibility of KDEL receptor recognition has limits. DDEL and ADEL motif variants have far lower affinities for the KDEL receptor. The presence of ligands bearing these sequences does not stimulate KDEL receptor-driven retrieval to the ER, instead resulting in KDEL receptor

accumulation in the Golgi (Gerondopoulos et al., 2021). Collectively, the KDEL motif and receptor studies of N2a, COS7, HEK293, and HeLa cells suggest the HEDL motif in the C-terminal tail of VNUT could be a functional ligand for the KDEL receptor.

5.3.2. Molecular Evidence of VNUT Localization to the ER-Golgi Complex

Throughout our experiments, my lab members and I noticed VNUT puncta in the perinuclear space. My experiments used anti-VNUT antibodies and genetically encoded EGFP-VNUT. N- and C-terminally tagged EGFP-VNUT constructs allowed visualization of differences in localization in case the conjugated EGFP impaired VNUT trafficking. Compared to the variability of the N-terminus, the risk of impaired trafficking seemed greater with the C-terminal EGFP-VNUT construct since mammalian C-termini are highly conserved in sequence and length (Fig 4.5A). However, both constructs were successfully expressed and trafficked in a similar manner to immunolabeled VNUT. The EGFP-VNUT clustered in the perinuclear space (Fig 3.16B,C). While some ER-Golgi aggregation of the overexpressed protein could be explained by limited availability of cellular transport machinery, I did not expect to see a similar degree of clustering in the immunocytochemistry-based experiments (Fig 3.16A). Other lab members noticed similar subcellular localization patterns of VNUT in their live-cell imaging experiments using VNUT-pHluorin.

Intense, perinuclear fluorescent signals were observed in live-cell imaging experiments using VNUT-pHluorin. Our lab developed several VNUT-pHluorin constructs to study real-time, stimulated vesicle release. Instead of seeing brief instances of signal corresponding to vesicular fusion and release events, other members of the Poburko lab noticed consistent, relatively stable fluorescence within the N2a cells. During live-cell imaging of N2a cells, the VNUT-pHluorin expression product aggregated primarily near the nucleus (Fig 3.17B). The intensity of the pHluorin emission signal intensifies with increasing pH (Grillo-Hill, Webb, & Barber, 2014). The correlation between pH and intensity allows general inferences to be made about the localization of the pHluorin. Largely diffuse labeling was observed throughout the cell in a compartment of near neutral pH, and a localized accumulation o the reporter in nucleus-adjacent compartments that had a slightly acidic pH (~6.5). These compartments were acidified with sodium butyrate, quenching the VNUT-pHluorin probe (Fig 3.17B). De-quenching

occurred with ammonium chloride, resulting in a maximal fluorescent signal. Approximations based on the normalized change in fluorescence relative to the range of fluorescence intensity suggests the pH of the VNUT-pHluorin-containing compartment ranges from pH 6-7 (Gastaldello & Poburko, 2021; unpublished observations). The ER has a pH of approximately 7.2 while the Golgi apparatus ranges from a pH of 6 to 6.7 (Rivinoja, Pujol, Hassinen, & Kellokumpu, 2012). The higher pH of these compartments could explain the intensity of the pHluorin in the perinuclear space, supporting the localization of VNUT to the ER-Golgi complex (Fig 3.17).

In contrast, when the Poburko Lab fused the red pH-sensitive fluorescent protein pHuji into the luminal S1-2 loop of VMAT2, this probe was largely localized to highly acidic vesicles. Some portion of the pHuji probe was externalized, indicated by rapid quenching with acidic MES buffered saline (pH 5.5) and dequenching with alkaline TRIS buffered saline (pH 8.2). However, a greater proportion of VMAT2-pHuji exhibited peak fluorescence when the cells were exposed to ammonium chloride buffered saline (Fig 3.17B). The relative differences between the initial-quenched intensity and the initial-maximal intensity indicated localization of most of the VMAT2-pHuji probe to acidified, fusion competent compartments. These observations are a stark contrast to the VNUT-pHluorin localization and responses, suggesting that VNUT is not localized to readily releasable, fusion competent compartments. Instead, VNUT-pHluorin is retained within the cell in compartments of slightly acidic to near neutral pH, which is most compatible with the ER-Golgi complex.

5.4. Future Studies and Concluding Remarks

To validate my findings of VNUT localization to the ER-Golgi complex, I identified several future experiments. Firstly, I suggest experiments to confirm the identity of the compartments as ER or Golgi. VNUT colocalization analyses using ER and/or Golgi markers are absent from my thesis due to time constraints, but this research would benefit from immunostaining of these compartments or transfecting cells with fluorescently tagged, genetically encoded markers. Examples of ER markers include the calcium binding chaperone calreticulin, synthesis chaperone binding immunoglobulin protein (BIP), and the enzyme protein disulphide-isomerase (PDI). Our lab has recently acquired the mDsRed-Golgi-7 Golgi-localizing fluorescent probe from Dr. Michael Davidson (Addgene plasmid # 55832). Colocalization analyses between ER and Golgi

markers and VNUT, as described in this thesis, would allow the quantification of the frequency of VNUT localization to these compartments.

Additional experiments using molecular techniques would complement immunolabeling. One such experiment would replicate the VMAT2-VAChT chimera experiments seen in the literature (Varoqui & Erickson, 1998). The Poburko lab has shown VMAT2 localization to highly acidified fusion competent compartments, likely synaptic vesicles, in N2a cells using genetically encoded VMAT2-pHuji. This construct functions in a similar manner to VNUT-pHluorin (B. Kim, 2019). I propose an experiment in which the C-terminal domains of the VMAT2-pHuji and the VNUT-pHluorin constructs are swapped. I predict the VNUT-pHluorin chimera with the VMAT2 C-terminal region would traffic to synaptic vesicles, while the VMAT2-pHuji chimera would exhibit perinuclear localization indicative of the ER-Golgi complex. This experiment serves to identify the C-terminal domain as being necessary and sufficient for targeting VNUT to the ER-Golgi complex. An additional experiment, which follows the same avenue of investigation, has two components. The first component involves truncating VNUT-pHluorin or the N-terminal, EGFP-tagged VNUT construct. Removing the HEDL portion of the C-terminus should alter targeting from the ER-Golgi complex. As shown in COS7 and HEK293 cells (Oh-hashi et al., 2011), altering the C-terminal HEDL sequence should result in increased secretion of VNUT. The second component of this experiment involves mutating the amino acids within the HEDL sequence, similar to the KDEL sequence mutation study (Raykhel et al., 2007). Mutations in the HEDL motif should result in a loss of ER-Golgi localization and most likely increased secretion. The use of N-terminal, EGFP-tagged VNUT or the VNUT-pHluorin is recommended due to the fluorescent probes residing well away from the C-terminal domain. Combined with the immunocytochemical analyses, these data could provide promising evidence of VNUT localization to the ER-Golgi complex.

In brief, my thesis work sought to identify the molecular fingerprint of a VNUT-containing vesicle. I predicted VNUT would localize to purinergic synaptic vesicles in my neuron-like N2a cell model. Immunolabeling and exogenous expression techniques identified sparse VNUT localization to vesicles. Large clusters of VNUT puncta were observed in the perinuclear space, possibly indicating the native trafficking pattern of VNUT to an organelle near the nucleus. Since perinuclear enrichment was observed with antibodies and genetically encoded probes, the accumulation of VNUT at the perinuclear space is

not due to sequestration of the fluorescent probe nor due to non-specific binding of the anti-VNUT antibodies. Bioinformatics-based studies identified a lack of synaptic vesicle targeting sequences in the C-terminal domain of VNUT, unlike other synaptic vesicle-associated transporters. Further, the C-terminus of mammalian VNUT contains an HEDL motif that bears a striking resemblance to the KDEL recognition motif responsible for retrieval of escaped ER proteins from the Golgi. Due to time constraints and COVID-19-related complications, I was unable to test my first sub-hypothesis that VNUT-mediated, Ca^{2+}-dependent ATP release from N2a cells is vesicular. I was able to do some troubleshooting identifying the optimal concentration of the calcium ionophore 4Br-A23187 (AbCam, cat# 142244), which I have described in Appendix A. In conclusion, the distribution of VNUT and pattern of colocalization with diverse marker proteins is most compatible with localization to the ER-Golgi complex in N2a cells. VNUT may be involved in indirect ATP-loading of synaptic vesicles by establishing an ATP-rich environment in Golgi outposts, ERGICS and/or endosomes that play a role in vesicle recycling.

References

Aasland, R., Abrams, C., Ampe, C., Ball, L. J., Bedford, M. T., Cesareni, G., … Winder, S. J. (2002, February 20). Normalization of nomenclature for peptide motifs as ligands of modular protein domains. *FEBS Letters*. Elsevier. https://doi.org/10.1016/S0014-5793(01)03295-1

Abeliovich, H. (2019, November 15). New gadget in the membrane trafficking toolbox: A novel inhibitor of SNARE priming. *Journal of Biological Chemistry*. American Society for Biochemistry and Molecular Biology Inc. https://doi.org/10.1074/jbc.H119.011334

Aberer, W., Stitzel, R., Winkler, H., & Huber, E. (1979). Accumulation of C[3H]ATP in small dense core vesicles of superfused vasa deferentia. *Journal of Neurochemistry*, *33*, 797–801. https://doi.org/10.1111/j.1471-4159.1979.tb05227.x

Aguet, F., Member, S., Ville, D. Van De, Unser, M., Van De Ville, D., & Unser, M. (2008). Model-based 2.5-D deconvolution for extended depth-of-field in brightfield microscopy. *IEEE Transactions on Image Processing*, *17*(7), 1144–1153. https://doi.org/10.1109/TIP.2008.924393

Ahdut-Hacohen, R., Duridanova, D., Meiri, H., & Rahamimoff, R. (2004). Hydrogen ions control synaptic vesicle ion channel activity in Torpedo electromotor neurones. *Journal of Physiology*, *556*(2), 347–352. https://doi.org/10.1113/jphysiol.2003.058818

Akopova, I., Tatur, S., Grygorczyk, M., Luchowski, R., Gryczynski, I., Gryczynski, Z., … Grygorczyk, R. (2012). Imaging exocytosis of ATP-containing vesicles with TIRF microscopy in lung epithelial A549 cells. *Purinergic Signalling*, *8*(1), 59–70. https://doi.org/10.1007/s11302-011-9259-2

Arthur, C. P., Dean, C., Pagratis, M., Chapman, E. R., & Stowell, M. H. B. (2010). Loss of Synaptotagmin IV Results in a Reduction in Synaptic Vesicles and a Distortion of the Golgi. *Neuroscience*, *167*(1), 135–142. https://doi.org/10.1016/j.neuroscience.2010.01.056.LOSS

Banfield, D. K. (2011). Mechanisms of Protein Retention in the Golgi. *Cold Spring Harbor Perspectives in Biology*, *3*(8). https://doi.org/10.1101/cshperspect.a005264

Bartholome, O., Van Den Ackerveken, P., Gil, J. S., Bonardeaux, O. de la B., Leprince, P., Franzen, R., & Rogister, B. (2017, May 22). Puzzling out synaptic vesicle 2 family members functions. *Frontiers in Molecular Neuroscience*. Frontiers Media S.A. https://doi.org/10.3389/fnmol.2017.00148

Beckel, J. M., Gómez, N. M., Lu, W., Campagno, K. E., Nabet, B., Albalawi, F., … Mitchell, C. H. (2018). Stimulation of TLR3 triggers release of lysosomal ATP in astrocytes and epithelial cells that requires TRPML1 channels. *Scientific Reports*, *8*(5726). https://doi.org/10.1038/s41598-018-23877-3

Bjelobaba, I., Janjic, M. M., & Stojilkovic, S. S. (2015). Purinergic Signaling Pathways in the Endocrine System. *Autonomic Neuroscience: Basic and Clinical*, *191*, 102–116. https://doi.org/10.1016/j.autneu.2015.04.010

Bodin, P., & Burnstock, G. (2001). Purinergic signalling: ATP release. *Neurochemical Research*, *26*(8–9), 959–969. https://doi.org/10.1023/A:1012388618693

Bolte, S., & Cordelières, F. P. (2006, December 1). A guided tour into subcellular colocalization analysis in light microscopy. *Journal of Microscopy*. Blackwell Publishing Ltd. https://doi.org/10.1111/j.1365-2818.2006.01706.x

Bonifacino, J. S., & Traub, L. M. (2003). Signals for Sorting of Transmembrane Proteins to Endosomes and Lysosomes. *Annu. Rev. Biochem*, *72*, 395–447. https://doi.org/10.1146/annurev.biochem.72.121801.161800

Boudreault, F., & Grygorczyk, R. (2002). Cell swelling-induced ATP release and gadolinium-sensitive channels. *American Journal of Physiology - Cell Physiology*, *282*(1 51-1), 219–226. https://doi.org/10.1152/ajpcell.00317.2001

Burnstock, G. (2007). Physiology and pathophysiology of purinergic neurotransmission. *Physiological Reviews*, *87*(2), 659–797. https://doi.org/10.1152/physrev.00043.2006

Burnstock, G. (2009, March 25). Autonomic neurotransmission: 60 Years since Sir Henry Dale. *Annual Review of Pharmacology and Toxicology*. Annual Reviews . https://doi.org/10.1146/annurev.pharmtox.052808.102215

Burnstock, G., Cocks, T., Kasakov, L., & Wong, H. K. (1978). Direct Evidence for ATP Release from Non-Adrenergic, Non-Cholinergic (“Purinergic”) Nerves in the Guinea-Pig Taenia Coli and Bladder. *European Journal of Pharmacology*, *49*, 145–149. https://doi.org/10.1016/0014-2999(78)90070-5

Cao, Q., Zhao, K., Zoë Zhong, X., Zou, Y., Yu, H., Huang, P., … Dong, X.-P. (2014). SLC17A9 Protein Functions as a Lysosomal ATP Transporter and Regulates Cell Viability *. *Journal of Biological Chemistry*, *289*(33), 23189–23199. https://doi.org/10.1074/jbc.M114.567107

Coco, S., Calegari, F., Pravettoni, E., Pozzi, D., Taverna, E., Rosa, P., … Verderio, C. (2003). Storage and Release of ATP from Astrocytes in Culture. *Journal of Biological Chemistry*, *287*(2), 1354–1362. https://doi.org/10.1074/jbc.M209454200

Colgan, L., Liu, H., Huang, S. Y., & Liu, Y. J. (2007). Dileucine motif is sufficient for internalization and synaptic vesicle targeting of vesicular acetylcholine transporter. *Traffic*, *8*(5), 512–522. https://doi.org/10.1111/j.1600-0854.2007.00555.x

Colocalization Analysis. (2020). Retrieved February 1, 2021, from https://imagej.net/Colocalization_Analysis

D'amico, M. A., Ghinassi, B., Izzicupo, P., Manzoli, L., & Di Baldassarre, A. (2014). Biological function and clinical relevance of chromogranin A and derived peptides. *Endocrine Connections*, *3*(2), R45–R54. https://doi.org/10.1530/EC-14-0027

Dahl, G. (2015). ATP release through pannexon channels. *Philosophical Transactions of the Royal Society B: Biological Sciences*, *370*(1672), 1–11. https://doi.org/10.1098/rstb.2014.0191

Davids, M., Kane, M. S., He, M., Wolfe, L. A., Li, X., Raihan, M. A., … Toro, C. (2016). Disruption of Golgi morphology and altered protein glycosylation in PLA2G6-associated neurodegeneration. *Journal of Medical Genetics*, *53*(3), 180–189. https://doi.org/10.1136/jmedgenet-2015-103338

Dean, C., Liu, H., Mark Dunning, F., Chang, P. Y., Jackson, M. B., & Chapman, E. R. (2009). Synaptotagmin-IV modulates synaptic function and long-term potentiation by regulating BDNF release. *Nature Neuroscience 2009 12:6*, *12*(6), 767–776. https://doi.org/10.1038/NN.2315

Denker, A., & Rizzoli, S. O. (2010, October 5). Synaptic Vesicle Pools: An Update. *Frontiers in Synaptic Neuroscience*. Frontiers. https://doi.org/10.3389/fnsyn.2010.00135

Diener, M., Helmle-Kolb, C., Murer, H., & Scharrer, E. (1993). Effect of short-chain fatty acids on cell volume and intracellular pH in rat distal colon. *European Journal of Physiology*, *424*, 216–223. https://doi.org/10.1007/BF00384345

Dobson, L., Reményi, I., & Tusnády, G. E. (2015a). CCTOP: a Consensus Constrained TOPology prediction web server. *Nucleic Acids Research*, *43*(W1), W408–W412. https://doi.org/10.1093/NAR/GKV451

Dobson, L., Reményi, I., & Tusnády, G. E. (2015b). The human transmembrane proteome. *Biology Direct*, *10*(1), 1–18. https://doi.org/10.1186/S13062-015-0061-X

Dunn, K. W., Kamocka, M. M., & McDonald, J. H. (2011, April). A practical guide to evaluating colocalization in biological microscopy. *American Journal of Physiology - Cell Physiology*. American Physiological Society Bethesda, MD. https://doi.org/10.1152/ajpcell.00462.2010

Estévez-Herrera, J., Domínguez, N., Pardo, M. R., González-Santana, A., Westhead, E. W., Borges, R., & Machado, J. D. (2016). ATP: The crucial component of secretory vesicles. *Proceedings of the National Academy of Sciences of the United States of America*, *113*(28), E4098–E4106. https://doi.org/10.1073/pnas.1600690113

Farhan, H., Reiterer, V., Kriz, A., Hauri, H.-P., Pavelka, M., Sitte, H. H., & Freissmuth, M. (2008). Signal-dependent export of GABA transporter 1 from the ER-Golgi intermediate compartment is specified by a C-terminal motif. *Journal of Cell Science*, *121*(6), 753–761. https://doi.org/10.1242/JCS.017681

Fletcher, P. A., Scriven, D. R. L., Schulson, M. N., & Moore, E. D. W. (2010). Multi-image colocalization and its statistical significance. *Biophysical Journal*, *99*(6), 1996–2005. https://doi.org/10.1016/j.bpj.2010.07.006

Freyberg, Z., Sonders, M. S., Aguilar, J. I., Hiranita, T., Karam, C. S., Flores, J., … Javitch, J. A. (2016). Mechanisms of amphetamine action illuminated through optical monitoring of dopamine synaptic vesicles in Drosophila brain. *Nature Communications*, *7*(1), 1–15. https://doi.org/10.1038/ncomms10652

Geisler, J. C., Corbin, K. L., Li, Q., Feranchak, A. P., Nunemaker, C. S., & Li, C. (2013). Vesicular nucleotide transporter-mediated ATP release regulates insulin secretion. *Endocrinology*, *154*(2), 675–684. https://doi.org/10.1210/en.2012-1818

Gerondopoulos, A., Bräuer, P., Sobajima, T., Wu, Z., Parker, J. L., Biggin, P., … Newstead, S. (2021). A signal capture and proofreading mechanism for the KDEL-receptor explains selectivity and dynamic range in ER retrieval. *ELife*, *10*, e68380. https://doi.org/10.7554/ELIFE.68380

Gómez-Villafuertes, R., Del Puerto, A., Díaz-Hernández, M., Bustillo, D., Díaz-Hernández, J. I., Huerta, P. G., … Miras-Portugal, M. T. (2009). Ca2+/calmodulin-dependent kinase II signalling cascade mediates P2X7 receptor-dependent inhibition of neuritogenesis in neuroblastoma cells. *FEBS Journal*, *276*(18), 5307–5325. https://doi.org/10.1111/j.1742-4658.2009.07228.x

Gould, S. J., Keller, G.-A., & Subramani, S. (1987). Identification of a Peroxisomal Targeting Signal at the Carboxy Terminus of Firefly Luciferase. *Journal of Cell Biology*, *105*(6), 2923–2931. https://doi.org/10.1083/jcb.105.6.2923

Gualix, J., Pintor, J., & Miras-Portugal, M. T. (1999). Characterization of nucleotide transport into rat brain synaptic vesicles. *Journal of Neurochemistry*, *73*(3), 1098–1104. https://doi.org/10.1046/j.1471-4159.1999.0731098.x

Guarnieri, F. G., Arterburn, L. M., Penno, M. B., Cha, Y., & August, J. T. (1993). The motif Tyr-X-X-hydrophobic residue mediates lysosomal membrane targeting of lysosome-associated membrane protein 1. *Journal of Biological Chemistry*, *268*(3), 1941–1946. https://doi.org/10.1016/S0021-9258(18)53945-4

Gutiérrez-Martín, Y., Bustillo, D., Gómez-Villafuertes, R., Sánchez-Nogueiro, J., Torregrosa-Hetland, C., Binz, T., … Artalejo, A. R. (2011). P2X7 receptors trigger ATP exocytosis and modify secretory vesicle dynamics in neuroblastoma cells. *Journal of Biological Chemistry*, *286*(13), 11370–11381. https://doi.org/10.1074/jbc.M110.139410

Hearn, S. A. (1987). Electron microscopic localization of chromogranin A in osmium-fixed neuroendocrine cells with a protein A-gold technique. *Journal of Histochemistry and Cytochemistry*, *35*(7), 795–801. https://doi.org/10.1177/35.7.3295032

Held, R. G., & Kaeser, P. S. (2018). ELKS active zone proteins as multitasking scaffolds for secretion. *Open Biology*, *8*(2). https://doi.org/10.1098/rsob.170258

Ho, T., Jobling, A. I., Greferath, U., Chuang, T., Ramesh, A., Fletcher, E. L., & Vessey, K. A. (2015). Vesicular expression and release of ATP from dopaminergic neurons of the mouse retina and midbrain. *Frontiers in Cellular Neuroscience*, *9*, 389. https://doi.org/10.3389/fncel.2015.00389

Holton, P. (1959). The liberation of adenosine triphosphate on antidromic stimulation of sensory nerves. *The Journal of Physiology*, *145*(3), 494–504. https://doi.org/10.1113/jphysiol.1959.sp006157

Hoon Huh, Y., Hoo Jeon, S., & Hyun Yoo, S. (2003). Chromogranin B-induced Secretory Granule Biogenesis COMPARISON WITH THE SIMILAR ROLE OF CHROMOGRANIN A*. *THE JOURNAL OF BIOLOGICAL CHEMISTRY*, *278*(42), 40581–40589. https://doi.org/10.1074/jbc.M304942200

Horton, A. C., & Ehlers, M. D. (2003). Dual Modes of Endoplasmic Reticulum-to-Golgi Transport in Dendrites Revealed by Live-Cell Imaging. *Journal of Neuroscience*, *23*(15), 6188–6199. https://doi.org/10.1523/JNEUROSCI.23-15-06188.2003

Ibata, K., Fukuda, M., Hamada, T., Kabayama, H., & Mikoshiba, K. (2000). Synaptotagmin IV Is Present at the Golgi and Distal Parts of Neurites. *Journal of Neurochemistry*, *74*(2), 518–526. https://doi.org/10.1046/J.1471-4159.2000.740518.X

Imura, Y., Morizawa, Y., Komatsu, R., Shibata, K., Shinozaki, Y., Kasai, H., … Koizumi, S. (2013). Microglia release ATP by exocytosis. *Glia*, *61*(8), 1320–1330. https://doi.org/10.1002/glia.22517

Intracellular transport: 4.2 Peptide signal sequences. (2020). Retrieved February 1, 2021, from https://www.open.edu/openlearn/science-maths-technology/science/biology/intracellular-transport/content-section-4.2

Jung, J., Shin, Y. H., Konishi, H., Lee, S. J., & Kiyama, H. (2013). Possible ATP release through lysosomal exocytosis from primary sensory neurons. *Biochemical and Biophysical Research Communications*, *430*(2), 488–493. https://doi.org/10.1016/j.bbrc.2012.12.009

Kalderon, D., Roberts, B. L., Richardson, W. D., & Smith, A. E. (1984). A short amino acid sequence able to specify nuclear location. *Cell*, *39*(3 PART 2), 499–509. https://doi.org/10.1016/0092-8674(84)90457-4

Kalkhoran, S. M., Chow, S. H. J., Walia, J. S., Gershome, C., Saraev, N., Kim, B., & Poburko, D. (2019). VNUT and VMAT2 segregate within sympathetic varicosities and localize near preferred Cav2 isoforms in the rat tail artery. *American Journal of Physiology-Heart and Circulatory Physiology*, *316*(1), H89–H105. https://doi.org/10.1152/ajpheart.00560.2018

Kato, Y., Hiasa, M., Ichikawa, R., Hasuzawa, N., Kadowaki, A., Iwatsuki, K., … Miyaji, T. (2017). Identification of a vesicular ATP release inhibitor for the treatment of neuropathic and inflammatory pain. *Proceedings of the National Academy of Sciences of the United States of America*, *114*(31), E6297–E6305. https://doi.org/10.1073/pnas.1704847114

Kelly, B. T., Graham, S. C., Liska, N., Dannhauser, P. N., Höning, S., Ungewickell, E. J., & Owen, D. J. (2014). AP2 controls clathrin polymerization with a membrane-activated switch. *Science*, *345*(6195), 459–463. https://doi.org/10.1126/science.1254836

Kennedy, C., McLaren, G. J., Westfall, T. D., & Sneddon, P. (1996). ATP as a co-transmitter with noradrenaline in sympathetic nerves--function and fate. *Ciba Foundation Symposium*, *198*, 223–235; discussion 235-8.

Kim, B. (2019). *Design and Validation of Genetically Encoded Probes for the Analysis of Neuronal Catecholamine and ATP Co-transmission*. Simon Fraser University.

Kim, S., Baek, J., Jung, U., Lee, S., Jung, W., Kim, J., & Kang, S. (2013). Mouse neuroblastoma cell-based model and the effect of epileptic events on calcium oscillations and neural spikes. In *Proc. SPIE 8879, Nano-Bio Sensing, Imaging, and Spectroscopy, 88790T* (Vol. 8879). https://doi.org/10.1117/12.2017666

Kinoshita, M., Hirayama, Y., Fujishita, K., Shibata, K., Shinozaki, Y., Shigetomi, E., … Koizumi, S. (2018). Anti-Depressant Fluoxetine Reveals its Therapeutic Effect Via Astrocytes. *EBioMedicine*, *32*, 72–83. https://doi.org/10.1016/j.ebiom.2018.05.036

Kirkpatrick, K., & Burnstock, G. (1987). Sympathetic nerve-mediated release of ATP from the guinea-pig vas deferens is unaffected by reserpine. *European Journal of Pharmacology*, *138*(2), 207–214. https://doi.org/10.1016/0014-2999(87)90434-1

Kloukina-Pantazidou, I., Chrysanthou-Piterou, M., Havaki, S., & Issidorides, M. R. (2013). Chromogranin A and Vesicular Monoamine Transporter 2 Immunolocalization in Protein Bodies of Human Locus Coeruleus Neurons. *Ultrastructural Pathology*, *37*(2), 102–109. https://doi.org/10.3109/01913123.2012.750410

Lange, A., Mills, R. E., Lange, C. J., Stewart, M., Devine, S. E., & Corbett, A. H. (2007, February 23). Classical Nuclear Localization Signals: Definition, Function, and Interaction with Importin α. *Journal of Biological Chemistry*. Papers in Press. https://doi.org/10.1074/jbc.R600026200

Larsson, M., Sawada, K., Morland, C., Hiasa, M., Ormel, L., Moriyama, Y., & Gundersen, V. (2012). Functional and anatomical identification of a vesicular transporter mediating neuronal ATP release. *Cerebral Cortex*, *22*(5), 1203–1214. https://doi.org/10.1093/cercor/bhr203

Lazarenko, R. M., DelBove, C. E., Strothman, C. E., & Zhang, Q. (2017). Ammonium chloride alters neuronal excitability and synaptic vesicle release. *Scientific Reports 2017 7:1*, *7*(1), 1–12. https://doi.org/10.1038/s41598-017-05338-5

Li, Haiyan, Santos, M. S., Park, C. K., Dobry, Y., & Voglmaier, S. M. (2017). VGLUT2 trafficking is differentially regulated by adaptor proteins AP-1 and AP-3. *Frontiers in Cellular Neuroscience*, *11*(October), 1–20. https://doi.org/10.3389/fncel.2017.00324

Li, Haiyan, Waites, C. L., Staal, R. G., Dobryy, Y., Park, J., Sulzer, D. L., & Edwards, R. H. (2005). Sorting of vesicular monoamine transporter 2 to the regulated secretory pathway confers the somatodendritic exocytosis of monoamines. *Neuron*, *48*(4), 619–633. https://doi.org/10.1016/j.neuron.2005.09.033

Li, Huinan, & Harlow, M. L. (2014). Individual synaptic vesicles from the electroplaque of *Torpedo californica* , a classic cholinergic synapse, also contain transporters for glutamate and ATP. *Physiological Reports*, *2*(1), e00206. https://doi.org/10.1002/phy2.206

Li, M., Zhong, Z., Zhu, J., Xiang, D., Dai, N., Cao, X., … Wang, D. (2010). Identification and Characterization of Mitochondrial Targeting Sequence of Human Apurinic/Apyrimidinic Endonuclease 1 * □ S. *Journal of Biological Chemistry*, *285*(20), 14871–14881. https://doi.org/10.1074/jbc.M109.069591

Li, S., Hu, K., Cao, W., Sun, Y., Sheng, W., Li, F., … Liang, X. J. (2014). pH-responsive biocompatible fluorescent polymer nanoparticles based on phenylboronic acid for intracellular imaging and drug delivery. *Nanoscale*, *6*(22), 13701–13709. https://doi.org/10.1039/c4nr04054f

Liu, H., Bai, H., Hui, E., Yang, L., Evans, C. S., Wang, Z., … Chapman, E. R. (2014). Synaptotagmin 7 functions as a Ca2+-sensor for synaptic vesicle replenishment. *ELife*, *2014*(3). https://doi.org/10.7554/eLife.01524.001

Liu, J., Liu, W., & Yang, J. (2016). ATP-containing vesicles in stria vascular marginal cell cytoplasms in neonatal rat cochlea are lysosomes. *Scientific Reports*, *6*(20903). https://doi.org/10.1038/srep20903

Locovei, S., Scemes, E., Qiu, F., Spray, D. C., & Dahl, G. (2007). Pannexin1 is part of the pore forming unit of the P2X7 receptor death complex. *FEBS Letters*, *581*(3), 483–488. https://doi.org/10.1016/j.febslet.2006.12.056

Marques, S. M., & Esteves Da Silva, J. C. G. (2009). Firefly bioluminescence: A mechanistic approach of luciferase catalyzed reactions. *IUBMB Life*, *61*(1), 6–17. https://doi.org/10.1002/iub.134

Masuda, T., Ozono, Y., Mikuriya, S., Kohro, Y., Tozaki-Saitoh, H., Iwatsuki, K., … Inoue, K. (2016). Dorsal horn neurons release extracellular ATP in a VNUT-dependent manner that underlies neuropathic pain. *Nature Communications*, *7*, 1–11. https://doi.org/10.1038/ncomms12529

Maximov, A. (2009). Synaptotagmins. In L. Squire (Ed.), *Encyclopedia of Neuroscience* (pp. 819–821). Elsevier L. https://doi.org/https://doi.org/10.1016/B978-008045046-9.01358-9

Meister, B., Grünebach, F., Bautz, F., Brugger, W., Fink, F.-M., Kanz, L., & Möhle, R. (1999). Expression of vascular endothelial growth factor (VEGF) and VEGF receptors in human neuroblastomas. *European Journal of Cancer*, *35*(3), 445–449. https://doi.org/10.1016/s0959-8049(98)00387-6

Meldrum, L. A., & Burnstock, G. (1983). Evidence that ATP acts as a Co-Transmitter with Noradrenaline in Sympathetic Nerves Supplying the Guinea-Pig Vas Deferens. *European Journal of Pharmacology*, *92*(1–2), 161–163. https://doi.org/https://doi.org/10.1016/0014-2999(83)90126-7

Menéndez-Méndez, A., Díaz-Hernández, J. I., & Miras-Portugal, M. T. (2015). The vesicular nucleotide transporter (VNUT) is involved in the extracellular ATP effect on neuronal differentiation. *Purinergic Signalling*, *11*(2), 239–249. https://doi.org/10.1007/s11302-015-9449-4

Menéndez-Méndez, A., Díaz-Hernández, J. I., Ortega, F., Gualix, J., Gómez-Villafuertes, R., & Miras-Portugal, M. T. (2017). Specific Temporal Distribution and Subcellular Localization of a Functional Vesicular Nucleotide Transporter (VNUT) in Cerebellar Granule Neurons. *Frontiers in Pharmacology*, *8*, 951. https://doi.org/10.3389/fphar.2017.00951

Merighi, A. (2018). Costorage of High Molecular Weight Neurotransmitters in Large Dense Core Vesicles of Mammalian Neurons. *Frontiers in Cellular Neuroscience*, *12*, 272. https://doi.org/10.3389/fncel.2018.00272

Miesenböck, G., De Angelis, D. A., & Rothman, J. E. (1998). Visualizing secretion and synaptic transmission with pH-sensitive green fluorescent proteins. *Nature 1998 394:6689*, *394*(6689), 192–195. https://doi.org/10.1038/28190

Mihara, H., Uchida, K., Koizumi, S., & Moriyama, Y. (2018). Involvement of VNUT-exocytosis in transient receptor potential vanilloid 4-dependent ATP release from gastrointestinal epithelium. *PLOS ONE*, *13*(10), e0206276. https://doi.org/10.1371/journal.pone.0206276

Mikhaylova, M., Bera, S., Kobler, O., Frischknecht, R., & Kreutz, M. R. (2016). A Dendritic Golgi Satellite between ERGIC and Retromer. *Cell Reports*, *14*, 189–199. https://doi.org/10.1016/j.celrep.2015.12.024

Miras-Portugal, M. T., Menéndez-Méndez, A., Gómez-Villafuertes, R., Ortega, F., Delicado, E. G., Pérez-Sen, R., & Gualix, J. (2019, May 14). Physiopathological role of the vesicular nucleotide transporter (VNUT) in the central nervous system: Relevance of the vesicular nucleotide release as a potential therapeutic target. *Frontiers in Cellular Neuroscience*. Frontiers Media S.A. https://doi.org/10.3389/fncel.2019.00224

Moreno, R. D., Ramalho-Santos, J., Chan, E. K. L., Wessel, G. M., & Schatten, G. (2000). The Golgi apparatus segregates from the lysosomal/acrosomal vesicle during rhesus spermiogenesis: Structural alterations. *Developmental Biology*, *219*(2), 334–349. https://doi.org/10.1006/dbio.2000.9606

Mori, Y., & Fukuda, M. (2011). Synaptotagmin IV acts as a multi-functional regulator of Ca 2+-dependent exocytosis. *Neurochemical Research*, *36*(7), 1222–1227. https://doi.org/10.1007/s11064-010-0352-7

Moriyama, S., & Hiasa, M. (2016). *Expression of Vesicular Nucleotide Transporter in the Mouse Retina*. *Biol. Pharm. Bull* (Vol. 564). https://doi.org/https://doi.org/10.1248/bpb.b15-00872

Moriyama, Y., Hiasa, M., Sakamoto, S., Omote, H., & Nomura, M. (2017). Vesicular nucleotide transporter (VNUT): appearance of an actress on the stage of purinergic signaling. *Purinergic Signalling*, *13*(3), 387–404. https://doi.org/10.1007/s11302-017-9568-1

Moriyama, Y., & Nomura, M. (2017). Clodronate: A Vesicular ATP Release Blocker. *Trends in Pharmacological Sciences*, *39*(1), 13–23. https://doi.org/10.1016/j.tips.2017.10.007

Murana, E., Pagani, F., Basilico, B., Sundukova, M., Batti, L., Di Angelantonio, S., … Ragozzino, D. (2017). ATP release during cell swelling activates a Ca2+-dependent Cl - Current by autocrine mechanism in mouse hippocampal microglia. *Scientific Reports*, *7*(1), 1–16. https://doi.org/10.1038/s41598-017-04452-8

Nagwaney, S., Harlow, M. L., Jung, J. H., Szule, J. A., Ress, D., Xu, J., … McMahan, U. J. (2009). Macromolecular connections of active zone material to docked synaptic vesicles and presynaptic membrane at neuromuscular junctions of mouse. *The Journal of Comparative Neurology*, *513*(5), 457–468. https://doi.org/10.1002/cne.21975

Namsi, A., Nury, T., Hamdouni, H., Yammine, A., Vejux, A., Vervandier-Fasseur, D., … Lizard, G. (2018). Induction of Neuronal Differentiation of Murine N2a Cells by Two Polyphenols Present in the Mediterranean Diet Mimicking Neurotrophins Activities: Resveratrol and Apigenin. *Diseases*, *6*(3), 67. https://doi.org/10.3390/diseases6030067

Obermüller, S., Lindqvist, A., Karanauskaite, J., Galvanovskis, J., Rorsman, P., & Barg, S. (2005). Selective nucleotide-release from dense-core granules in insulin-secreting cells. *Journal of Cell Science*, *118*(18), 4271–4282. https://doi.org/10.1242/jcs.02549

Offermanns, S., & Rosenthal, W. (Eds.). (2004). Non-adrenergic Non-cholinergic (NANC) Transmission/Mediators. In *Encyclopedic Reference of Molecular Pharmacology* (p. 663). https://doi.org/10.1007/3-540-29832-0

Oh-hashi, K., Koga, H., Ikeda, S., Shimada, K., Hirata, Y., & Kiuchi, K. (2009). CRELD2 is a novel endoplasmic reticulum stress-inducible gene. *Biochemical and Biophysical Research Communications*, *387*(3), 504–510. https://doi.org/10.1016/j.bbrc.2009.07.047

Oh-hashi, K., Kunieda, R., Hirata, Y., & Kiuchi, K. (2011). Biosynthesis and secretion of mouse cysteine-rich with EGF-like domains 2. *FEBS Letters*, *585*(15), 2481–2487. https://doi.org/10.1016/J.FEBSLET.2011.06.029

Oh-Hashi, K., Norisada, J., Hirata, Y., & Kiuchi, K. (2015). Characterization of the Role of MANF in Regulating the Secretion of CRELD2. *Biol. Pharm. Bull*, *38*(5), 722–731. https://doi.org/10.1248/bpb.b14-00825

Omote, H., & Moriyama, Y. (2013). Vesicular Neurotransmitter Transporters: An Approach for Studying Transporters With Purified Proteins. *Physiology*, *28*(1), 39–50. https://doi.org/10.1152/physiol.00033.2012

OneZoom Tree of Life Explorer. (n.d.). Retrieved May 29, 2021, from https://www.onezoom.org/

Onoa, B., Li, H., Gagnon-Bartsch, J. A., Elias, L. A. B., & Edwards, R. H. (2010). Vesicular monoamine and glutamate transporters select distinct synaptic vesicle recycling pathways. *Journal of Neuroscience*, *30*(23), 7917–7927. https://doi.org/10.1523/JNEUROSCI.5298-09.2010

Ori-McKenney, K. M., Jan, L. Y., & Jan, Y. N. (2012). Golgi Outposts Shape Dendrite Morphology by Functioning as Sites of Acentrosomal Microtubule Nucleation in Neurons. *Neuron*, *76*(5), 921–930. https://doi.org/10.1016/j.neuron.2012.10.008

Oya, M., Kitaguchi, T., Yanagihara, Y., Numano, R., Kakeyama, M., Ikematsu, K., & Tsuboi, T. (2013). Vesicular nucleotide transporter is involved in ATP storage of secretory lysosomes in astrocytes. *Biochemical and Biophysical Research Communications*, *438*(1), 145–151. https://doi.org/10.1016/j.bbrc.2013.07.043

Öztürk, Z., O'Kane, C. J., & Pérez-Moreno, J. J. (2020). Axonal Endoplasmic Reticulum Dynamics and Its Roles in Neurodegeneration. *Frontiers in Neuroscience*, *14*(January), 1–33. https://doi.org/10.3389/fnins.2020.00048

Pandey, K. N. (2009). Functional roles of short sequence motifs in the endocytosis of membrane receptors. *Frontiers in Bioscience*, *14*(14), 5339–5360. https://doi.org/10.2741/3599

Pankratov, Y., Lalo, U., Verkhratsky, A., & North, R. A. (2006, August 26). Vesicular release of ATP at central synapses. *Pflugers Archiv European Journal of Physiology*. Springer. https://doi.org/10.1007/s00424-006-0061-x

Pelegrin, P., & Surprenant, A. (2006). Pannexin-1 mediates large pore formation and interleukin-1β release by the ATP-gated P2X7 receptor. *EMBO Journal*, *25*(21), 5071–5082. https://doi.org/10.1038/sj.emboj.7601378

Pérez de Lara, M. J., Guzmán-Aránguez, A., de la Villa, P., Díaz-Hernández, J. I., Miras-Portuga, M. T., & Pintor, J. (2015). Increased levels of extracellular ATP in glaucomatous retinas: Possible role of the vesicular nucleotide transporter during the development of the pathology. *Molecular Vision*, *21*, 1060–1070. Retrieved from http://www.molvis.org/molvis/v21/1060

Pierzynska-Mach, A Janowski, P. A., & Dobrucki, J. W. (2014). Evaluation of Acridine Orange, LysoTracker Red, and Quinacrine as Fluorescent Probes for Long-Term Tracking of Acidic Vesicles. *Cytometry Part A*, *85*(8), 729–737. https://doi.org/10.1002/cyto.a.22495

Poburko, D. (n.d.). Image Analysis Tools. Retrieved February 1, 2021, from https://www.sfu.ca/mcpg/PoburkoLabMain/imageAnalysisTools.html

Prado, V. F., & Prado, M. A. M. (2002, December). Signals Involved in Targeting Membrane Proteins to Synaptic Vesicles. *Cellular and Molecular Neurobiology*. Springer. https://doi.org/10.1023/A:1021884319363

Raykhel, I., Alanen, H., Salo, K., Jurvansuu, J., Van, D. N., Latva-Ranta, M., & Ruddock, L. (2007). A molecular specificity code for the three mammalian KDEL receptors. *Journal of Cell Biology*, *179*(6), 1193–1204. https://doi.org/10.1083/jcb.200705180

Reimer, R. J. (2013). SLC17: A functionally diverse family of organic anion transporters. *Molecular Aspects of Medicine*, *34*(2–3), 350–359. https://doi.org/https://doi.org/10.1016/j.mam.2012.05.004

Roy, C., Gagné, V., Fernandes, M. J. G., & Marceau, F. (2013). High affinity capture and concentration of quinacrine in polymorphonuclear neutrophils via vacuolar ATPase-mediated ion trapping: Comparison with other peripheral blood leukocytes and implications for the distribution of cationic drugs. *Toxicology and Applied Pharmacology*, *270*(2), 77–86. https://doi.org/10.1016/j.taap.2013.04.004

Rudnick, G. (2008). Vesicular ATP transport is a hard (V)NUT to crack. *PNAS*, *105*(16), 5949–5950. https://doi.org/10.1073/pnas.0802774105

Sabirov, R. Z., Dutta, A. K., & Okada, Y. (2001). Volume-dependent ATP-conductive large-conductance anion channel as a pathway for swelling-induced ATP release. *Journal of General Physiology*, *118*(3), 251–266. https://doi.org/10.1085/jgp.118.3.251

Sakamoto, S., Miyaji, T., Hiasa, M., Ichikawa, R., Uematsu, A., Iwatsuki, K., … Moriyama, Y. (2014). Impairment of vesicular ATP release affects glucose metabolism and increases insulin sensitivity. *Scientific Reports*, *4*(1), 1–10. https://doi.org/10.1038/srep06689

Sankaranarayanan, S., De Angelis, D., Rothman, J. E., & Ryan, T. A. (2000). The Use of pHluorins for Optical Measurements of Presynaptic Activity. *Biophysical Journal*, *79*(4), 2199–2208. https://doi.org/10.1016/S0006-3495(00)76468-X

Sawada, K., Echigo, N., Juge, N., Miyaji, T., Otsuka, M., Omote, H., … Moriyama, Y. (2008). Identification of a vesicular nucleotide transporter. *Proceedings of the National Academy of Sciences of the United States of America*, *105*(15), 5683–5686. https://doi.org/10.1073/pnas.0800141105

Schindelin, J., Arganda-Carreras, I., Frise, E., Kaynig, V., Longair, M., Pietzsch, T., … Cardona, A. (2012). Fiji: An open-source platform for biological-image analysis. *Nature Methods*, *9*(7), 676–682. https://doi.org/10.1038/nmeth.2019

Schmid, S. L. (1997, November 28). Clathrin-coated vesicle formation and protein sorting: An integrated process. *Annual Review of Biochemistry*. Annual Reviews 4139 El Camino Way, P.O. Box 10139, Palo Alto, CA 94303-0139, USA . https://doi.org/10.1146/annurev.biochem.66.1.511

Shastry, P., Basu, A., & Rajadhyaksha, M. S. (2001). Neuroblastoma cell lines - a versatile in vitro model in neurobiology. *International Journal of Neuroscience*, *108*(1–2), 109–126. https://doi.org/10.3109/00207450108986509

Shin, Y. H., Lee, J., & Jung, J. (2012). Secretion of ATP from Schwann cells through lysosomal exocytosis during Wallerian degeneration. *Biochemical and Biophysical Research Communications*, *429*(3–4), 163–167. https://doi.org/10.1016/j.bbrc.2012.10.121

Smythe, L. M., Yamboliev, I. A., & Mutafova-Yambolieva, V. N. (2008). N-type and P/Q-type calcium channels regulate differentially the release of noradrenaline, ATP and β-NAD in blood vessels. *Neuropharmacology*, *56*(2), 368–378. https://doi.org/10.1016/j.neuropharm.2008.09.007

Sneddon, P., & Westfall, D. P. (1984). Pharmacological evidence that adenosine triphosphate and noradrenaline are co-transmitters in the guinea-pig vas deferens. *The Journal of Physiology*, *347*(1), 561–580. https://doi.org/10.1113/jphysiol.1984.sp015083

Stjärne, L. (2001). Novel dual “small” vesicle model of ATP- and noradrenaline-mediated sympathetic neuromuscular transmission. *Autonomic Neuroscience: Basic and Clinical*, *87*(1), 16–36. https://doi.org/10.1016/S1566-0702(00)00246-0

Suedhof, T. (2012). The Presynaptic Active Zone. *Neuron*, *75*(1), 11–25. https://doi.org/10.1016/j.neuron.2012.06.012.The

Swayne, L. A., Sorbara, C. D., & Bennett, S. A. L. (2010). Pannexin 2 is expressed by postnatal hippocampal neural progenitors and modulates neuronal commitment. *Journal of Biological Chemistry*, *285*(32), 24977–24986. https://doi.org/10.1074/jbc.M110.130054

Teasdale, R. D., Jackson, M. R., & Johnson, R. W. (1996). *Signal-mediated Sorting of Membrane Proteins Between the Endoplasmic Reticulum and the Golgi Apparatus*. *Annu. Rev. Cell Dev. Biol* (Vol. 12). Retrieved from www.annualreviews.org

Todorov, L. D., Mihaylova-Todorova, S., Craviso, G. L., Bjur, R. A., & Westfall, D. P. (1996). Evidence for the differential release of the cotransmitters ATP and noradrenaline from sympathetic nerves of the guinea-pig vas deferens. *The Journal of Physiology*, *496*(3), 731–748. https://doi.org/10.1113/jphysiol.1996.sp021723

Todorov, L. D., Mihaylova-Todorova, S. T., Bjur, R. A., & Westfall, D. P. (1999). Differential cotransmission in sympathetic nerves: Role of frequency of stimulation and prejunctional autoreceptors. *Journal of Pharmacology and Experimental Therapeutics*, *290*(1), 241–246.

Tremblay, R. G., Sikorska, M., Sandhu, J. K., Lanthier, P., Ribecco-Lutkiewicz, M., & Bani-Yaghoub, M. (2010). Differentiation of mouse Neuro 2A cells into dopamine neurons. *Journal of Neuroscience Methods*, *186*(1), 60–67. https://doi.org/10.1016/j.jneumeth.2009.11.004

Vacca, F., Scott, C., & Gruenberg, J. (2016). The Late Endosome. In *Encyclopedia of Cell Biology* (Vol. 2, pp. 201–210). https://doi.org/10.1016/B978-0-12-394447-4.20017-5

Van Ael, E., & Fransen, M. (2006, December 1). Targeting Signals in Peroxisomal Membrane Proteins. *Biochimica et Biophysica Acta - Molecular Cell Research*. Elsevier. https://doi.org/10.1016/j.bbamcr.2006.08.020

Varoqui, H., & Erickson, J. D. (1998). The Cytoplasmic Tail of the Vesicular Acetylcholine Transporter Contains a Synaptic Vesicle Targeting Signal. *Journal of Biological Chemistry*, *273*(15), 9094–9098. https://doi.org/10.1074/jbc.273.15.9094

Verkhratsky, A., & Krishtal, O. (2009). Adenosine Triphosphate (ATP) as a Neurotransmitter. *Encyclopedia of Neuroscience*, *1*, 115–123. https://doi.org/10.1016/B978-008045046-9.01245-6

Weng, W. C., Lin, K. H., Wu, P. Y., Ho, Y. H., Liu, Y. L., Wang, B. J., … Lee, H. (2017). VEGF expression correlates with neuronal differentiation and predicts a favorable prognosis in patients with neuroblastoma. *Scientific Reports*, *7*(1), 1–11. https://doi.org/10.1038/s41598-017-11637-8

Westfall, D. P., Todorov, L. D., Mihaylova-Todorova, S. T., & Bjur, R. A. (1996). Differences between the regulation of noradrenaline and ATP release. *Journal of Autonomic Pharmacology*, *16*(6), 393–395. https://doi.org/10.1111/j.1474-8673.1996.tb00061.x

Wicki-Stordeur, L. E., Dzugalo, A. D., Swansburg, R. M., Suits, J. M., & Swayne, L. A. (2012). Pannexin 1 regulates postnatal neural stem and progenitor cell proliferation. *Neural Development*, *7*(1), 11. https://doi.org/10.1186/1749-8104-7-11

Wimalasena, K. (2011). Vesicular monoamine transporters: Structure-function, pharmacology, and medicinal chemistry. *Medicinal Research Reviews*, *31*(4), 483–519. https://doi.org/10.1002/med.20187

Wreden, C. C., Wlizla, M., & Reimer, R. J. (2005). Varied mechanisms underlie the free sialic acid storage disorders. *Journal of Biological Chemistry*, *280*(2), 1408–1416. https://doi.org/10.1074/jbc.M411295200

Wu, L. G., Hamid, E., Shin, W., & Chiang, H. C. (2014, February). Exocytosis and endocytosis: Modes, functions, and coupling mechanisms*. *Annual Review of Physiology*. NIH Public Access. https://doi.org/10.1146/annurev-physiol-021113-170305

Wu, P. Y., Lin, Y. C., Chang, C. L., Lu, H. T., Chin, C. H., Hsu, T. T., … Sun, S. H. (2009). Functional decreases in P2X7 receptors are associated with retinoic acid-induced neuronal differentiation of Neuro-2a neuroblastoma cells. *Cellular Signalling*, *21*(6), 881–891. https://doi.org/10.1016/j.cellsig.2009.01.036

Wu, Z., He, K., Chen, Y., Li, H., Pan, S., Li, B., … Li, Y. (2021). An ultrasensitive GRAB sensor for detecting extracellular ATP in vitro and in vivo. *BioRxiv*, 2021.02.24.432680. https://doi.org/10.1101/2021.02.24.432680

Xiong, Y., Sun, S., Teng, S., Jin, M., & Zhou, Z. (2018). Ca2+-Dependent and Ca2+-Independent ATP Release in Astrocytes. *Frontiers in Molecular Neuroscience*, *11*, 224. https://doi.org/10.3389/fnmol.2018.00224

Xu, X., Wicki-Stordeur, L. E., Sanchez-Arias, J. C., Liu, M., Weaver, M. S., Choi, C. S. W., & Swayne, L. A. (2018). Probenecid disrupts a novel pannexin 1-collapsin response mediator protein 2 interaction and increases microtubule stability. *Frontiers in Cellular Neuroscience*, *12*(May), 1–13. https://doi.org/10.3389/fncel.2018.00124

Yin, Y., Hong, J., Phạm, T. L., Shin, J., Gwon, D. H., Kwon, H. H., … Kim, D. W. (2019). Evans blue reduces neuropathic pain behavior by inhibiting spinal ATP release. *International Journal of Molecular Sciences*, *20*(18). https://doi.org/10.3390/ijms20184443

Ying, M., Flatmark, T., & Saraste, J. (2000). The p58-positive pre-Golgi intermediates consist of distinct subpopulations of particles that show differential binding of COPI and COPII coats and contain vacuolar H+-ATPase. *Journal of Cell Science*, *113*(20), 3623–3638. https://doi.org/10.1242/jcs.113.20.3623

Yoon, T. Y., & Munson, M. (2018). SNARE complex assembly and disassembly. *Current Biology*, *28*(8), R397–R401. https://doi.org/10.1016/j.cub.2018.01.005

Yoshihara, M., Adolfsen, B., Galle, K. T., & Littleton, J. T. (2005). Retrograde signaling by Syt 4 induces presynaptic release and synapse-specific growth. *Science*, *310*(5749), 858–863. https://doi.org/10.1126/SCIENCE.1117541

Zhang, Z., Chen, G., Zhou, W., Song, A., Xu, T., Luo, Q., … Duan, S. (2007). Regulated ATP release from astrocytes through lysosome exocytosis. *Nature Cell Biology*. https://doi.org/10.1038/ncb1620

Zhong, X. Z., Cao, Q., Sun, X., & Dong, X. P. (2016). Activation of lysosomal P2X4 by ATP transported into lysosomes via VNUT/SLC17A9 using V-ATPase generated voltage gradient as the driving force. *Journal of Physiology*, *594*(15), 4253–4266. https://doi.org/10.1113/JP271893

Appendix A.

VNUT-Mediated, Ca^{2+}-Dependent ATP Release from N2a Cells is Vesicular

This sub aim sought to corroborate literature findings by visualizing A23187-induced ATP release in real-time using the novel GRAB-$ATP_{1.0}$ sensor, as shown in Figure A.1. Further, I planned to assess relative changes in GRAB-$ATP_{1.0}$ response when the cells were exposed to pharmacological agonists of VNUT, the SNARE complex, and pannexin channels using clodronate, NEM, and probenecid, respectively. As discussed in Section 1.2.1, clodronate is a selective inhibitor of VNUT, unlike Evans Blue or DIDs. Clodronate has been used to study VNUT-mediated purinergic signaling involved in neuropathic pain (Mihara et al., 2018; Y. Moriyama & Nomura, 2017). NEM is an inhibitor of the SNARE complex dissociation mediator N-ethylmaleimide-sensitive factor (NSF) that has been in use since the 1980s (Abeliovich, 2019). Probenecid has been used to study the role of Panx1 during neuritogenesis in N2a cells as well as primary neural stem and progenitor cells (Wicki-Stordeur et al., 2012; Xu et al., 2018). The calcium ionophore A23187 has been used to induce ATP release in rat hippocampal neurons (Kato et al., 2017; Larsson et al., 2012). Figure A.2 illustrates predicted effects of each inhibitor. The first step in setting up an experimental protocol for assessing changes in the relative amounts of ATP release in response to the describe inhibitors was identifying the optimal concentration of 4-Br-A23187 for inducing ATP release.

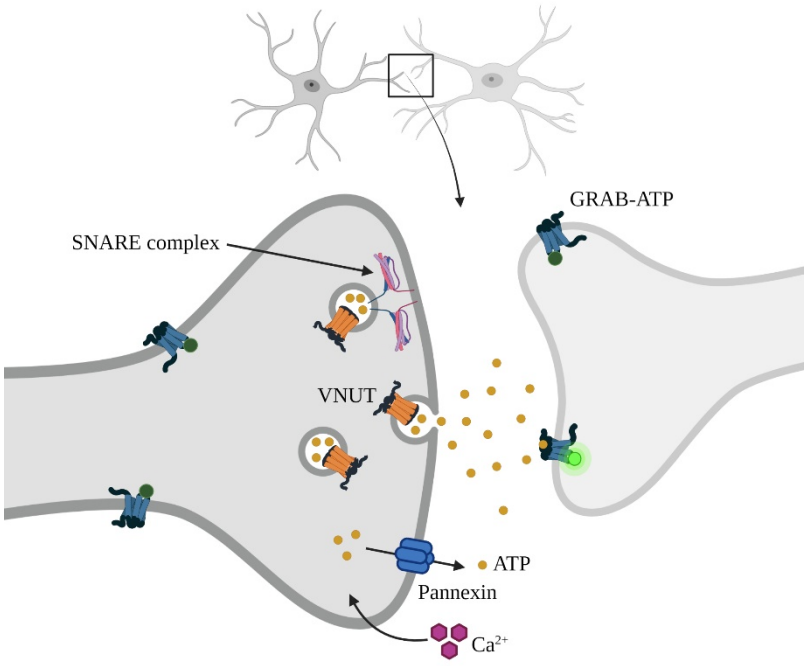

Figure A.1 Overview of ATP release mechanisms and GRAB$_{ATP1.0}$ activation
Created with BioRender.com.

Subsequently, the optimal concentrations of each inhibitor would be determined. Complications due to the COVID-19 pandemic reduced my ability to troubleshoot my protocol, however I was able to elicit an intracellular calcium response to 4-Br-A23187.

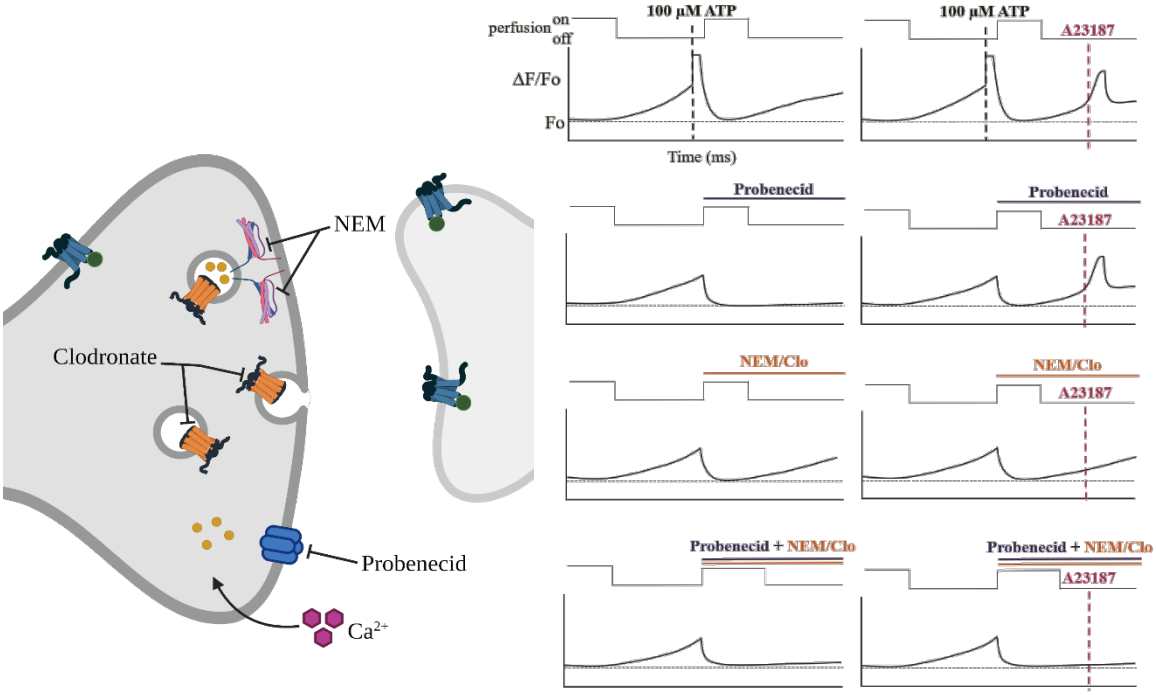

Figure A.2 Predicted changes in GRAB-ATP$_{1.0}$ fluorescence in response during application of ATP release inhibitors
Created in Part with BioRender.com.

Methods and Materials

In preparation for live-cell experiments, N2a cells were seeded at 5 K cells per well of a 96-well plate (Greiner Bio-One, cat# 655090). The cells were stored in a humidified cell culture incubator that maintained an internal environment of 37°C, 5% CO_2, and 95% air. One day post-seeding, the cells were transfected with the GRAB-ATP$_{1.0}$ sensor at a 1:2 ratio of DNA to jetPRIME reagent using the jetPRIME DNA transfection kit and protocol from Polyplus (cat# 114-07). After the four-hour transfection incubation time, the transfection media was replaced with fresh, warmed GM. Cells were allowed to recover for one day prior to differentiation. After two days of differentiation in DM (described in Section 2.1.1), the cells were imaged. The cell preparation methodology is summarized in Figure A.3.

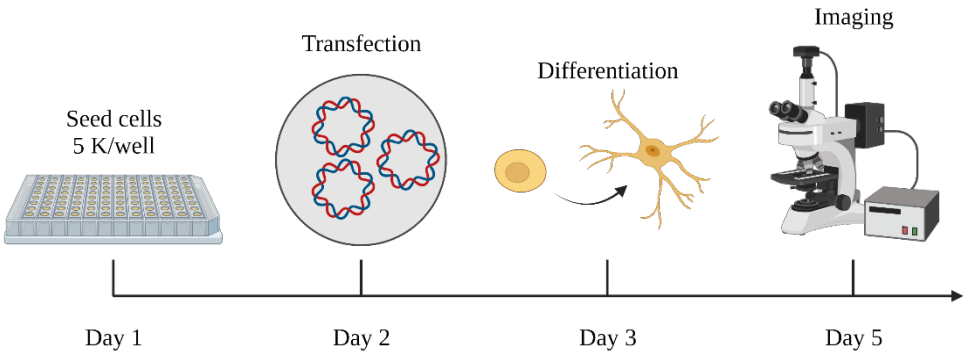

Figure A.3 Cell preparation for live-cell imaging of GRAB-ATP
Created with BioRender.com.

Transfected cells were incubated for 30 minutes in GM containing 3 µg/mL Hoeschst-33342 (Invitrogen Molecular Probes, cat# H3570). To visualized calcium dynamics, CalBryte was loaded into untransfected cells with a CalBryte loading solution containing 2.5 µM CalBryte-520L AM from a 1 mM stock in DMSO (AAT Bioquest, cat# 20640), 0.1% pluronic F-127, and 3 µg/mL Hoeschst-33342 in GM. After a 30-minute incubation at 37°C, the loading solutions for transfected and untransfected cells were replaced with 100 µL HEPES buffer (140 mM NaCl, 5 mM KCl, 10 mM HEPES, 2 mM $CaCl_2$, 1.5 mM $MgCl_2$, 10 mM glucose, pH 7.4), as shown in Figure A.4.

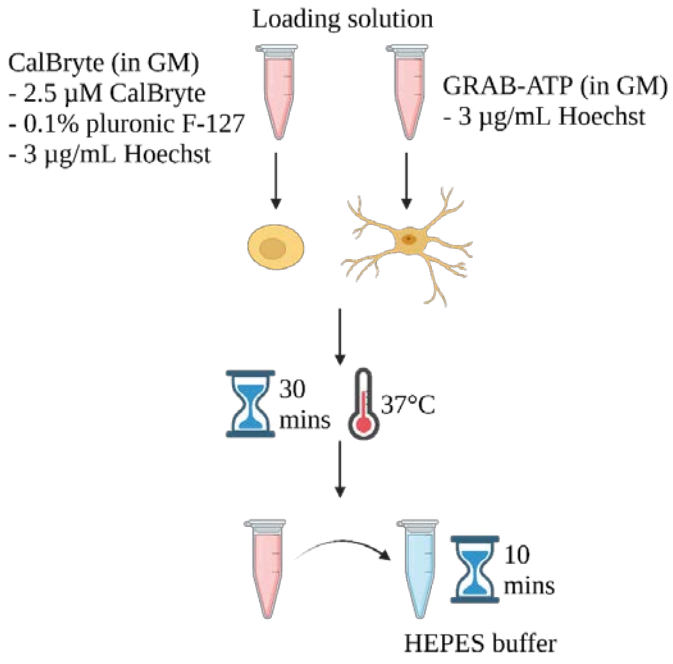

Figure A.4 Pre-imaging DNA staining and calcium dye loading
Created with BioRender.com.

Unless otherwise stated, perfusion solutions were prepared in HEPES buffer and delivered onto the cells manually using a pipet. Successive acquisition of the GFP (488 nm) and mCherry (510 nm) signals from the genetically encoded $GRAB_{ATP1.0}$ probe used QD480 and QD560 dichroic mirrors, respectively. The mCherry signal stably identified transfected cells, while the GFP signal was only visible when the receptor bound to a ligand (ATP). CalBryte signals were acquired using the same settings as GFP

acquisition. Time-lapse data were acquired using the same microscope and camera equipment as described in Section 2.3. Twice concentrated working solutions of 4-Bromo-A23187 was prepared at concentrations ranging from 2 µM to 10 mM. To induce

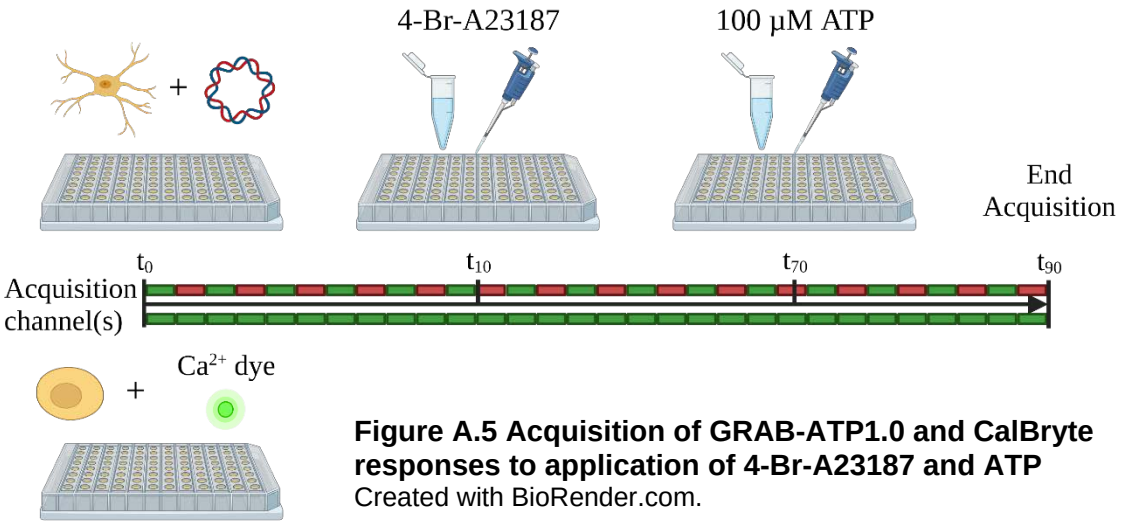

Figure A.5 Acquisition of GRAB-ATP1.0 and CalBryte responses to application of 4-Br-A23187 and ATP
Created with BioRender.com.

a maximal GRAB-ATP$_{1.0}$ response, a 3X concentrated working solution of 300 µM was prepared from a 100 mM stock in HEPES buffer. The 4-Br-A23187 and ATP were added sequentially to the 100 µL HEPES already present in the wells, resulting in a 1X concentration of each reagent. The 4-Br-A23187 was added to the cells 10 seconds into acquisition, followed by ATP at approximately 70 seconds into acquisition. Each round of acquisition was 90 seconds. The acquisition set-up is illustrated in Figure A.5.

Results

The calcium sensing dye CalBryte confirmed increased levels of intracellular calcium in response to 200 µM 4-Br-A23187, shown in Figure A.6. The CalBryte signal steadily increased after addition of the calcium ionophore, followed by maximum fluorescence when 100 µM ATP was added to the well.

The GRAB-ATP$_{1.0}$ sensor did not show a response to concentrations of 4-Br-A23187 ranging from 1 µM to 200 µM final well concentration. The sensor was functional, indicated by immediate, robust responses to the manually added ATP as shown in Figure A.7. Further troubleshooting is needed to optimize the concentration of 4-Br-A23187 needed to illicit ATP release.

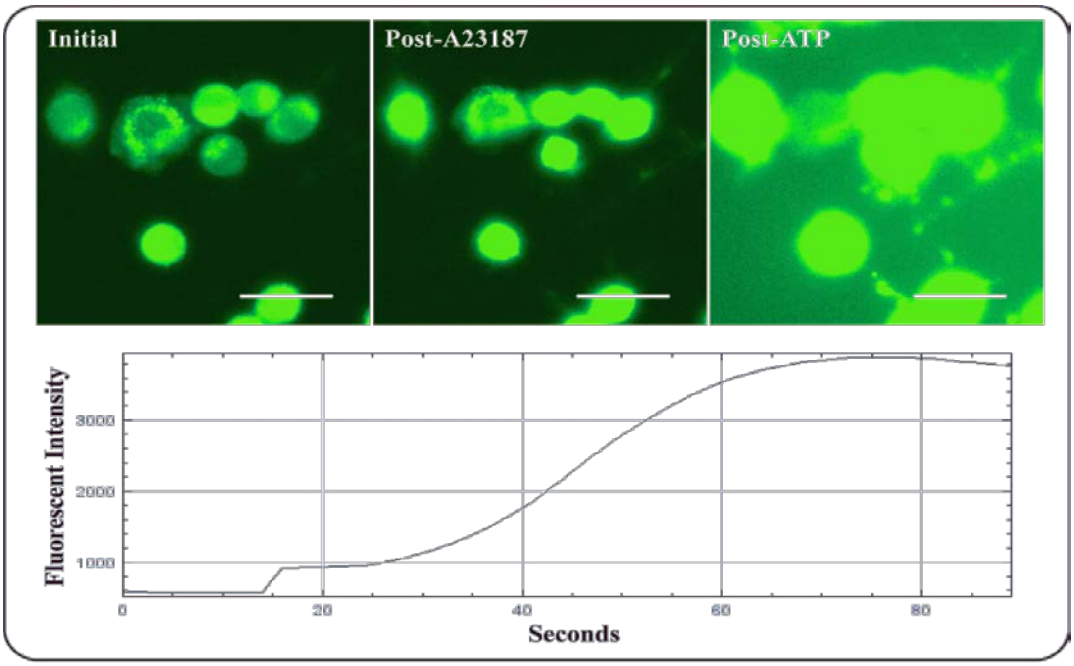

Figure A.6 Changes in CalBryte signal in response to 200 µM 4-Br-A23187 and ATP
Scale bar = 10 µM.

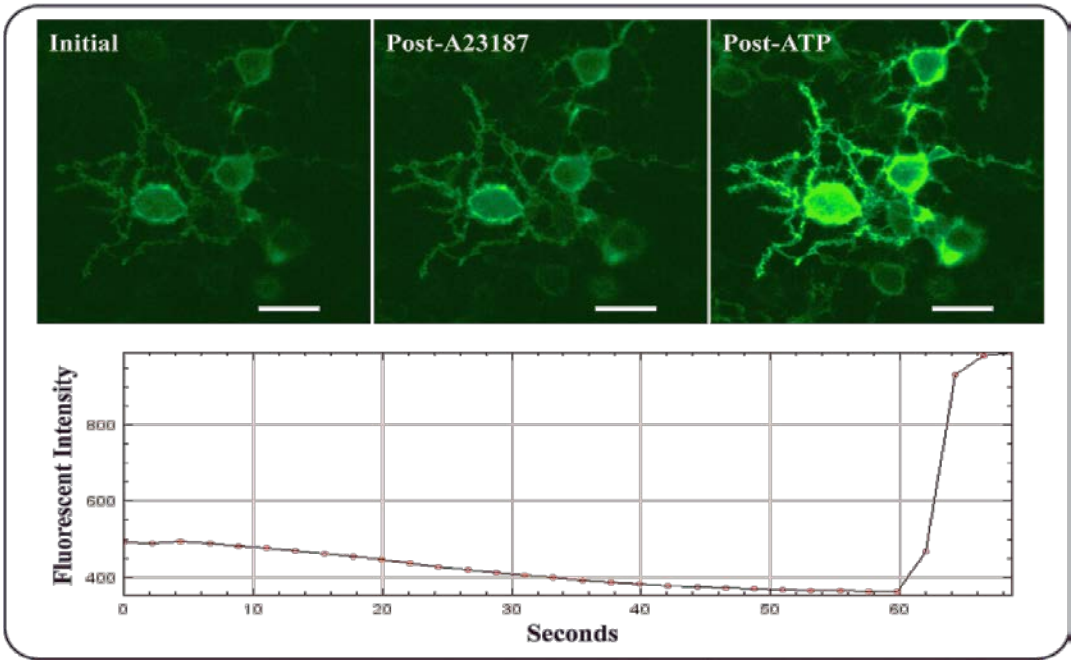

Figure A.7 Representative images and trace of GRAB-ATP1.0 response to 4-Br-A23187 and ATP
Scale bar = 10 µM. Emission of mCherry at 510 nm not shown.

Appendix B.

Testing Anti-VNUT Antibody Specificity using shRNA-Mediated Knockdown of VNUT

To test if the anti-VNUT polyclonal antibody was specific for VNUT, I designed shRNA constructs using pEGFP-C1 RPEL1-EGFP-3XNLS gifted from Dr. Dyche Mullins (Addgene plasmid # 58469). This plasmid encoded a nuclear localized EGFP, which identified successfully transfected cells. Based on the pEGFP backbone, I designed two recombinant plasmids. The first contained a firefly luciferase (FFL) shRNA sequence and served as a negative control for VNUT knock down (5'-CTGACGCGGAATACTTCGA -3') and the second contained a VNUT shRNA sequence (5'-GAACAAGAAGGAGGCTGGTATCGTGCTCA-3') (Menéndez-Méndez et al., 2015). The shRNA sequences were designed as gBlocks Gene Fragments (IDT) to allow future use in other plasmids. The gBlocks included priming sequences, Esp3I TypeIIS restriction enzyme consensus sequences (New England BioLabs, cat# R0734S), and an H1 promoter sequence. The backbone and gBlocks were assembled using a Golden Gate Assembly-based protocol.

The first step of assembling the recombinant pEGFP construct was linearizing of the backbone. Using primers that would simultaneously insert complementary Esp31 sequence onto either end of the backbone, the plasmid was linearized after the third nuclear localization sequence and before the SV40 poly(A) signal via PCR. The backbone and gBlocks were combined using same-reaction restriction and ligation using Esp3I and T4 DNA ligase (New England BioLabs, cat# M0202S). Figure B.1 illustrates the molecular workflow for constructing the recombinant VNUT shRNA and firefly luciferase shRNA constructs, referred to as pEGFP-C1 EGFP-3XNLS-VNUTshRNA and pEGFP-C1 EGFP-3XNLS-FFLshRNA, respectively. Unfortunately, the constructs failed to ligate successfully despite multiple cloning attempts. Sequencing data indicated no insertion of the gBlocks into the backbone. To troubleshoot, plasmid DNA extracted from DH10ß *Escherichia coli* cells thought to be transformed with linearized plasmid was digested with DpnI restriction enzyme (New England BioLabs, cat# R0176S), which digests methylated DNA such as the non-linearized backbone plasmid. The DpnI-treated

PCR products should have cleaved all parent plasmid. Due to COVID-19 related complications, this project was not completed.

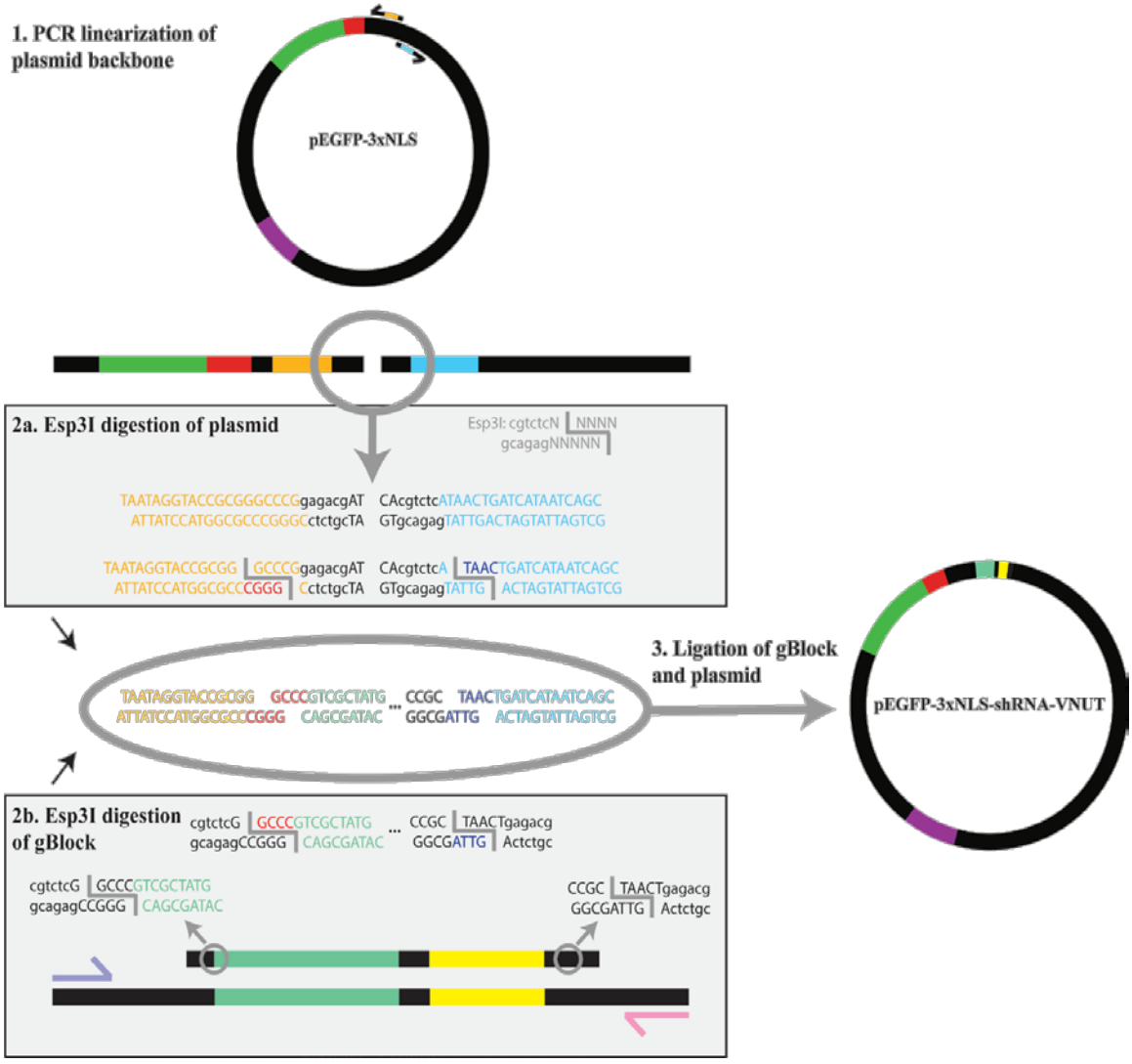

Figure B.1 Molecular workflow to build shRNA constructs using an EGFP-expressing backbone and gBlock gene fragments coding for VNUT and FFL
Top grey box shows the generation of sticky ends on the pEGFP construct, while the lower grey box shows the same process for the gBlock containing the VNUT shRNA sequence. At the center of the figure, both components are ligated via their complementary sticky ends to generate the pEGFP-3xNLS-shRNA-VNUT construct.

Appendix C.

Summary of Protein BLAST Results for the Predicted Cytosolic Domains of Murine VNUT

Table C.1 summarizes series of NCBI protein BLAST results for the cytosolic domains of mouse VNUT (NCBI accession number Q8VCL5). A subset of each BLAST analysis is shown, of which the matched proteins share 100% identity with VNUT. Notes were made for this subset of the BLAST results using the corresponding UniProt and NCBI descriptions. Where multiple isoforms of a protein matched with VNUT, only one isoform was described to compact the table. Some protein names were too long to fit into the .txt results file that was downloaded from NCBI and are incomplete in the table, as denoted by ellipses (…).

Table C.1 Summary of NCBI protein BLAST results

Cytosolic Domain	Protein Name	NCBI Accession	Subcellular Location (typical or predicted)	Gene	Notes on Function/Structure (from UniProt)
N-terminus					
	protein 4.1 isoform 2	NP_001122078.1	Cytoplasm	*EPB41*	major structural element of erythrocyte membrane skeleton; interacts with spectrin and actin filaments; calmodulin binding
	protein RUFY3 isoform 4	NP_001346137.1	Cytoplasm	*RUFY3*	neuronal plastificty & axon growth; interacts with actin filaments

Cytosolic Domain	Protein Name	NCBI Accession	Subcellular Location (typical or predicted)	Gene	Notes on Function/Structure (from UniProt)
	complement component C1q receptor precursor	NP_034870.1	Plasma Membrane	*CD93*	receptor for C1q; might be involved in phagocytosis (monocytes and macrophages) and cell adhesion; calcium binding
	general transcription factor 3C polypeptide 4 isoform 2...	NP_001159505.1	Nucleus	*GTF3C3*	involved in RNA III mediated transcription; DNA binding
S2-3 loop					
	neurogenic locus notch homolog protein 2 precursor	NP_035058.2	Nucleus, Plasma Membrane, Golgi	*NOTCH2*	receptor for ligands related to cell fate determination; calcium binding
	alanine-tRNA ligase, cytoplasmic	NP_666329.2	Cytoplasm	*AARS1*	catalyzes attachment of alanine to tRNA(ala)
	lysine-specific histone demethylase 1B	NP_758466.1	Nucleus	*KDM1B*	corepressor of epigenetic transcriptional activation; demethylates Lys-4 of histone H3
	E3 ubiquitin-protein ligase SMURF1 isoform 1	NP_001033716.1	Plasma Membrane	*SMURF1*	promotes ubiquitination of TRAF family members; role in dendrite formation in melanocytes
	neuronal tyrosine-phosphorylated phosphoinositide-3-kinase...	NP_001343326.1	Mitochondria, Cytoplasm (Human Protein Atlas)	*Nyap2*	regulates neuronal morphologenesis
	sphingomyelin phosphodiesterase 3	NP_067466.1	Golgi, Plasma Membrane	*SMPD3*	catalyzes hydrolysis of spingomyelin

Cytosolic Domain	Protein Name	NCBI Accession	Subcellular Location (typical or predicted)	Gene	Notes on Function/Structure (from UniProt)
	zinc finger protein Eos isoform 1	NP_035902.2	Nucleus	*IKZF4*	DNA binding; recognizes 5'-GGGAATRCC-3' Ikaros binding sequence; transcriptional repressor
	tripartite motif-containing protein 43A isoform 1	NP_001344616.1	Cytoplasm	*Trim43a*	ubiquitin protein ligase; zinc binding; regulation of gene expression
	SPRY domain-containing protein 3	NP_001028449.2	Cytoplasm	*SPRY3*	inhibits neurite growth/arborization
	syntaxin-6	NP_067408.1	Golgi, Endosome, Nucleus, Plasma Membrane	*STX6*	intracellular vesicle trafficking
	rab11 family-interacting protein 1 isoform 1	NP_001074282.1	Endosomes, Phagosomes, Cytoplasm	*RAB11FIP1*	involved in endosomal recycling; Rab11 effector
	actin-binding protein IPP	NP_032415.2	Cytoplasm	*IPP*	might be involved in cytoskeletal organization (actin); actin binding
	dystonin isoform 1	NP_001263693.1	Cytoplasm, Nucleus, ER	*DST*	cytoskeletal linker protein; integrator of intermediate filaments, actin, and microtubules; calcium binding
	dynein heavy chain 8, axonemal	NP_038839.2	Cytoplasm	*DNAH8*	motor protein; ATPase; involved in sperm motility

Cytosolic Domain	Protein Name	NCBI Accession	Subcellular Location (typical or predicted)	Gene	Notes on Function/Structure (from UniProt)
	dynein heavy chain 5, axonemal	NP_579943.3	Cytoplasm	*DNAH5*	motor protein; ATPase; involved in cilium assembly, cardiac development, and left/right symmetry
	ATP-binding cassette sub-family A member 2 isoform 2...	NP_001355553.1	Endosomes, Lysosomes	*ABCA2*	cholestrol sequestration into late endosomes/lysosomes; ATPase activity; ATP binding
	multiple PDZ domain protein isoform 1	NP_001292213.1	Plasma Membrane	*MPDZ*	NMDAR signalling complex member (may have a role in AMPAR potentiaton and synaptic plasticity; promotes clustering of (5)HT2RC (i.e., serotonin receptors) at cell suface
	sodium channel protein type 5 subunit alpha isoform 1...	NP_067519.2	Plasma Membrane, Nucleus, ER	*SCN5A*	mediates permeability to Na^+ ions in a voltage-dependent manner
	sodium channel protein type 1 subunit alpha isoform 1...	NP_001300926.1	Nuclear Body, Plasma Membrane,	*SCN1A*	mediates permeability to Na^+ ions in a voltage-dependent manner
	sodium channel protein type 2 subunit alpha isoform 2...	NP_001333608.1	Plasma Membrane	*SCN2A*	mediates permeability to Na^+ ions in a voltage-dependent manner
	sodium channel protein type 3 subunit alpha isoform 1...	NP_001342095.1	Plasma Membrane	*SCN3A*	mediates permeability to Na^+ ions in a voltage-dependent manner
S4-5 loop					

Cytosolic Domain	Protein Name	NCBI Accession	Subcellular Location (typical or predicted)	Gene	Notes on Function/Structure (from UniProt)
	myosin-15	NP_001159682.1	Cytosol	*MYO15*	intracellular movement; actin binding; ATPase activity; ATP binding; calmodulin binding
	dynein heavy chain 9, axonemal	NP_001093103.1	Cytosol	*DNAH9*	force generating protein for cilia beating; ATP binding
	rab11 family-interacting protein 5 isoform 1	NP_001003955.1	Endosomes, Golgi, Mitochondria	*RAB11FIP5*	Rab effector; protein trafficking from recycling endosomes to plasma membrane
	angiopoietin-1 isoform 2 precursor	NP_001272991.1	Extracellular	*ANGPT1*	binds and activates TEK/TIE2 receptor; regulation of angiogenesis, endothelial cell survival, proliferation, migration, adhesion, and cell spreading, reorganization of action cytoskeletion, maintenace of vascular quiescence
S6-7 loop					
	VNUT	Q8VCL5	Vesicles	*SLC17A9*	involved in vesicular storage and release of ATP
S8-9 loop					
	G protein-activated inward rectifier potassium channel 2 isofo...		Plasma Membrane	*KCNJ6*	influx of potassium

Cytosolic Domain	Protein Name	NCBI Accession	Subcellular Location (typical or predicted)	Gene	Notes on Function/Structure (from UniProt)
	retinoic acid receptor RXR-gamma isoform 1	NP_033133.1	Nucleus	*RXRG*	receptor for retinoic acid; involved in differentiation
	glycosyltransferase 6 domain-containing protein 1 precursor...	NP_001034184.1	Golgi, possibly Vesicles and Plasma Membrane	*GLT6D1*	transferase activity (glycosyl and hexosyl groups)
	roundabout homolog 2 isoform 6 precursor	NP_001345423.1	Plasma Membrane	*ROBO2*	receptor for SLIT2 and maybe SLIT1 (SLITs are possible molecular guidance cues for cellular migration); axonal navigation; differentiation from neural tube during development
	receptor-type tyrosine-protein phosphatase delta isoform 6...	NP_001355921.1	Plasma Membrane	*PTPRD*	bidirectional induction of pre- and post-synaptic differentiation of neurons
S10-11 loop					
	nesprin-2	NP_001005510.2	Sarcoplasmic Reticulum, Nucleus, Plasma Membrane	*SYNE2*	cytoskeletal component; actin binding; maintains organellar organization; might interact with dynein-dynactin motor complexes
	protein argonaute-2	NP_694818.3	Cytoplasm	*AGO2*	involved in RNAi; endoribonuclease activity
	protein argonaute-3	NP_700451.2	Cytoplasm	*AGO3*	involved in RNAi; endoribonuclease activity

Cytosolic Domain	Protein Name	NCBI Accession	Subcellular Location (typical or predicted)	Gene	Notes on Function/Structure (from UniProt)
	protein timeless homolog isoform 3	NP_001157552.1	Nucleus	*TIMELESS*	DNA repair, circadian clock, genome stability; stabilizes replication forks; DNA binding
	cordon-bleu protein-like 1 isoform 2	NP_081501.1	Extracellular	*COBLL1*	actin binding; cadherin binding
	A-kinase anchor protein 11 isoform 1	NP_001157975.1	Cytosol	*AKAP11*	binds and anchors type II regulatory subunits of PKA
	unconventional myosin-XVIIIa isoform 4	NP_001278143.1	Cytosol, Golgi	*MYO18A*	may link Golgi membranes to cytoskeleton; participate in tensile force for vesicle budding from Golgi; may have a role in Golgi membrane trafficking; ATP/ADP binding; DNA binding; RNA binding; actin filament binding
	ATP-binding cassette sub-family A member 13	NP_839990.2	Plasma Membrane, Lysosome	*ABCA13*	ATP binding; ATPase-coupled transporter
C-terminus					
	VNUT	Q8VCL5	Vesicles	*SLC17A9*	involved in vesicular storage and release of ATP